Technische Universität München
Wissenschaftszentrum Weihenstephan für Ernährung, Landnutzung und Umwelt
Lehrstuhl für Systemverfahrenstechnik

Triboelectric separation – A new method to separate fine organic powders?

Johann Landauer

Vollständiger Abdruck der von der Fakulät Wissenschaftszentrum Weihenstephan für Ernährung, Landnutzung und Umwelt der Technischen Universität München zur Erlangung des akademischen Grades eines Doktor-Ingenieurs (Dr.-Ing.) genehmigten Dissertation.

Vorsitzende: Prof. Dr.-Ing. Mirjana Minceva

Prüfer der Dissertation:
1. apl. Prof. Dr.-Ing. habil. Petra Först
2. Prof. Dr. rer. nat. Sonja Berensmeier

Die Dissertation wurde am 01.10.2019 bei der Technischen Universität München eingereicht und durch die Fakultät Wissenschaftszentrum Weihenstephan für Ernährung, Landnutzung und Umwelt am 27.02.2020 angenommen.

Contents

Abstract

Triboelectric separation is a technique to separate dry powders according to their ability to generate charge. Charge generation takes place due to contact and subsequent separation of two surfaces. For instance, this surface-physical effect occurs when children rub a balloon on their hair. To date, an universal and agreed-upon physical description of the triboelectric effect for insulating materials is still missing. Since triboelectric charging is a surface effect, surface properties might play a decisive role for the generated electric potential differences.
Hitherto, triboelectric separation is used to separate plastics, salts, and organic raw materials containing starch and protein. Only few studies have shown that triboelectric separation is a suitable technique to separate powders containing of particles with different chemical compositions. These studies mostly address the properties of the separation step of triboelectrically charged particles and try to predict the charge generation of particles due to the empirical triboelectric series; however, to understand, to apply, and to improve the separation of powders using triboelectric charging, the separation of charged particles in an electrical field should not be the focus, but the charge generation due to the interaction of surfaces must be examined. In this thesis, powder mixtures of whey protein and barley starch with particle sizes below 50 µm are used in order to investigate the influence of particle-particle and particle-wall interaction on triboelectric separation; however, separation selectivity is used as an indicator for the formation of charge. Furthermore, the generated charge by triboelectric charging of single particles was quantified using a specially constructed setup. Thus, all studies carried out accompanying with this thesis are focused on the control parameters of triboelectric charging, since separation of particles in an electrical field is state of the art. Hence, derived from the fundamental description of the triboelectric effect, contact numbers of particles are found to be decisive.
For the first time, triboelectric separation was used to separate fine organic powders with similar size and true density. A variation of the tube material along with the empirical triboelectric series showed no differences in the separation performance. In further experiments, particle-wall interactions were inhibited using a boundary-layer control setup and a similar separation performance was shown. Furthermore, particle-particle contact numbers varied due to the flow profile and the particle size distribution of the used powder. An increase in contact number leads to a linear increase of the separation selectivity. Thus, particle-particle interactions are significant for charge generation and subsequent separation. In summary, both contact number and surface properties influence triboelectric charging, whereby the contact number can easily be influenced by flow properties, particle size, and surface properties.

Zusammenfassung

Der triboelektrische Effekt kann zur Trennung von Pulvern verwendet werden. Das Trennmerkmal ist die Aufladung der Partikeln. Die Ladung entsteht durch Kontakt und nachfolgende Trennung von Oberflächen. Dieser oberflächenphysikalische Effekt tritt auf, wenn ein Kind einen Luftballon an den Haaren reibt – dadurch werden Haare und Luftballon elektrisch geladen. Der genaue physikalische Zusammenhang ist für Isolatoren bisher noch nicht bekannt. Da es sich um einen Oberflächeneffekt handelt, spielen Oberflächeneingenschaften eine entscheidende Rolle.

Die triboelektrische Trennung kann für die Trennung von Kunststoffen, Salzen und organischen Rohstoffen bestehend aus Stärke und Protein verwendet werden und wird nur von einigen Studien als geeignete Technik zur Aufbereitung von Pulvern mit Partikeln verschiedener chemischer Zusammensetzung beschrieben. Im Fokus steht dabei hauptsächlich das Verhalten von triboelektrisch geladenen Partikeln in der Trennkammer, wobei das Aufladen der Partikeln über die empirische triboelektrische Reihe abgeschätzt wird. Jedoch ist es notwendig den Aufladevorgang betreffende Parameter zu untersuchen, um die triboelektrische Trennung von Pulvern besser verstehen, anwenden und verbessern zu können. Deshalb sollen in dieser Arbeit Pulvermischungen aus Molkenprotein und Gerstenstärke mit einer Partikelgröße kleiner 50 µm verwendet werden, um den Einfluss von Partikel-Partikel- und Partikel-Wand-Interaktionen auf die triboelektrische Trennung zu untersuchen. Dabei wird die Selektivität der Trennung als Indikator für die Ladungsbildung verwendet. Zusätzlich werden auch Ladungsverteilungen von einzelnen Partikeln in einem eigens aufgebauten Versuchsstand gemessen. Alle für diese Arbeit durchgeführten Studien untersuchen Regelgrößen des triboelektrischen Effekts, da die Trennung im elektrischem Feld Stand des Wissens ist. Daher ist ausgehend von der prinzipiellen Beschreibung des triboelektrischen Effekts die Kontakthäufigkeit der Partikeln als Haupteinflussgröße zu untersuchen.

Zum ersten Mal war es möglich feine organische Pulver durch den triboelektrischen Effekt zu trennen. Eine Variation des Materials der Ladungsstrecke anhand der empirischen *triboelektrischen Reihe* führte zu keiner Veränderung der Trennergebnisse. Mit einem zusätzlichen Aufbau konnte die Partikel-Wand-Interaktion durch Grenzschichtausblasen verhindert werden, wobei ähnliche Trennergebnisse erreicht wurden. Weiter wurden die Partikel-Partikel-Interaktionen durch eine Variation von Strömungsprofil und Partikelgröße der Pulver verändert. Eine Zunahme der Kontakthäufigkeit geht mit einer Zunahme der Trennselektivität einher. Ein wesentlicher Parameter für die Ladungsbildung und die darauffolgende Trennung ist demnach die Partikel-Partikel-Interaktion. Zusammenfassend konnte gezeigt werden, dass sowohl Kontakthäufigkeit als auch Oberflächeineigenschaften der Partikeln Einfluss auf die triboelektrische Trennung haben, wobei sich die Kontakthäufigkeit durch Strömungsbedingungen und Partikelgröße einstellen lässt.

Acknowledgement

First of all, I would like to thank Prof. Dr.-Ing. Petra Först for the possibility to work out this topic and her support though the last years. Furthermore, I would like to thank Prof. Dr.-Ing. Heiko Briesen for his support and the fruitful discussions as well as Prof. Dr. rer. nat. Sonja Berensmeier for the readiness to review this thesis and Prof. Dr.-Ing Mirjana Minceva for acting as chief examiner.

My students, who worked on tiboelectic separation and further *academic hobbies* of mine: Felicitas Aigner, David Andlinger, Lion Beck, Long Chen, Gao Di, Lukas Hans, Matthias Kilger, Dominik Nönninger, Rebecca Röhrenbach, Johannes Seitz, Yuting Tan, Melina Tauwald, Chong Yin, Yaowen Zhang; thank you all.

In addition, I would like to thank all colleagues of the Chair of Process Systems Engineering for the pleasant working atmosphere. A special thank goes to Carsten, Christoph, Michi, and Steve; thank you for your fruitful discussions even in the unlikely case of nonsense and the fun we had during and after work.

I would like to thank my parents and my brother Flo; thank you for the faith in me and your support during my long way in education. Furthermore, life is not only work, but also free time. I want to thank my friends who supported me through their distraction.

Thank you Thesi for your time, your support, your faith in me, and your patience.

1. Introduction

1.1. State-of-the-art dry separation techniques

1.1.1. Air classification

Since the chaff of the grains were removed by air classification in order to improve flour quality, separation is one of the oldest classes of unit operations. The threshed cereals are thrown up into the air and differences in particle weight result in different sedimentation velocities, and thus are classified. If the particles are just thrown up and no futher force is acting, the particles will sediment at the same location. Thus, a perpendicular force acting on the particles like wind is necessary. This enables a difference in displacement of particles according to their sedimentation velocity (related to particle mass). This very old and very simple example forms the basis of all air classification techniques used in process engineering until now; however, modern air classification systems have well defined flow conditions, use different kinds of vortexes, enable cut sizes up to a few microns, and mass flow rates of several tons an hour (Furchner and Zampini, 2010).
In this simple example, the terms of mass, size, and sedimentation velocity are mixed up. In order to clarify the physics and to classify air classification in the context of further particle separation techniques, a detailed consideration must be done. As shown, at least two perpendicular forces are necessary to separate particles. Predominantly, one force is linked to properties of the particles, whereas the other is independent of the particles. As in the simple air classification example, in almost every air classification setup the flow profile/velocity (wind) is independent (meaning that the particles do not influence the flow profile/velocity) of the drag force of the particles. The drag force $\vec{F}_D$ consists of the mass force $\vec{F}_M$, the buoyancy force $\vec{F}_B$, and the resistance force $\vec{F}_R$. The mass force $\vec{F}_M$ for a single particle with the mass m_p can be calculated by:

$$\vec{F}_M = m_p \cdot \vec{a}, \tag{1.1}$$

whereby the acceleration $\vec{a}$ can be the gravity $\vec{g}$ or the centrifugal acceleration $r\,\vec{\omega}^2$. Under the assumption of monodisperse particles, the mass of the particles is expressed by $m_p = \rho_s V_p$. The buoyancy force $\vec{F}_B$ causes a static buoyancy,

$$\vec{F}_B = -V_p \cdot \rho_f \cdot \vec{a}, \tag{1.2}$$

which contains the same acceleration $\vec{a}$ as the mass force. Due to the interaction between particle and fluid, a resistance force is calculated by:

$$\vec{F_R} = c_w(\mathrm{Re}_p) \cdot A_p \cdot \frac{\rho_f}{2} \cdot \vec{v_{rel}}^2, \tag{1.3}$$

with the relative velocity v_{rel} of the particle, the inflow cross-section A, and the drag coefficient c_w as a function of the particle Reynolds number $\mathrm{Re}_p = \frac{v_{rel} \cdot d_p \cdot \rho_f}{\eta}$. In most cases, the drag coefficient is calculated for spherical particles with actual flow conditions (Re_p) (Allen, 1997).
The motion of particles in a fluid can be calculated as the balance of forces (Equations (1.1), (1.2), (1.3)):

$$\begin{aligned} \vec{F_M} - \vec{F_B} &= \vec{F_R}, & (1.4) \\ V_p \cdot (\rho_s - \rho_f) \cdot \vec{a} &= \frac{\rho_f}{2} \vec{v_{rel}}^2 \cdot \frac{\pi}{4} d_p^2 \cdot c_w(\mathrm{Re}_p), & (1.5) \end{aligned}$$

and thus outline the influencing factors particle motion and air classification. These relevant parameters can be assigned to the particles or the fluid. Particle characteristics are volume, true density, mass, and shape, whereas the fluid parameters are density, viscosity, flow conditions (indicated by the Reynolds number), and acceleration. The separation features of air classification are particle size and true density. Tomas (2004) showed the separation parameters for turbulent flow conditions. Derived from the motion of particles, the separation feature of air classification is the density and the volume of each particle. The particle shape is excluded and spherical particles are presumed, because particle shape is difficult to integrate in the used models. As shown in equation (1.5), to separate fine and low-density powders, the acceleration due to the use of different vortexes and/or the flow profile has to be optimised. Consequently, several types of air classifiers were developed and cut sizes of $\sim$1 µm (Galk et al., 1999) are available with different flow profiles and vortexes (Rumpf and Leschonski, 1967; Shapiro and Galperin, 2005).

Besides the optimisation of the flow profile, the use of air classification as a tool to separate organic/biological materials like starch and protein in flours is limited, because organic/biological powders have almost the same density. Further, the method of selective comminution is no promising strategy, because after grinding the powder both starch and protein are in the same size range (Vose, 1978). Thus, a selective separation of starch and protein is restricted.

1.1.2. Sieving

Besides air classification, sieving is a common technique to separate dry powders. A sieve usually consists of a mesh with defined open spaces. These defined open spaces are usually quadratic and specify the size of particles which can pass the sieve. To separate fine powders finer meshes are necessary; however, below certain sizes problems in manufacturing of meshes, passing probability, and particle interaction arise. Especially fine powders tend to agglomerate and the formed agglomerates are not dispersed by the motion of the sieve. The separation feature of sieving is the particle size. In some cases, particle shape can be also the

separation feature when sieves have open spaces with defined shapes (Schmidt, 2010). For the separation of fine organic/biological powders sieving has a limited suitability (Liu et al., 2009).

1.1.3. Problems with *classical* separation techniques

Hitherto, classical separation techniques like air classification or sieving showed no satisfactory separation of organic materials like protein and starch. In fact, air classification has a very small cut size and can separate powders accurately according to their size. Sieving is limited due to agglomeration of particles and the low passing probability. The separation features referred to particle properties of air classification and sieving are the volume (size), true density, and shape of the particles. The size and shape of the particles can be adjusted by comminution; however, both starch and protein will likewise become finer and the separation issue is not solved but moved to a finer scale. To separate particles of different chemical composition, it is desired to use a separation feature which is linked with the surface properties of particles. The surface properties are closely correlated to the chemical composition.

1.2. Triboelectric charging

1.2.1. The triboelectric effect

When two uncharged surfaces are brought into contact and subsequently separated, charge remains on both surfaces. This experiment describes the triboelectric effect. This well-known effect occurs everywhere in nature (Lacks and Mohan Sankaran, 2011). When children play with a balloon and rub it on their hair, they rejoice the generated electrical charge. The discovery of the triboelectric effect was made by ancient Greek philosophers and often Thales of Miletus is credited with the discovery (Iversen and Lacks, 2012; O'Grady, 2002). They rubbed amber[1] with fur and generated electricity (Park, 1898). A more intense rubbing of surfaces results in a higher amount of generated charge. This observation and also the subword *tribo* are misleading, because both might indicate that friction is necessary to obtain charged surfaces. The rubbing of a balloon only increases the contact/separation probability between balloon and hair and causes a higher net charge; nevertheless, a single contact suffices to generate charge. To prevent this misunderstanding, triboelectric or tribo-charging is also called contact or surface charging (Matsusaka et al., 2010; Matsusaka and Masuda, 2003). However, a detailed physical description, which considers all factors influencing triboelectric charging, is still missing for this very early discovered, well known, and common effect.

1.2.2. The physics behind the triboelectric effect

As triboelectric charging depends on surface properties, chemical composition, and physical structure of the surfaces plays a major role in the charging step. The usual classification

[1] The word *electricia* was first used by William Gilbert in *De Magnete*. It is derived from the Latin word *ēlectrum* and came from the greek word for amber $\grave{\eta}\lambda\varepsilon\kappa\tau\rho o\nu$.

of the triboelectric effect is based on the conductivity of the materials. The reason for it might be historical, because for conductors and semiconductors a physical description has been established. Thus, for arranging different phenomena, conductor-conductor, insulator-insulator, and hybrid contacts are usually distinguished (Lacks and Mohan Sankaran, 2011).

In a conductor and semiconductors, the conductivity can be explained by the Fermi gas (Fermi, 1926). The Fermi gas describes the electrons in a solid (crystal) without any interaction between the electrons and the ions of the crystal lattice. Thus, the electrons behave like an ideal gas in classical physics. In reality, the electrons in metals are not able to move without any interaction. They move in the periodic potential of the metal ions which are located at the crystal lattice. Thus, the interaction between electrons and ions play a major role for the mobility of the electrons. The order of ions in the crystal is periodic, and thus the potential (energy) of the electrons is also periodic. Bloch (1929) showed based on the Einstein solid that the probability of electrons in a solid is periodic and there are areas where no electrons are found (band gap). These so called Bloch waves just matter for electrons which are located in bands further from the nucleus. Electrons in bands near the nucleus must comply the Pauli Exclusion Principle and are bound very strongly to the nucleus, and thus their mobility is limited. The allocation of the electrons to the bands depends on the Fermi energy E_f (dependent on the material). If voltage is applied to a solid, electrons in a full band can not absorb energy, because no free spaces are available in allowed areas (band). To reach the next band, the band gap energy $\Delta E_g \gg k_B T$, whereby k_B is the Boltzmann constant and T the absolute temperature, has to be overcome, which is higher than the feasible voltage. The solids with the Fermi energy within the band gap are called insulators (Figure 1.1). For all conductive materials, the Fermi energy is within the conductive or valence band. Thus, applied voltage can increase the energy of electrons and these electrons can move along the electrical field.

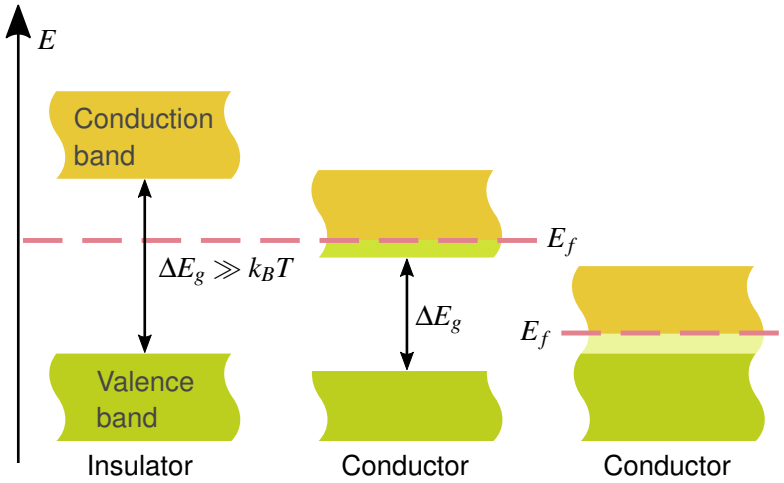

Figure 1.1.: Simplified scheme of the band model of conductors and insulators. If the Fermi energy E_f is within the band gap, energy supplied by an applied voltage is insufficient to overcome the energy of the prohibited zone ΔE_g. In conductors, the Fermi energy is within a band, and thus the electrons can reach easily the next band and can move along the applied electrical field.

Conductor-conductor contact

Triboelectric charging upon conductor-conductor contact can be explained according to the band model. In a metal with infinite extension, electrons are only replaced by applying voltage, because all electrons in the condition band are attracted homogeneously by the ions. The surfaces of real solids result in areas where ions are in a half space. Thus, the electrons near the surface are bound weaker to the ions than those within the metal. The thermodynamic work (energy) that is needed to remove an electron from a solid into vacuum is called *work function* W and is defined as the difference between the energy of the electron nearby the surface $-e\phi$ and the Fermi energy E_f:

$$W = -e\phi - E_f, \tag{1.6}$$

with the charge of an electron $-e$ and the electrostatic potential in the vacuum nearby the surface ϕ. The difference of the work function of different metals is shown in Figure 1.2. Thus, the dependency of the crystal structure is clearly visible due to the influence of different surfaces according to the orientation in crystal lattice.

When two conductors come into contact, the difference in the surface potential/work function leads to charged solids after contact and subsequent separation (Figure 1.3). Before the contact, metal A and B have different Fermi levels (Figure 1.3A) and different specific surface potentials ϕ_A and ϕ_B. Due to the contact, the Fermi levels are equalised and a surface potential difference $\Delta\phi$ is generated (Figure 1.3B). The surface potential difference is equivalent to the charge that remains on both solids after a separation of the two metals. In our case, metal A is charged negatively and B is charged positively, because $\phi_A > \phi_B$, and the charge is equivalent to the surface potential difference $\Delta\phi = |\phi_A - \phi_B|$. (Harper, 1951; Matsusaka and Masuda, 2003)

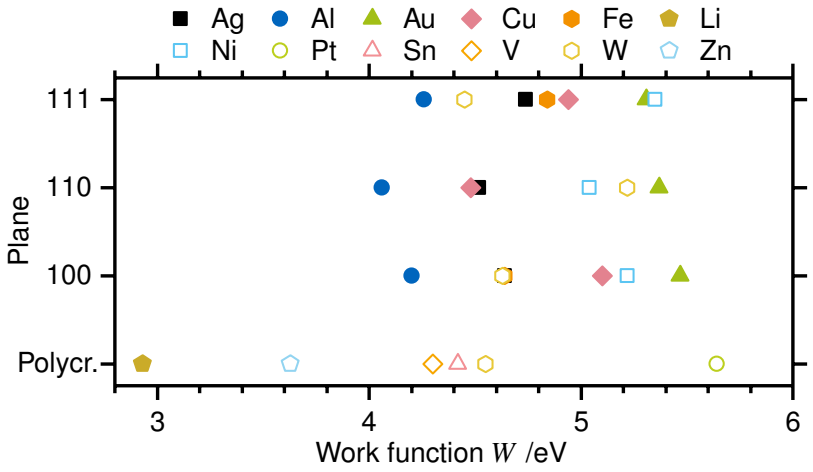

Figure 1.2.: Work functions of different metals on different crystal plains and in the polycrystalline state (Hölzl and Schulte, 1979).

First experiments with different metal powders to generate electric charge were carried out by Vollrath (1932). Iron and antimony powders were dispersed in air and blown through a

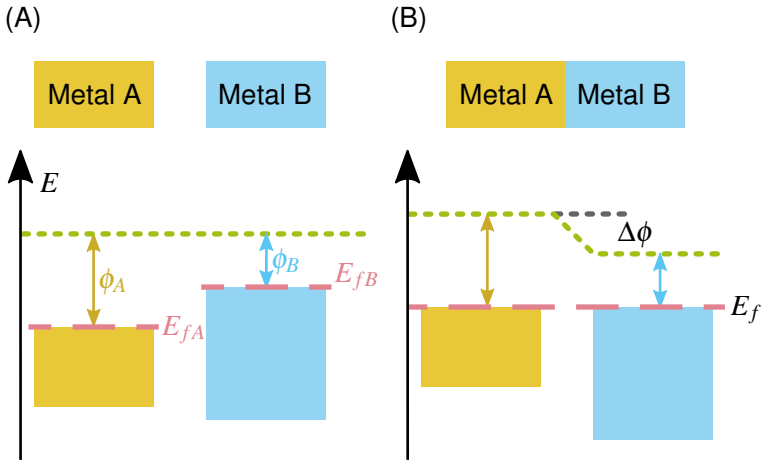

Figure 1.3.: (A) Energy distribution of metal A and B with different Fermi levels E_fA, E_fB and the surface potentials ϕ_A, ϕ_B without contact. (B) Energy distribution of two metals during and after contact. Due to the contact, Fermi levels are equalised and electrons flow from the higher to the lower surface potential, which leads to a negative charge on metal A and a positive charge on metal B after separation.

copper tube and the resulting voltage of 260 kV was measured. This work founded the currently highly investigated field of triboelectric nanogenerators (Wang et al., 2015b; Wu et al., 2019). Further experiments demonstrated that for conductors the contact potential difference $\Delta\phi$ describes triboelectric charging of particulate materials (Gupta et al., 1993; Harper, 1951). In summary, the contact or triboelectric charge between conductive materials is driven by the difference in potential difference between the different materials. For all cases, a calculation of the expected charge with a slight difference to the measured charge is possible.

Conductor-insulator contact

In insulators electrons require a high amount of energy to reach the conductive band, which is always above the Fermi level as shown in Figure 1.1. As the required energy, $\Delta E_g \gg k_B T = 0.025\,\text{eV}$ (at 293.15 K), in most cases the temperature required to reduce the band gap is higher than the disintegration temperature. However, a linear relationship between charge density on polymer insulators and metal work functions support an electron transfer mechanism (Davies, 1969; Gallo and Lama, 1976; Harper, 1967). Gallo and Lama (1976) also assumed a size dependency of triboelectric charging, because this might lead to charges in thunderstorms (Mareev and Dementyeva, 2017). These findings assume an apparent or effective work function for insulators ϕ_I and conductors ϕ_C through contact:

$$\Delta q_{eff} = c_0 \frac{-(\phi_I - \phi_C)}{e}, \tag{1.7}$$

where c_0 is the contact capacitance between materials (Davies, 1969). Some effective work functions and dielectric constants are published for insulators (Gallo and Lama, 1976). This model is based on the idea of an available *free electron* in an insulator, which is in contrary

to the thermodynamic states of the electrons in an insulator. The theory of band model assumes a homogenous energy distribution over the whole materials and neglects the surfaces of solids. To allow an electron transfer between conductor and insulator, the energy level of the donator or acceptor states of the insulator has to be lower closer to the surfaces. Therefore, Lowell and Rose-Innes (1980) assumed an exponential decrease of the energy levels towards the surface, the so called *surface state*. These lower energy levels might allow insulators to be charged during a conductor-insulator contact (Anderson, 1994; Bailey, 2001).
The description of an insulator as shown in Figure 1.1 is idealised. In actual insulators, defects or *trap states* in the band gaps are present and can be occupied by non-equilibrated electrons. The non-equilibrated electrons are not in their lowest energy state (Lowell and Truscott, 1986a). For the conductor-insulator contact, the behaviour of the conductor is known, but the charging mechanism of insulators remains ambiguous.

Insulator-insulator contact

Electron transfer. As already outlined, for the conductor-insulator, contact electrons can be transferred in spite of the large band gap, because lower energy levels due to *surface states* (Lowell and Rose-Innes, 1980) and *trap states* (Lowell and Truscott, 1986a) are possible. Furthermore, the electron transfer model is supported by experiments carried out with the redox couple $[Fe(CN)_6]^{3-}$ and $[Fe(CN)_6]^{4-}$. This reaction allows a selectivity between electrons and ions, because it can only take place with electrons (Liu and Bard, 2008). It is also possible to coat a PMMA (Poly(methyl methacrylate)) surface with Cu by immersing the tribocharged PMMA in a solution containing $CuSO_4$ and small amounts of Cu^{2+} (Liu and Bard, 2009). A further study carried out by Piperno et al. (2011) showed complementary results to those reported by Liu and Bard (2008, 2009), but offer an alternative interpretation based on material transfer. The static charge might be induced by uncompensated ions (Apodaca et al., 2010; McCarty and Whitesides, 2008; Salaneck, 1976) on the surfaces (Piperno et al., 2011). A further study describes the formation of mechanoradicals, which are created due to the polymer-polymer contact and can drive chemical reactions (Baytekin et al., 2012a). To describe or correlate triboelectric charging of insulating materials with bulk electronic properties, like the dielectric constant, or atomic properties, such as the work function, ionisation energy, or electron affinity, these approaches are insufficient (Wiles et al., 2003).
In addition to redox reactions, a correlation between the Lewis acid-base concept and triboelectric charging was observed and interpreted as evidence for electron transfer. Surfaces with a Lewis acidity tend to become negatively charged, whereas surfaces with a Lewis basicity tend to become positively charged (Clint and Dunstan, 2001). The approach of acid-base interaction in general (including Brønsted and Lewis acid-base theory) was used to describe surface adhesion (Fowkes, 1987, 1990). Based on these theories charging was described (Horn and Smith, 1992; Horn et al., 1993). The concept of Lewis acid-base interaction, which is used to elucidate triboelectric charging is unusual, because in a chemical way an electron pair from a Lewis base is shared with a Lewis acid; no electrons are transferred from the electron donor to the electron acceptor as in redox-reactions (McCarty and Whitesides, 2008).

Ion transfer. For insulating materials with mobile ions present, like polymers with salt ions on the surface or ionomers, charge transfer due to ions is comprehended. On the surface of these materials, there are strongly bound ions of one charge polarity and loosely bond ions of a contrary polarity. Through the contact with another surface, the loosely bound ions can be transferred to the other surface. Thus, both surfaces remain charged after contact (Fenzel-Alexander et al., 1994; Mizes et al., 1998). These results showed that ion transfer is an essential and general mechanism in charge transfer, not only for materials with inherently loosely-bound ions (McCarty and Whitesides, 2008). If no mobile ions are present inherently, the water layer which is present on every surface contains hydroxide ions. During the contact, a redistribution of the hydroxide ions takes place and after separation charge remains on both surfaces. In experiments, the charge of a surface was changed by changing the relative humidity, probably due to the exchange of ions between the water layer and the atmosphere (Ducati et al., 2010).

Material transfer. The contact of two solids is usually violent on a nanoscale. Thus, small amounts of material (on the nanometre scale) can splinter off of each surface and subsequently adhere on original surface or on the opposite surface. Since these interactions are on atomic scale, contact momentum cannot affect the splintering. Also, small particles adhering on the surface can change the surfaces due to the contact. These small particles are likely to carry charge, because bonds must be broken in order to splinter material (Salaneck, 1976) and radicals are formed (Baytekin et al., 2012a). On a polymer film of PS (Polystyrene), material transfer from PTFE (Polytetrafluoroethylene) balls was determined using X-ray photoelectron spectroscopy and confocal Raman spectroscopy. The matching surface potentials and surface topographies were detected using Kelvin force microscopy and atomic force microscopy (AFM), respectively.
Correlation of material characteristics like Young's Modulus and surface potentials rise a hint to a link between triboelectric charging properties and material characteristics (Baytekin et al., 2012b). The charge on surfaces induced by material transfer can be also strengthened due to the formation of ions on the surfaces (Piperno et al., 2011). Baytekin et al. (2011b) showed that due to the contact of different polymer films the charge is distributed on both surfaces in a mosaic structure and sections with opposite charge are stable side by side (Albrecht et al., 2009).

Mechanoions. Fission of chemical bonds induced by mechanical stress is called mechanochemistry, and thus ions are formed due to mechanical stress are named mechanoions. The contact of two surfaces can lead to newly formed interactions between molecules. Subsequent separation results in stress for newly formed surface interactions and fission of bonds. These bonds can be the newly formed or pre-existing ones which can lead to the formation of radicals on both surfaces or a cation and an anion for a homogenous or heterogeneous fission, respectively (Sakaguchi et al., 2014, 1990). The formation of mechanoions contains charge formation and material transfer (Baytekin et al., 2012a).

Summary. The physics of triboelectric charging is only partly understood. For conducting materials, contact charging is described by a physical model which contains the concept of Fermi (1926) gas and the band model derived from it which corresponds to experimental findings. Charging of insulating materials is more complex and no universal and agreed-upon description was found. Different charge transfer mechanisms are discussed and recent studies point out the significance of material transfer (including fission of chemical bonds) and ions. The transfer of electrons is discussed controversial. "Perhaps we are now learning why the field of electrostatic charging has not followed a trajectory similar to those of the other scientific fields, which were founded in ancient Greece" (Lacks, 2012).

1.2.3. Prediction of charge

For insulating materials, no general charging mechanism is known yet; however, several studies were carried out to predict the polarity and amount of generated charge.

Empirical triboelectric series. In the empirical triboelectric series, materials are ordered due to their charge after triboelectric charging. Nernst (1896) presented the triboelectric series for conductors; it follows the work function of the materials as shown in Figure 1.2. As the charging mechanism of insulators is still unknown, no series of materials can be calculated. However, lots of triboelectric charging experiments for insulators were carried out and the polarity as well as the amount of charge of materials in the charging setup were recorded. Coehn (1898) showed the first triboelectric series for insulating materials containing solids and fluids. Shaw (1917) coined the term *triboelectric series* and ordered metals and insulators empirically. The concept was adapted and the number of materials extended by further studies (Clint and Dunstan, 2001; Henniker, 1962; Hersh and Montgomery, 1955; Park et al., 2008b) as also reviewed by Gooding and Kaufman (2011). An example of a triboelectric series of polymer materials is shown in Figure 1.4.
A correlation of position in the triboelectric series and the functional groups showed that nitrogen containing polymers developed most positive charge. In PA (Polyhexamethylene adipamide), the repeating units are linked with an amide bond, whereas PI (Polyimide) appears uncharged. Halogenated polymers such as PTFE (Polytetrafluoroethylene) and PVC (Polyvinyl chloride) exhibit the highest negative charge. Thus, PTFE is designated to be the negative end of the triboelectric series. Polymers containing hydrocarbons show almost no charge (PET(Polyethylene terephthalate), PP (Polypropylene), PS (Polystyrene), PC (Polycarbonate), PMMA (Polymethylmethacrylate), and PVAc (Polyvinyl acetate)) (Diaz and Felix-Navarro, 2004) (Figure 1.4). However, Diaz and Felix-Navarro (2004) already point out that the ordering of materials with a low positive or without charge is questionable. The efforts to link the empirical triboelectric series, which is based on experimental observations, to different material properties was of limited success (Lacks, 2012).

Cyclic triboelectric series. Since charging conditions, material composition, and pretreatment plays a decisive role, different experiments result in different orders of the tribo-

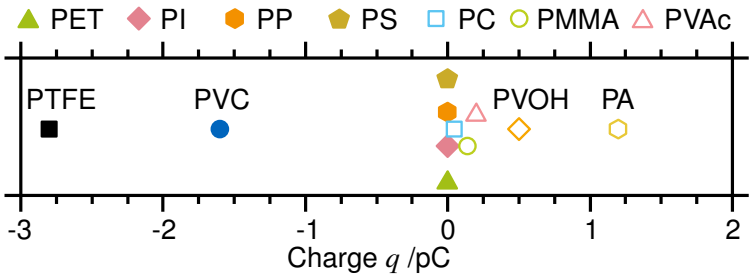

Figure 1.4.: Triboelectric series of the insulating polymer materials PTFE (Polytetrafluoroethylene), PVC (Polyvinyl chloride), PET (Polyethylene terephthalate), PI (Polyimide), PP (Polypropylene), PS (Polystyrene), PC (Polycarbonate), PMMA (Polymethylmethacrylate), PVAc (Polyvinyl acetate), PVOH (Polyvinyl alcohol), and PA (Polyhexamethylene adipamide). Materials form a group round zero exhibit only very few charge (Diaz and Felix-Navarro, 2004).

electric series. Some experimental results are unambiguously incompatible with the concept of the triboelectric *series*. For example, the series of zinc, silk, paper, cotton, and glass is known as the *cyclic triboelectric series*. The shown order is in series with increasing negative charge; however, the order cotton, glass, zinc, silk, and paper is also valid, and thus these materials can be ordered circular (Gooding and Kaufman, 2011; Harper, 1967; McCarty and Whitesides, 2008).

Triboelectric charging of identical materials. When two chemically-identical surfaces are brought into contact and are subsequently separated, intuitively no charge should be generated; however, several studies determined charge on both surfaces (Apodaca et al., 2010; Lowell and Truscott, 1986a; Pähtz et al., 2010; Sow et al., 2012; Waitukaitis et al., 2014; Xie et al., 2014, 2013). On flat surfaces, the charge generation follows a random, microscopic level fluctuation (Apodaca et al., 2010), but it is affected by deformation of materials (Xie et al., 2014). For particulate systems, the particle size might play a major role. It is found that larger particles are prevalently charged positively and smaller ones are charged negatively (Sow et al., 2012; Waitukaitis et al., 2014). It is likely that the contacting surface area is crucial for charge transfer (Xie et al., 2013) and the amount of charge q is proportional to the square root of the contacting area A, i.e., $q \propto \sqrt{A}$ (Apodaca et al., 2010).

Summary. Under the objective that for conductors the contact charge can be predicted by the work function, this concept was transferred to insulating materials. Empirical experiments without standardised conditions and standardised materials showed no clear tendency towards one specific series. Furthermore, only contacts of binary material combinations have been determined and no cross-correlations were used to create triboelectric series. Over time, more precise measurements and an enhanced understanding of charging mechanisms have led to contradictions in the triboelectric series and it is questioned whether triboelectric series exists, not least because triboelectric charging of identical materials. Thus, the triboelectric series could be an indication but not an evidence for predicting triboelectric charging.

1.2.4. External influences

Humidity As already expected by dealing with ions as *charge carrier*, humidity of the surrounding medium has a considerable influence on triboelectric charging due to the water adsorbed on the surface of solids. Moreover, humidity affects the electrical conductivity of surfaces. Lots of studies dealing with the influence of relative humidity on triboelectric charging and showed a decline in charge by increasing relative humidity (Albrecht et al., 2009; Ducati et al., 2010; Gouveia and Galembeck, 2009; Hemery et al., 2009; Kolehmainen et al., 2017; Mohanta et al., 2016; Pence et al., 1994; Schella et al., 2017; Schönert et al., 1996; Trigwell et al., 2003a). Since water is ubiquitous in technical conditions, water forms a thin layer of 1-2 nm on every surface. Therefore, Baytekin et al. (2011a) raised the question "Is Water Necessary for Contact Electrification?" Different polymer surfaces were brought into contact and separated subsequently under absence of water using a sophisticated setup in a glove box submerged in paraffin oil. After contact, the charge was determined using a Faraday cup and compared with experiments under presence of atmospheric water. Results showed that water is not necessary for triboelectric charging. But, contrary to the assumption that water/humidity reduces electrical conductivity, water helps to stabilise the surface charge during and after formation. As water is not required but enhances triboelectric charging, the role of water in the empirical triboelectric series arises. The charge of water in contact with different materials when flowing through tubes was examined. Water is charged positively due to material contact and negatively when flowing through air. Thus, water should be located at the positive end of the triboelectric series (Burgo et al., 2016; Coehn, 1898).
As remarkably described in the review of McCarty and Whitesides (2008), water might be essential for the charge transfer by ion transfer. Pence et al. (1994) showed for toner particles that charge depends on relative humidity. At 0 % relative humidity almost no charge was measured. An increase of relative humidity higher than 40 % results in rapid decrease of charge determined on particles made of toner and polymers (Kolehmainen et al., 2017; Schella et al., 2017). The amount of charge formed by particle-particle interaction increases with increasing humidity. Same findings were made by determining the charge of particles induced by changing the humidity, and thus absorbing and desorbing water (Gouveia and Galembeck, 2009).

The role of humidity in triboelectric charging not only has a preventing ability as water affects the electrical conductivity but also promotes and stabilises charging. Since the charging mechanism(s) still remain(s) vague, the role of humidity for triboelectric charging and within the proposed mechanisms could not be comprehended; however, there might be an optimal humidity level for triboelectric charging with regard to used materials. But, to prevent triboelectric charging in industrial applications, humidity might play a subordinate role, because most applications are in the *unpersuasive range* of humidity.

Contact mode. The contact of surfaces can take place in different modes like rolling, sliding, or static contact. Besides the relative velocity of two surfaces, the normal forces of the contact can differ and lead to higher contact areas according to the Hertzian theory of

the non-adhesive elastic contact (Hertz, 1881). Considering the different suggested charging mechanisms (cf. 1.2.2) the contact mode is ignored. However, various different studies determined an influence of the contact mode (Akande and Lowell, 1987; Atroune et al., 2015; Ema et al., 2003; Ireland, 2010, 2019; Matsusaka et al., 2007; Matsusyama and Yamamoto, 2006; Matsuyama et al., 2003; Matsuyama and Yamamoto, 1994, 1995; Sow et al., 2012; Watanabe et al., 2007; Yao et al., 2016). Sliding of particles results in higher particle charge than a single contact (Atroune et al., 2015). A higher contact momentum of particles also generates higher amounts of charge (Watanabe et al., 2007). To investigate the influence of contact mode, single particle collisions are popular. The contact angle (angle between particle trajectory and the colliding plate) evokes different amounts of charge. An increase in plate angle results in higher amounts of charge; angels larger $\approx 60°$ result in a decrease of charge (Ema et al., 2003), whereas Ireland (2019) found a maximum of 50°. The decrease of charge with higher angles results from the transition of slip to roll over the plate (Ema et al., 2003). For sliding particles, charge is increasing with normal force and length of the slide. The *available* contact area might be increased and the contact between particle and plate should be more tightly (Yao et al., 2016). The increase of charge due to higher contact momentum is attributed to an increase in contact area (Matsuyama et al., 2003; Matsuyama and Yamamoto, 1994, 1995). The relevance of increasing contact area is shown by a contact of a hard sphere with a very elastic surface (Sow et al., 2012). This might only be a reason if the particles have no atomic flat surface and a relative velocity is applied (Baytekin et al., 2011b).
For slipping/bouncing particles an increase in contact time and residence time results in an increase in charge to mass ratio. Also, a higher sliding and bouncing fraction leads to higher amounts of charge (Ireland, 2010). These patterns are not describable with a simple *capacitor model* as proposed by Matsusyama and Yamamoto (2006). The differences of these studies are that Matsusyama and Yamamoto (2006) used conducting particles and plates, whereas Ireland (2010) used a conducting plate and insulating particles.

The contact mode in itself might be merged to a higher probability of surface area interaction. This higher accessible contact area results in an increase in charge generation probability (Lowell and Truscott, 1986a,b); however, if charged particles collide, a decrease of the generated charge can also occur in the same interaction rate. Thus, for every interaction case there might be an equilibrium. This equilibrium could be calculated due to charging and discharging frequency distributions (Haeberle et al., 2018).

Particle size. When particles are charged, bipolar charging occurs (Zhao et al., 2003). Thus, in a powder negatively and positively charged particles are present. Several studies showed that particle size influences the polarity of charge. Larger particles are charged predominantly positive, while smaller particles charge negatively (Forward et al., 2009; Kok and Lacks, 2009; Lacks et al., 2008; Lacks and Levandovsky, 2007; Zhao et al., 2002, 2003); however, also opposite findings were made – larger particles are charged negatively and smaller particles are charged positively (Mehrani et al., 2005; Sowinski et al., 2010). In order to understand why bipolar charging occurs depending on particle size, Lacks and co-workers

carried out a simulative approach and experimental investigations. The simulative approach deals with the combination of fundamental physics of triboelectric charging and the altered collision rate of charged particles according to their charge (Lacks et al., 2008; Lacks and Levandovsky, 2007). In the experimental setup, a bed of particles is partly fluidised like a fountain through a thin gas stream. Therefore, charging by particle-wall interaction is excluded. Bipolar charging was measured for monodisperse, spherical particles, indicating that charge generation of the material is feasible, and for bimodal, spherical particles (Forward et al., 2009). The same setup is used to investigate different materials and same findings were made: small particles are charged negatively, whereas large particles are charged positively (Forward et al., 2009; Kok and Lacks, 2009).

Triboelectric charging of particulate systems is very complex. Under the opinion that charging mechanisms remain unknown, empirical findings of particle size and polarity of charge are hazy. All experiments ignore particle morphology and thereby different surface properties (especially for the differences between small and large particles). The surface properties might influence charging the most, since triboelectric charging is a surface-physics phenomenon.

1.2.5. Role of triboelectric charging in process engineering

Hitherto, it was focused on the explanation of triboelectric charging. Process engineering deals with the utilisation or prevention of physical properties in order to transform raw materials to products.

Triboelectric charging occurs everywhere; in particular, when particles are involved. Triboelectric charging is observed in dust storms (Mareev and Dementyeva, 2017), volcanic clouds (Anderson et al., 1965; Tanaka et al., 2002), and even in space applications on Mars (Forward et al., 2009) and Moon (Jackson et al., 2015). Particulate system have obviously many factors that promote triboelectric charging. Particles have a large specific surface area, and when they are set in motion, the interaction rate between them is very high. Thus, high amounts of charged particles are generated.

In process engineering, triboelectric charging is considered to be bane instead of boon, and mostly the prevention of triboelectric charging is focused on. Triboelectric charged particles and charged plant components can cumulate high amounts of voltage. These high amounts of voltage can lead to spontaneous discharges and the formed flashes can lead to dust explosions within the plant (Glor, 2003). Besides these dangerous properties, triboelectric charging influences further particle characteristics. These can be summarised to electrostatic agglomeration (Lee et al., 2015) and the decline in granular flow properties (Boland and Geldart, 1972; Hendrickson, 2006).

Triboelectric charging occurs mainly in plants comprising fluidised beds, pneumatic conveying systems, or dry powder mixing; so mainly where particles are moved. Fluidised beds are mainly used for drying, coating, and reaction applications. In all cases, applications of fluidised beds are operated with particles distributed in size. Geldart (1973) correlated the fluidisation behaviour according to the particle size. Due to the particle size distribution packing

density and van der Waals forces between the particles are implied. But due to moving particles, charge is generated. Therefore, electrostatic interaction is added to the influence forces on single particles, which affects the fluidisation properties of powder (Boland and Geldart, 1972). Triboelectric charging in fluidised beds depends predominantly on particle size, bubble size and superficial gas velocity (Chen et al., 2003). In a fluidised bed (under bubbling conditions), negative and positive zones are detected. The charge distribution can be affected by altering the gas inlet conditions (Tiyapiboonchaiya et al., 2012). Charge generation in a fluidised bed is not affected by adding larger particles of the same chemical composition; whereas the addition of smaller particles showed both an increase or a decrease of charge generation according to the amount of particles added (Wu and Bi, 2011; Yu et al., 2010). Of course, in fluidised beds the charge of particles and hydrodynamic bed properties influences each other. Size and frequency of bubbles in the fluidised bed are decreasing and the buble rising zone is decreasing due to an increase in generated charge. The reason for this might be electrostatic agglomeration (Dong et al., 2015a,b).
In contrast to fluidised beds, recent research of pneumatic conveying with the focus on triboelectric charging deals with prediction of charge due to the conveying process. Therefore, most studies are predictive ones (Bunchatheeravate et al., 2013; Cangialosi et al., 2006; Grosshans and Papalexandris, 2016; Korevaar et al., 2014). The charge of particles can play a significant role in the spatial distribution of particles. If the particle charge is sufficiently low, the interaction of particles is not altered by the electrostatic forces (Korevaar et al., 2014). An increase in conveying air velocity results in an increase in the charge of the powder. The higher charge might be generated due to a more frequent particle-wall interaction and a higher turbulent dispersion (Grosshans and Papalexandris, 2016). However, higher air velocities lead to smaller charge magnitudes, because the residence time for particles in the tube is shorter (Cangialosi et al., 2006).
Mixing properties in dry powder mixing are mainly influenced by the cohesiveness between particles. The cohesiveness depends on the acting forces between particles, primary van der Waals forces and Coulomb force. The Coulomb force depends on the charge of a particle. Particle charge is increasing due to the triboelectric effect during the mixing process, because the motion of the particles leads to recurring contacts and subsequent separations of particle surfaces. The generated charge during powder mixing depends on particle size, amount of fine particles (0-40 µm), and mixing container size (Karner and Urbanetz, 2012). For binary mixtures of charged particles, there is an optimal shear velocity which induces a maximum segregation of the particles (Yoshimatsu et al., 2018). In contrast, an increase of Coulomb force between particles increased the mixing degree (Lu and Hsiau, 2005). Since higher particle interactions result in a challenging design of the mixing process, triboelectric charging disturbs dry powder mixing and is tried to be prevented during the mixing process.

In most process-engineering applications, triboelectric charging is a lack. An increase in charged particles is accompanied with higher Coulomb forces, and thus with a decrease in granular flowability as bipolar charging is always present in powders. In summary, motion

of the particles leads to worse flowability due to the triboelectric effect. Thus, triboelectric charging is tried to be prevented by discharging particles.

1.2.6. Triboelectric separation

Triboelectric separation is a technique in process engineering where triboelectrically charged particles are separated due to their different polarity of charge in an electrical field. The actual separation step is very simple. Charged particles are defected in a homogenous electrical field due to their charge. Similar to the horizontal throw, the deflection trajectory depends on initial velocity of the particle, electrical-field strength, particle mass, and particle charge. Thus, the separation properties within an electrical field can be easily adjusted by the electrical-field strength for a given powder. Figure 1.5 shows three common types of separators. The plate separators consists of a capacitor with parallel plates (Figure 1.5 a) or plates with an aperture angle (Figure 1.5 b), which causes a homogenous (Trigwell et al., 2003b) or heterogeneous field (Shin and Lee, 2002), respectively. The charged particles are conveyed pneumatically or due to their gravity in the electrical field. This separation setup allows the separation of particle sizes up to a minimal size of $\sim$1 µm. For larger particles (>200 µm) also drum separators (Figure 1.5 c) are used. The particles are conveyed over a rotating drum electrode and the other electrode is placed nearby (Dizdar et al., 2018). Thus, the relations of the separation of triboelectrically charged particles are known and can be adapted to different requirements like particle charge, flow properties, or throughput.

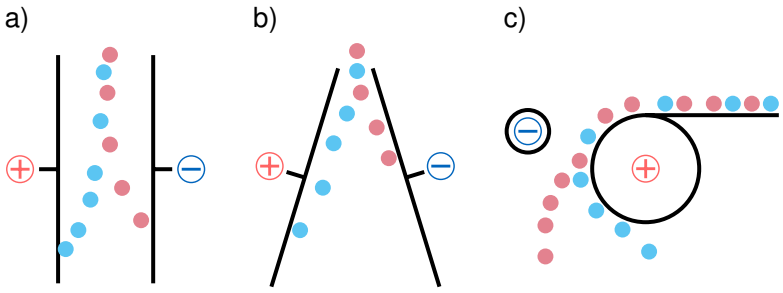

Figure 1.5.: Common designs of electrostatic separators: a) parallel-plate, b) angular-plate, and c) drum separator.

Since the separation step of triboelectric separation is well understood and can be designed for particles carrying various charge, most studies dealing with triboelectric separation address the charging step and different technical possibilities of particle charging are discussed. The technical possibilities can be divided in tube, gutter, rotary, and fluidised-bed setups. In tube setups, the particles are conveyed through a tube and the particles are charged due to particle-particle or particle-wall interaction whereby straight (Gupta et al., 1993; Hemery et al., 2011, 2009; Sibakov et al., 2014; Wang et al., 2015a, 2014, 2016a,b) and coiled tubes (Chen and Honaker, 2015; Chen et al., 2014; Wang et al., 2019; Xing et al., 2018) are used. Coiled tubes are intended to raise particle-wall interaction. Horizontal vibrated gutters charge particles predominantly due to particle-wall interaction (Atroune et al., 2015; Dizdar et al., 2018; Dwari et al., 2015; Gupta et al., 1993). In rotary setups, the particles are pneumatically

conveyed into cyclones and charged due to particle-particle interaction (Mohanta et al., 2016; Park et al., 2008a; Trigwell et al., 2003b). Furthermore, fluidised beds are used to charge particles due to particle-particle interaction (Calin et al., 2008; Messafeur et al., 2019; Shin and Lee, 2002; Tabtabaei et al., 2016a,b, 2017; Zelmat et al., 2015). Thus, the method of triboelectric charging of particles can be divided into particle-particle and particle-wall interaction. For particle-particle interaction/collision, the flow properties of the gas phase are most important (Smoluchowski, 1917). Saffman and Turner (1956) showed that an increase in turbulence dissipation rate results in a higher interaction rate. These correlations are only applicable for small particles (Wang et al., 1998). For pneumatically conveyed particles, particle-wall interaction depends also on the flow profiles and boundary-layer theory should not be ignored (Schlichting and Gersten, 2017; Sommerfeld, 1992). The boundary layer can prevent particle-wall interaction especially for fine particles. Besides flow induced particle-wall interaction, for all non flow condition induced particle-wall interactions like particles on a vibrated gutter, Ireland (2010) described particle-wall interaction with regard to triboelectric charging (cf. 1.2.4).

Various studies do not merely address differences in particle-particle and particle-wall interaction, in order to understand factors affecting triboelectric separation, but also the ability of triboelectric separation to separate granular materials and particles. Triboelectric separation performance is predominately investigated by separating minerals, plastic waste, and cereals. The processing of raw and recyclable material starts with comminution. Since comminution provides a homogenous powder with a narrow particle size distribution, a separation of particles according to different materials using air classification (cf. 1.1.3) is not expedient, because particles after comminution differ neither in size, nor in density. Hence, triboelectric separation is used to purify coal (Soong et al., 2001). A two-stage beneficiation showed significant reduction on sulphur and ash, whereas fine grinding improved bipolar charging and separation (Trigwell et al., 2003b). Due to triboelectric separation of cocking washery coal, the proportion of fly ash could be reduced (Mohanta et al., 2016). Furthermore, the mixing-ratio of coal-silica had an influence on the separation properties (Chen and Honaker, 2015). The separation properties of coal and sulphur were increased by surface modification with ethanol (Wang et al., 2017). Until now, triboelectric separation is used in an industrial scale to separate potash ores, fly-ash, and coal in an industrial scale (Dötterl et al., 2000).
The separation of PVC and PET in a fluidised bed tribocharger leads to highly concentrated PVC powder in a single processing stage (Shin and Lee, 2002). To separate a mixture of PVC, PET, and ABS (acrylonitrile butadiene styrene), a setup with cyclone chargers made of different materials was used. In the first step, PVC was separated from PET and ABS using a PP cyclone. In the second step, the charged PET and ABS was neutralised and after that charged using a HIPS (high-impact polystyrene) cyclone charger. PET was charged negatively and ABS was charged positively. Furthermore, an increase in air velocity results in a higher recovery rate (Park et al., 2008a). Thus, triboelectric separation is a promising process for the recycling of plastic waste. Lots of studies were carried out to propose different triboelectric

separation setups with appropriate operating parameters, in order to transfer these setup to an industrial scale (Wu et al., 2013).

Besides separation of minerals and recycling of plastic waste, triboelectric separation is applied to cereals. In most cases, as also in this thesis, an enrichment of protein of comminuted cereals is examined. Cereals and other organic raw materials are very heterogeneous in their natural structure depending on environmental conditions and plant source. Thus, to produce intermediate food and feed products, different valuable substances can be enriched using triboelectric separation. Hemery et al. (2011) carried out one of the first studies on triboelectric separation of cereals. They found that a multi-step purification of wheat bran results in fraction with higher amounts of ferulic acid, mineral, β-glucans, vitamins, and fibres. Furthermore, combined triboelectric separation and comminution enriched β-glucan from oat bran (Sibakov et al., 2014) and lupine protein (Wang et al., 2016b). Both studies showed that a decrease in particle size leads to higher separation selectivity and efficiency, because the surface area is increased and the particles with different chemical composition are segregated. Recent studies used tube (Chen et al., 2014; Pelgrom et al., 2015; Wang et al., 2015a, 2014, 2016a,b; Xing et al., 2018) and fluidised bed (Tabtabaei et al., 2016a,b, 2017) setup to charge cereals and legumes. The separation selectivity $\beta_{S,i}$ is the quotient of the mass of material i separated on one electrode $m_{\mathrm{i,el}}$ and the mass of powder on the same electrode m_{el}, whereas the separation efficiency $\beta_{E,i}$ is the quotient of the mass of material i on one electrode $m_{i,el}$ and the the mass of material i in the powder before separation $m_{i,0}$:

$$\beta_{S,i} = \frac{m_{i,el}}{m_{el}}, \tag{1.8}$$

$$\beta_{E,i} = \frac{m_{i,el}}{m_{i,0}}. \tag{1.9}$$

In addition, separation performance is an often used term to describe both separation selectivity and separation efficiency.

Wang et al. (2014) estimated the potential of triboelectric charging for food powders, the charging conditions of wheat gluten were investigated relating to particle size distribution, gas velocity, flow conditions, and humidity. A decrease in particle size and an increase in gas velocity/flow conditions showed an increase in generated charge on particles. The humidity of the gas flow improves charge generation up to 40 % relative humidity. Thus, the influencing factors for triboelectric charging of wheat gluten are present, and separation properties of a gluten-starch mixture can be evaluated. An increase in initial protein concentration leads to higher protein concentrations and higher yields in the positively charged fraction. However, the separation was not as high as predicted by measuring cumulated charge of powder and the formation of agglomerates is presumed to be the reason. An increase in gas flow rate and electrical-field strength showed an increase in separation selectivity and efficiency as expected (Wang et al., 2015a). To enrich dietary fibre from rice bran, a two-step triboelectric separation setup was used. Triboelectric separation showed a higher amount of smaller particles compared with sieving, but the same amount of dietary fibre (Wang et al., 2016a). Lupine protein was enriched after pin milling to approximately ∼50 wt. % in a single step separation.

Two further separation steps raised the protein content to ∼65 wt. %, but the yield decreased from 22 wt. % to 2 wt. %. In contrast, a recycling and repeated separation of the *uncharged* powder results in an increase in protein concentration and yield (Wang et al., 2016b). Xing et al. (2018) showed that powder preparation plays a decisive role for triboelectric separation of organic materials. Finer particle size distributions predominantly showed higher protein contents.
Tabtabaei et al. (2016b) used a fluidised bed to charge and subsequently separate navy bean flour. In preliminary tests PTFE was found to be the most suitable material for the charging setup. In the protein rich fraction, 43.5 % of the total protein with a protein content of 40.3 wt. % were increased. To increase the efficiency and selectivity of the triboelectric separation setup, a *Design of experiment* study including the parameters flow rate, electrical-field strength, plate angle, and tribocharger length was carried out. The optimised operating conditions show a high protein content and a high yield (Tabtabaei et al., 2016a). Flow condition in the separation step and plate voltage influence the separation conditions in single stage separation. A two-stage separation enables to enrich protein content to ∼38 wt. % at a total protein yield of 60 % (Tabtabaei et al., 2017).

Triboelectric charging can be a suitable tool to separate particles due to their ability of charge generation by contact. Recent publications on triboelectric separation show that it is already used in processing minerals, but the scope of application to separate plastic waste materials and organic materials for food and feed production is not yet exploited. This might be the reason, because for complex organic materials triboelectric charging is more challenging due to the number of lots of different materials. However, empirical studies show that triboelectric separation is an excellent method to separate particles due to their chemical composition.

1.3. Aim of the thesis

The knowledge on triboelectric charging and separation is multifariously, but in most cases incoherent. The best example for this is the so called empirical triboelectric series, where different authors found different series (cf. 1.2.3). However, different results under different experimental conditions are usual for triboelectric charging experiments. Nevertheless, triboelectric charging holds great potential to separate materials due to their chemical composition and the charging process can be influenced by several external factors (cf. 1.2.4).
Gaps in mechanistic understanding identified in the literature, as well as perspectives for novel applications of triboelectric separation leads to the main hypotheses of this thesis:

H I Triboelectric charging is a suitable tool to separate fine organic powders, and the main influencing parameters are flow conditions in the charging tube and particle size distribution.

These two parameters might be essential, because both refer to the fundamental concept of triboelectric charging – the contact of two surfaces. The turbulence intensity increases the interaction frequency and, thereof, the contact and subsequent separation

of surfaces. The particle size distribution is related to surface area of a particle, and thus for finer particles a higher amount of surface is available within a sample.

H II Particle-particle interaction plays a decisive role in triboelectric charging and separation.

Since triboelectric charging is a surface phenomenon, the surface area available for particles is very high. This high surface area might lead to a high interaction probability. Furthermore, contacts between particles with different and same materials could also facilitate charge generation. Therefore, the probability of generating charge might increase.

H III Particle-wall interaction has no influence on triboelectric separation.

The surface area of the wall material in the charging section is small compared to the surface area of the particles. Boundary-layer theory also shows a low interaction probability of particles close to the walls compared to the centre of the flow. Thus, a choice of the wall material according to the empirical triboelectric series cannot improve or impair triboelectric separation.

H IV Particle-particle interaction shows multimodal charge distributions according to their chemical composition.

Since contact between identical materials generates charge and particle size has an influence on polarity of charge, a charge distribution for a powder might arise. For binary mixtures, contacts between identical and different materials as well as between different particle sizes occur.

H V Polarity and amount of charge are independent from particle size in a binary powder mixture.

It is assumed that the polarity of charge depends predominantly on the chemical composition of the particle surface. The interaction between two surfaces results in a different amount of charge. Particle size might have a minor influence on the surface composition. Thus, polarity and amount of charge are independent and depend on contact probability.

In summary, the main message of the five hypotheses puts the focus on particle-particle interaction with regard to triboelectric separation. To control and to optimise triboelectric charging and subsequent separation due to particle-particle interaction and chemical composition might be an expedient possibility from a process-engineering perspective.

2. Results

2.1. Paper I: Triboelectric separation of a starch-protein mixture – Impact of electric field strength and flow rate (Landauer and Foerst, 2018)

Brief introduction

This paper examines the influence of gas flow rate in a turbulent flow regime in the charging tube and electrical-field strength in the separation chamber on the separation efficiency and selectivity of triboelectric separation. For the first time, triboelectric separation is used to separate fine organic powders with a particle size below 50 µm and a mean particle size of ∼10 µm. The used model powder consists of barley starch and whey protein in a proportion of 85 % and 15 %, respectively.
A simple bench-top triboelectric separator is developed containing a charging section and a parallel-plate separation chamber. The charging section consists of a Venturi nozzle to insert powder in a nitrogen gas flow and a charging tube ($d_i = 10\,\text{mm}$, $l_t = 450\,\text{mm}$). Both components are made of PTFE. The investigated flow rates are 2.0, 2.5, and 3.0 $\text{m}^3\,\text{h}^{-1}$, which corresponds to Reynolds numbers of 5408, 6759, and 8111, respectively. The rectangular separation chamber consists of a parallel plate capacitor ($l_c = 400\,\text{mm}$, $d_{pl} = 46\,\text{mm}$, $h_c = 32\,\text{mm}$). Electrical-field strengths of 22, 66, and 109 $\text{kV}\,\text{m}^{-1}$ are applied.

Study findings

Triboelectric separation is a suitable way to separate fine organic powders. Starch and protein are separated with a high protein separation efficiency (yield) and a very high separation selectivity. On the cathode a protein content of 80 wt. % and on the anode a starch content of 96 wt. % are determined. Contray to expectations, the increase in turbulence showed no change in separation selectivity and efficiency for protein and starch. An increase in electrical-field strength results in a higher selectivity and efficiency of the triboelectric separation process. Furthermore, an analysis of the particle size distribution shows different patterns for cathode and anode; the powder separated on the cathode is finer than the initial particle size distribution and an increase in electrical-field strength results in a decrease of the mean particle size, which might represent the high amount of protein powder. The particle size distribution of powder separated on the anode showed the same patten like barley starch and stays unaffected by an increase in electrical-field strength.

Conclusion

i Triboelectric separation is an excellent possibility to separate the fine organic powders according to their chemical composition.

ii A variation of the turbulence intensity had no influence on separation efficiency and selectivity assuming that a maximum charge (equilibrium cf. (Haeberle et al., 2018)) has been achieved.

iii An increase in electrical-field strength results in higher separation efficiency and selectivity.

Author contributions

Johann Landauer did the conception and design of the study as well as the experimental work and wrote the manuscript. Petra Foerst participated to the writing and supervised the study.

Advanced Powder Technology 29 (2018) 117–123

Contents lists available at ScienceDirect

Advanced Powder Technology

journal homepage: www.elsevier.com/locate/apt

Original Research Paper

Triboelectric separation of a starch-protein mixture – Impact of electric field strength and flow rate

Johann Landauer *, Petra Foerst

Chair of Process System Engineering, TUM School of Life Sciences Weihenstephan, Technical University of Munich, Germany

ARTICLE INFO

Article history:
Received 11 July 2017
Received in revised form 4 October 2017
Accepted 20 October 2017
Available online 31 October 2017

Keywords:
Electrostatic separation
Protein purification
Separation efficiency
Triboelectric charging

ABSTRACT

Triboelectric separation is a method for separating dry particulate systems due to their different electrostatic chargeability. Previous applications are limited to the separation of coarse powders. The aim of the present study is to examine the influence of the flow conditions and the influence of the electric field strength on the separation efficiency of starch and protein particles. Very fine organic powders are separated in a simple bench scale electrostatic separator to extend this technique to powders below 50 μm. The influence of different gas flow rates in the turbulent flow regime on particle charging and subsequent separation is investigated.

As an organic model substrate, a mixture of barley starch and whey protein was used. The tribocharger consists of a PTFE charging tube and a rectangular separation chamber where an electric field is applied between two electrodes. The particles are conveyed through the charging tube and charged by frictional contact with the tube wall. It is shown that different gas flow rates at a turbulent flow regime in the charging tube did not change the separation characteristics. In contrast, increasing electrical field strength increases separation efficiency of protein particles regardless of gas flow conditions. The proportion of starch at the anode is the same for all the investigated parameters.

© 2017 The Society of Powder Technology Japan. Published by Elsevier B.V. and The Society of Powder Technology Japan. All rights reserved.

1. Introduction

Triboelectric charging occurs when two contacted solid surfaces are separated again [1]. It is a poorly understood phenomenon, though ubiquitous in handling of dry particulate systems [2–5]. In powder handling, triboelectric charging can promote undesirable aggregation in pneumatic conveying systems [6–8]. Furthermore, it can encourage dust explosion hazards [9]. On the other hand, the triboelectric effect can be employed for the separation of fine powders with different triboelectric properties [10].

In order to separate powders based on their triboelectric properties, the particles must be charged first. However, electrostatic separation is so far only applied for the separation of coarse bulk materials with particle sizes larger than 100 μm [11,12]. In this study, we investigated for the first time the effect of triboelectric charging on the separation of fine organic powders with a mean particle sizes of 10 μm. The possible combinations of different materials to induce triboelectric charging are widespread [13,14]. Basically, electrostatic charging can be classified by the electric conductivity of the contacted materials, namely insulator-insulator, insulator-conductor and conductor-conductor [2,15–18]. The precise mechanism is not yet known for insulating materials [19,20]. For insulating materials triboelectric charging depends on surface properties. The surface properties can be described by the roughness and the chemical composition [21–23] as well as the morphology of the particle [24,25].

Triboelectric charging has been studied for the separation of powders by a number of authors. Triboelectric charging is mainly used for the separation of silica from coal [26–28], α-lactose from pharmaceuticals [29–32], plastics from waste [33–35] and for separating ground cereals [36–44]. In particular, dry electrostatic separation of ground cereals is a qualified method to enrich functional ingredients like protein or bran from wheat [36,37], rice [38], or legume [41–43]. As powders of natural origin usually consist of a mixture of numerous functional molecules, dry electrostatic separation has the potential to enable the efficient separation of functional ingredients [45,46].

Devices for the triboelectric separation of the ingredients of ground cereals are usually based on two different material combinations. Either, the powder is charged by insulator-conductor contact [36,38–40,43], where the particles come in contact with an aluminum plate before they are separated in an electric field with

* Corresponding author at: Chair of Process Systems Engineering, Gregor-Mendel-Straße 4, 85354 Freising, Germany.
E-mail address: johann.landauer@tum.de (J. Landauer).

https://doi.org/10.1016/j.apt.2017.10.018
0921-8831/© 2017 The Society of Powder Technology Japan. Published by Elsevier B.V. and The Society of Powder Technology Japan. All rights reserved.

a field strength between 100 and 250 kV/m. It was reported that the separation efficiency of a starch-gluten mixture can be controlled by the applied electrical field strength [39]. In the other works, ground cereals are triboelectrically charged by the contact with a polytetrafluorethylene (PTFE) surface. The particles can reach a higher charge due to the contact with PTFE compared to other insulating materials [28]. Therefore, lower electrical field strengths are sufficient to separate the protein-starch powder for this material combination [41,42,44].

Barley starch consists of large and small starch granules. The large starch granules from barley have an elliptical shape and an average particle size of about 20 μm. The small starch granules are spheres with a mean particle size of 5 μm. The proportion in the number of small granules is about 90 %. Thus, barley starch has a bimodal particle size distribution with maxima at 5 and 20 μm [47].

The aim of our work was to investigate the potential of triboelectric charging as a method for the separation of a very fine-grained protein-starch mixture. Both mixture components are in the same order of magnitude in size and density (mean particle size of 10 μm). This powder is not separable by conventional air classification. Therefore, novel methods for the separation of these kinds of mixtures have to be developed [45]. The protein and starch particles are similar in size but different in their chemical composition and particle morphology. Therefore, the driving force for separation is not size but triboelectric chargeability of the powder components.

2. Materials and methods

2.1. Materials

Barley starch was purchased from Altia Corporation, Finland, with a protein content below 0.5 wt% and a fat content below 0.6 wt%. The starch content was examined by a method where starch is hydrolyzed enzymatically and the formed glucose content is determined using 4-Aminoantipyrine in a dye reaction [48]. The moisture content was measured by Karl Fischer titration using a pretreatment for starch and protein powders [49]. Barley starch was determined to a starch content of 97.0 ± 1.5 wt% in dry matter and a moisture content of 10.9 ± 0.6 wt%. Whey protein isolate powder was obtained from Davisco Foods International, USA, with a protein content of 97.6 wt% in dry matter. The moisture content was determined to 7.5 ± 0.5 wt%.

2.2. Particle preparation

To obtain protein particles in the same size range as the starch particles, whey protein powder was dry comminuted in a lab-scale agitator bed mill with a *MoliNex* eccentric disk agitator (PE 075, Netzsch Feinmahltechnik, Selb, Germany) for 15 min at 2000 rpm. Zirconium dioxide grinding balls with a size of 1.25 mm were used. The target diameter $x_{50,3}$ was 4 μm.

2.3. Particle analysis

Particle size distributions were measured using the laser diffraction system Helos with the dry dispersing unit Rhodos and the wet dispersing unit Quixel (Sympatec, Clausthal-Zellerfeld, Germany). To disperse the powder in wet stage, ethanol was used as dispersant.

Scanning electron microscopy (SEM) pictures of used powders were made using GeminiSEM 500 (Carl Zeiss, Oberkochen, Germany) at a voltage of 1 kV.

2.4. Statistics

All measurements were performed in triplicate and are presented with the 95% confidence interval of the mean using Student's *t*-test. The uncertainty of quantities depending on multiple variables is given by the propagation of error.

2.5. Electrostatic separator

A benchscale electrostatic separator was constructed to perform separation experiments with very fine powders (Fig. 1). The separator consists of three parts. The Venturi nozzle (1) is used for dispersing the powder mixture in a nitrogen stream [50]. To disperse the manually added powder in the gas flow, a funnel was installed at the narrowing of the nozzle. A polytetrafluorethylene (PTFE) tube (2) with an inner diameter of 10 mm and a length of 450 mm was used as charging segment directly behind the Venturi nozzle. The particles are triboelectrically charged by particle-particle and particle-wall collisions inside the tube. In the separation part (3), the applied voltage of the parallel plate capacitator is adjustable from 1 to 5 kV, which corresponds to an electrical field strength between 22 and 109 kV/m. The nitrogen stream conveys the triboelectrically charged particles into the separation setup. The charged particles are separated by the interaction with the applied electrical field between the parallel stainless steel capacitor plates.

2.6. Separation procedure

The bulk material for separation experiments consist of a mixture of starch and protein powder with a weight ratio of 20:3 (starch/protein). This refers to a protein content of 15 wt% The gas volumetric flow rate was adjusted to 2.0 m^3/h, 2.5 m^3/h, and 3.0 m^3/h and the electrical field strength of the capacitator to 22 kV/m, 66 kV/m and 109 kV/m, respectively. To perform a separation experiment, gas flow rate and electrical field strength were set and approximately 2.5 g of the powder were dispersed within 5 min in the nitrogen stream.

To evaluate the selectivity of the separation experiment, both mass fraction and protein content of the bulk material adhered to both electrodes was analyzed. The purity of enriched protein β_i on the electrode i was calculated by (1).

$$\beta_i = \frac{m_{i,p}}{m_i} \tag{1}$$

where $m_{i,p}$ is the mass of protein and m_i is the total mass on the electrode i. The protein separation efficiency $\beta_{i,p}$ on the electrode i is defined as the quotient of the protein purity β_i and the initial protein content β_p scaled with the mass yield w_i (2).

$$\beta_{i,P} = \frac{\beta_i w_i}{\beta_P} = \frac{m_{i,p}}{m_p} \tag{2}$$

2.7. Protein concentration

The protein content was determined by taking an aliquot of the bulk material and dispersing it in 0.15 M NaCl, pH 7 buffer to achieve a protein concentration between 0.2 and 1.0 mg/ml. After an incubation time of 10 min, the probe was centrifuged at 2000 rpm for 5 min to separate the indissoluble starch particles and the absorbance of the supernatant was determined photometrically at 280 nm [51]. The protein content was then calculated using a calibration line, which was prepared by serial dilution of whey protein powder.

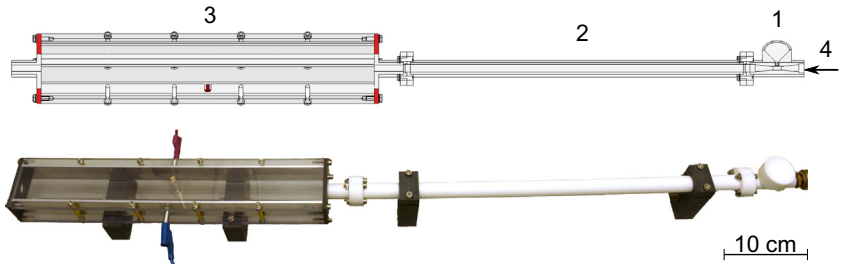

Fig. 1. Bench scale electrostatic separator schematic representation (top) and photo (bottom) with Venturi nozzle and funnel (1), charging tube (2), and rectangular separation chamber (3). The arrow indicates the direction of flow (4).

3. Results

3.1. Particle size distribution of the used powder

Fig. 2 shows the measured cumulative distribution $q_3(x)$ of the used protein powder, the starch powder and the protein-starch mixture. All particle sizes are in the same order of magnitude between 0.1 and 30 μm. The comminuted protein and starch particles are smaller than 20 μm and 30 μm, respectively. The particle size distribution of the protein-starch mixture (15 wt% protein) is located between starch and protein. Up to 30% of the volume of particles has a size smaller than 10 μm and about 42% of the volume lie in the range of 10–20 μm.

Fig. 3 shows SEM images of starch, protein, and protein-starch mixture. Starch particles have elliptical shape a very smooth surface. On the other hand protein particles are have a rough surface and no defined shape. In protein-starch mixture protein particles adhere on the starch particle surface.

3.2. Separation characteristics

3.2.1. Gas flow rate

Triboelectric charging of particles is induced by contacting different materials, in this case protein and starch particles with the PTFE tube wall. The impact of the gas flow rate on charging and separation was studied in a first step as the flow conditions influence the particle-particle and particle-wall collision frequency. Reynolds numbers were calculated for the chosen gas flow rates of 2.0, 2.5 and 3.0 m^3/h corresponding to 5408 ± 87, 6759 ± 96, and 8111 ± 107, respectively. Reynolds numbers in the rectangular separation chamber are 1720 ± 18, 2150 ± 15, and 2580 ± 15 corresponding to the chosen gas flow rates. For Reynolds numbers larger than 2400, inside the charging tube, turbulent flow was assumed [52]. In the rectangular separation chamber, flow conditions are in the laminar-turbulent transition regime or in the turbulent regime. Turbulent flow or high gas velocities are necessary to disperse particles in a gaseous phase [50].

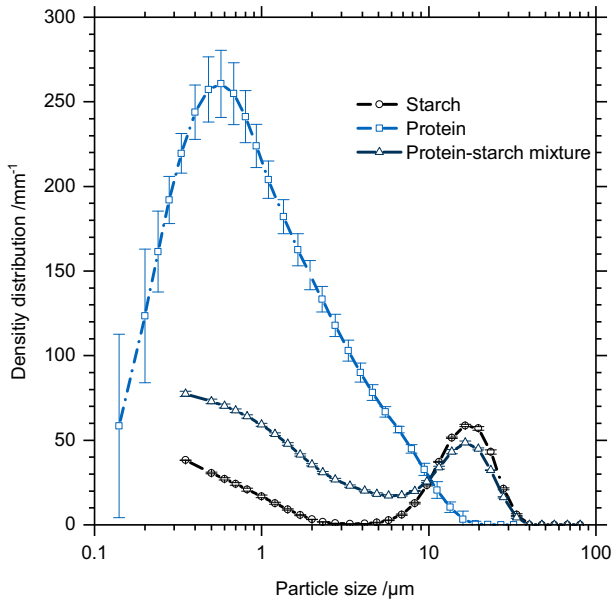

Fig. 2. Cumulated particle size distribution of protein, starch, and protein-starch mixture.

Fig. 4 shows the deposited mass fraction of the powder remaining on both the cathode (negative electrode) and the anode (positive electrode). After experimental procedure about 80% of the dispersed powder was collected on the electrodes. The experimental setup was cleaned after each experiment and a thin, not weighable layer of the remained powder was removed. No significant ($\alpha = 0.05$) differences were observed when increasing the gas flow rate within the studied range of Reynolds numbers (5408–8111). Independent from the electrical field strength, 94 ± 4% of the total mass is charged negatively and collected on the anode.

Only a small proportion is charged positively after the particle wall interaction. Thus, in the investigated flow regime, the mass fractions on the electrodes are independent on gas flow rate. Lower gas flow rates could not be investigated due to insufficient dispersibility of the powder in the gas stream.

3.2.2. Electrical field strength

The separation characteristics of the contact-charged particles depend on the net charge of every particle and the applied capacity of the parallel plate capacitator. In order to influence the separation efficiency of triboelectrically charged organic particles, different electrical field strength were applied on the capacitator. Fig. 4 shows the impact of an incremented electrical field strength from 22 kV/m to 109 kV/m on the mass deposition. A significant increase between 22 kV/m and 109 kV/m of the mass fraction on the cathode was observed. Analogously, the mass fraction decreases on the anode. The observed effect of increasing electrical field strength is very weak.

3.3. Selectivity of separation

3.3.1. Gas flow rate

In order to investigate the influence of the gas flow rate on the selectivity of the separation, the protein content of the powder on both the cathode and the anode were analyzed (Fig. 5). The protein content on the cathode was consistently higher than on the anode. In addition, an enrichment of protein on the cathode compared to the initial powder (15 wt%) is seen for each gas flow rate. In contrast, the protein concentration at the anode is a considerably smaller than the initial protein concentration. Thus, protein particles are preferably positively charged by the contact with the PTFE

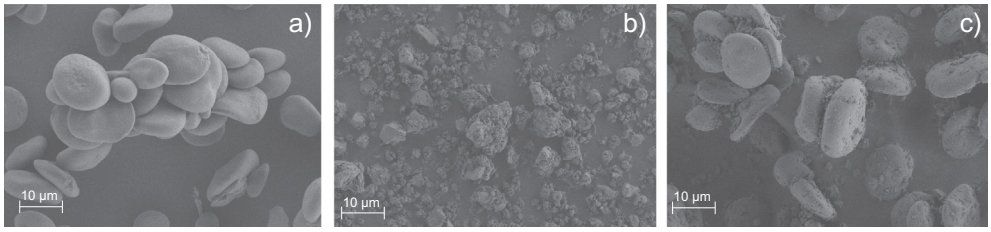

Fig. 3. Scanning electron microscope images of starch (a), protein (b), and protein-starch mixtures.

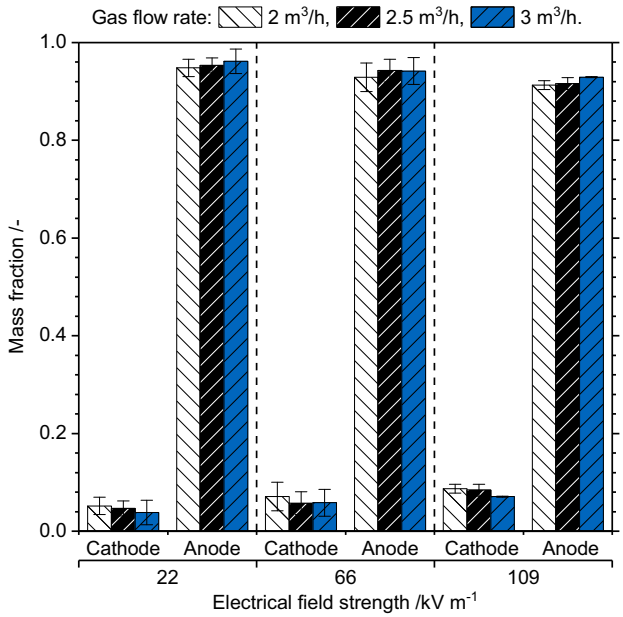

Fig. 4. Mass fraction on the cathode and the anode depending on the gas flow rate at 2, 2.5, and 3 m^3/h at different electrical field strengths. The mass fraction is not affected by an increased gas flow rate.

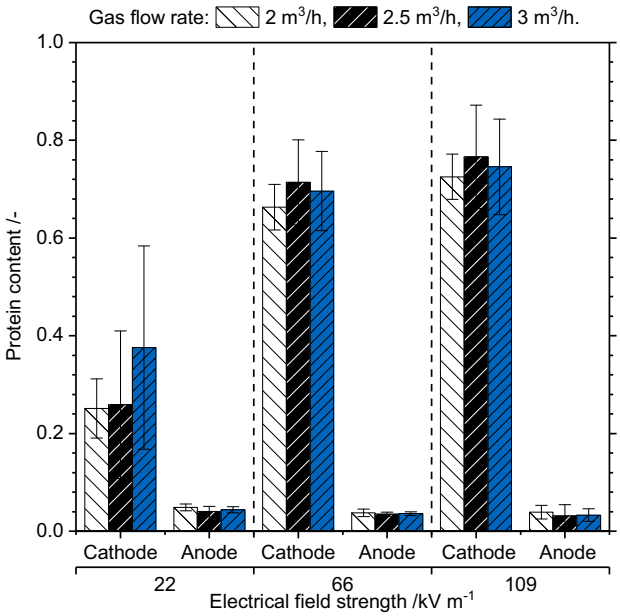

Fig. 5. Protein content on the cathode and the anode depending on the gas flow rate at 2, 2.5, and 3 m^3/h and different electrical field strengths. The initial protein content of the powder was 15 wt%. The gas flow rate has no significant impact on protein content or purity on the cathode. An increasing electrical field strength leads to an increase in protein content on the cathode. The protein content on the anode remains unaffected and a starch powder with high purity is separated.

insulator. No significant changes in protein content on both electrodes could be shown by increasing the gas flow rate within the turbulent flow regime. It is, therefore, concluded that an influence of different turbulent gas flow rates on electrostatic protein separation for small particles is negligible.

3.3.2. Electrical field strength

Fig. 5 also includes the protein content at the electrodes for different electrical field strengths. The protein content on the cathode increases with an increasing electrical field strength. To ensure a reproducible enrichment of protein on the cathode, an electrical field strength of 66 kV/m is necessary. No significant increase in protein content could be measured by further increasing the electrical field strength to 109 kV/m. On the other hand, the protein content on the anode is not significantly affected by increasing the electrical field. Similar results are obtained for gas flow rates of 2, 2.5, and 3 m^3/h.

The results show that triboelectric separation is a potential technology to separate fine powders to obtain high purity. A high protein concentration of 80 wt% on the anode and a high starch concentration of 96 wt% on the cathode could be achieved. The selectivity of the separation for the used model system is, therefore, very high.

3.4. Protein separation efficiency

To evaluate the selectivity of the triboelectric separation process, Fig. 6 shows the protein separation efficiency under varied test conditions. Like for the mass deposition and protein content, the gas flow rate in the studied range of Reynold numbers has no significant influence on the protein separation efficiency. In contrast, the change in capacitator electrical field strength leads to successively increasing protein yields on the cathode. For an electrical field strength of 109 kV/m, a separation efficiency of 0.58 can be achieved. On the other hand, the protein separation efficiency on the anode is statistically unaffected by the chosen electrical field strength and remains at about 0.24. The mass balance could not be closed due to the small amounts of powder used for the experiment. Thus, small weight losses have a very strong impact on the mass balance and thereby on the protein separation efficiency.

3.5. Particle size distribution of the collected powder

Fig. 7 shows the particle size distribution of the powder deposited on cathode and anode for a gas flow rate of 2.5 m^3/h. On the anode, the particle size distribution remains unaffected by an increase in the electrical field strength. The distribution shows a typical mode for barley starch powders at approximately 20 µm [47]. This indicates that there is a variety of so called large starch granules in the powder separated on the anode. Thus, the powder composition is not affected by the electrical field strength. In con-

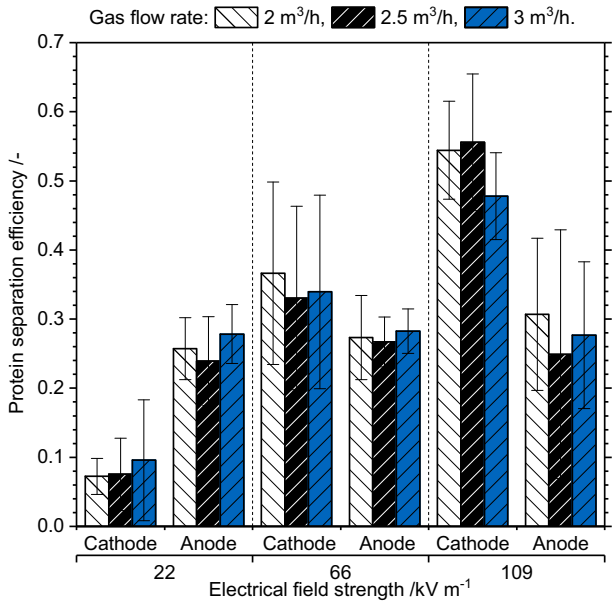

Fig. 6. Protein separation efficiency at gas flow rate of 2, 2.5, and 3 m^3/h and different electrical field strengths. The gas flow rate has no influence on the protein separation yield. An increase in the electrical field strength leads to higher protein yields on the cathode.

trast, the particle size distribution on the cathode is strongly influenced by the electrical field strength. At an electrical field of 22 kV/m, the distribution has a peak at approximately 20 μm. Thus, the volume fraction of the larger starch particles is substantial. When the electrical field strength is increased to 66 kV/m, the peak is shifted to lower particle sizes. Further increase in electrical field strength leads to a decrease of the particle mean diameter and the peak at 6 μm is elevated.

4. Discussion

4.1. Gas flow rate

Triboelectric separation is only slightly influenced by the applied flow conditions within the investigated flow regime. Increasing turbulence, and the accompanied higher particle-wall collision frequency, which was not tracked, showed no significant influence on separation characteristics. It can be assumed that an increase in turbulence might not increase particle charging. Therefore, it can be assumed that the impact momentum plays a minor role in the contact charge of particles below 30 μm (Fig. 2) contrary to larger particles [53]. On the other hand, the consistent geometry leads to a turbulent transition in the separation chamber when increasing the gas flow rate. However, the protein separation efficiency is statistically unaffected by the gas flow rate and turbulent flow conditions. These findings expand the results that a transition from laminar to turbulent flow regime has an influence on triboelectric charging and leads to an increase in protein separation efficiency [1]. This indicates that turbulent flow conditions are sufficient for triboelectric charging for both starch and protein particles and a further increase in turbulence does not improve the separation efficiency.

4.2. Electrical field strength and overall separation efficiency

In order to investigate the separation characteristics of the triboelectrically charged particles, the influence of electrical field strength is investigated. Starch particles are preferentially negatively, protein particles positively charged (Fig. 5). Higher electrical field strength increasingly deflect charged particles and, therefore, both the protein yield and the mass deposited at the cathode are increasing (Fig. 4). A further increase of the electrical field strength over the chosen maximum of 109 kV/m for very fine powders could be necessary. Separation efficiency is heavily influenced by increasing the electrical field strength and no stagnancy is observed in this study (Fig. 6). Furthermore, particle size distribution and separation efficiency show the same tendencies. In contrast, electrical field strength was in the same magnitude as shown elsewhere [39,41].

4.3. Protein content and particle size distribution

For the discussion on separation efficiency, both the particle size distribution (Fig. 7) and the protein content (Fig. 5) are employed. The powder, which is deposited at the anode, is neither affected by the gas flow rate nor by the electrical field strength. It is therefore likely that in contact with PTFE the starch particles are

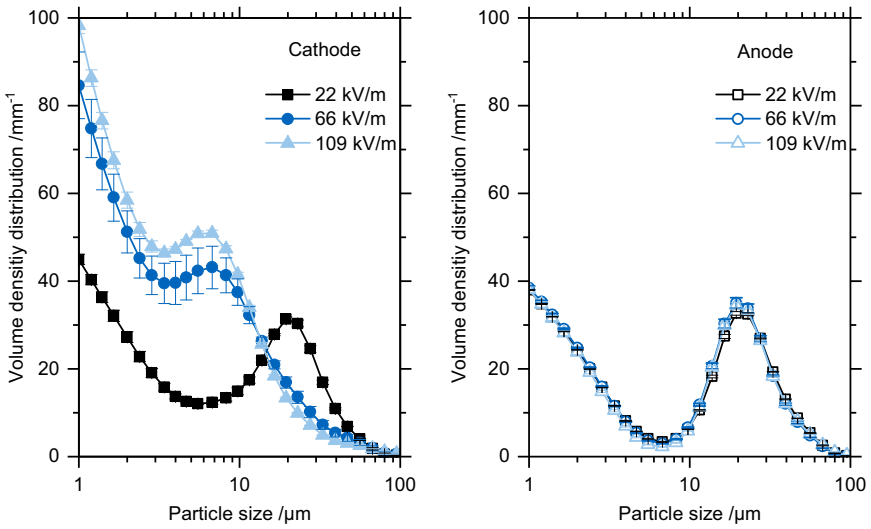

Fig. 7. Particle size distribution of powder collected on the cathode (left) and on the anode (right) after triboelectric separation at a gas flow rate of 2.5 m^3/h. Triangle square and circles mark an electrical field strength of 22, 66, and 109 kV/m, respectively. The powder collected on the cathode is significantly finer than on the anode. At an electrical field strength of 22 kV/m, no separation between the finer protein and the coarser starch particles can be seen. As the electrical field strength is increased, the peak at 20 μm vanishes and a new peak at 6 μm appears. The particle size on the anode is not affected by the electrical field strength.

charged stronger than the protein particles. Second, the composition of the powder deposited on the cathode is influenced by the electrical field strength but not by gas flow rate within turbulent flow regime. However, turbulent flow leads to an increase in protein content and smaller particles on the anode [44]. With increasing electrical field strength, the particle size distribution is shifted to smaller particles and the purity of the powder was increased (Fig. 5). When comparing particle size distribution and protein content at 22 and 66 kV/m, a significantly decrease in mean particle size and increase in purity is apparent. This is attributed to the large starch granules from barley represented by the peak at 20 μm in the particle size distribution. Fig. 3c shows small protein particles adhere on large starch granules. Thus, at low electrical field strength adhesion of protein particles cannot be overcome. This could be an explanation why large starch particles are detected on the cathode at low electrical field strength. In addition, at an increased electrical field strength a new peak at 6 μm is formed indicating an increasing amount of protein particles. In addition, small starch granules with a mean diameter of 5 μm can contribute to the peak forming at 6 μm. These effects have not yet been observed so far [38,44]. Therefore, a certain electrical field strength is necessary to separate triboelectrically charged starch and protein particles. A relationship between peak height at 6 μm and protein content is clearly recognizable. Furthermore, if a separation of elliptical and spherical starch granules can be assumed, triboelectric separation might be a reliable separation method.

5. Conclusion

In order to separate very fine powders, triboelectric separation is shown to be a useful method. For the first time, we were able to separate a very fine protein-starch powder mixture within the same order of magnitude in size and density with a mean particle size of 10 μm. It is assumed that the driving force for separation is mainly the composition of the surface of the particles. The powders made of starch and protein were separated with a protein separation efficiency of up to 0.6 on the cathode in one single step. Furthermore, high purity of protein (80 wt%) and starch (96 wt%) were achieved. Different turbulent gas flow rates in the charging section of the bench scale electrostatic separator did not influence the particle charge with regard to separation efficiency To ensure a sharp separation of the oppositely charged particles, a minimum necessary electrical field strength resulting from the applied voltage is required. Moreover, large starch granules are charged negatively, which is visible from the absence of large particles in the powder remaining on the cathode. Further work will be done to investigate the influence of the protein-starch ratio on the separation efficiency. On the one hand, the design of the electrostatic separator needs to be improved to increase the separation efficiency by decreasing powder loss. Therefore, the laminar flow conditions in the separation chamber should be improved and the construction should be modularized in order to enable a series connection of triboelectric separators which can enhance throughput for the industrial application. On the other hand, to apply the gained knowledge to further particle systems with different chemical and surface properties like roughness and ability of wetting, a prediction of the chargeability should be necessary. Here, analytical methods should be used to develop a correlation between the particle system, the particle properties, and the chargeability adapted.

Acknowledgements

This research did not receive any specific grant from funding agencies in the public, commercial, or not-for-profit sectors. The authors would like to thank Junwei Wang, LFG, FAU Erlangen-Nürnberg, for the help in taking SEM images.

References

[1] R.G. Horn, D.T. Smith, Contact electrification and adhesion between dissimilar materials, Science (New York, N.Y.) 256 (5055) (1992) 362–364.
[2] D.J. Lacks, R. Mohan, Sankaran, contact electrification of insulating materials, J. Phys. D Appl. Phys. 44 (45) (2011) 453001.
[3] S. Matsusaka, H. Maruyama, T. Matsuyama, M. Ghadiri, Triboelectric charging of powders: a review, Chem. Eng. Sci. 65 (22) (2010) 5781–5807.
[4] A.G. Bailey, Electrostatic phenomena during powder handling, Powder Technol. 37 (1) (1984) 71–85.
[5] S. Matsusaka, H. Masuda, Electrostatics of particles, Adv. Powder Technol. 14 (2) (2003) 143–166.
[6] P. Bunchatheeravate, J. Curtis, Y. Fujii, S. Matsusaka, Prediction of particle charging in a dilute pneumatic conveying system, AChE J. 59 (7) (2013) 2308–2316.
[7] S.-C. Liang, J.-P. Zhang, L.-S. Fan, Electrostatic characteristics of hydrated lime powder during transport, Ind. Eng. Chem. Res. 35 (8) (1996) 2748–2755.
[8] M.W. Korevaar, J.T. Padding, M.A. van der Hoef, J.A.M. Kuipers, Integrated DEM–CFD modeling of the contact charging of pneumatically conveyed powders, Powder Technol. 258 (2014) 144–156.
[9] F. Riedewald, A fire in a secondary pharmaceutical powder transfer operation, Process Saf. Prog. 31 (4) (2012) 390–392.
[10] K. Schönert, K. Eichas, F. Niermöller, Charge distribution and state of agglomeration after tribocharging fine particulate materials, Powder Technol. 86 (1) (1996) 41–47.
[11] T. Matsuyama, H. Yamamoto, Electrification of single polymer particles by successive impacts with metal targets, IEEE Trans. Ind. Appl. 31 (6) (1995) 1441–1445.
[12] T. Matsuyama, M. Ogu, H. Yamamoto, J.C.M. Marijnissen, B. Scarlett, Impact charging experiments with single particles of hundred micrometre size, Powder Technol. 135–136 (2003) 14–22.
[13] M.K. Mazumder, R.A. Sims, A.S. Biris, P.K. Srirama, D. Saini, C.U. Yurteri, S. Trigwell, S. De, R. Sharma, Twenty-first century research needs in electrostatic processes applied to industry and medicine, Chem. Eng. Sci. 61 (7) (2006) 2192–2211.
[14] S. Matsusaka, M. Oki, H. Masuda, Control of electrostatic charge on particles by impact charging, Adv. Powder Technol. 18 (2) (2007) 229–244.
[15] J. Lowell, A.C. Rose-Innes, Contact electrification, Adv. Phys. 29 (6) (1980) 947–1023.
[16] J. Lowell, W.S. Truscott, Triboelectrification of identical insulators. I. An experimental investigation, J. Phys. D Appl. Phys. 19 (7) (1986) 1273–1280.
[17] Y. Soong, M.R. Schoffstall, T.A. Link, Triboelectrostatic beneficiation of fly ash, Fuel 80 (6) (2001) 879–884.
[18] W.R. Harper, Contact and frictional electrification, in: Monographs on the Physics and Chemistry of Materials, Clarendon Press, Oxford, 1967.
[19] H.T. Baytekin, A.Z. Patashinski, M. Branicki, B. Baytekin, S. Soh, B.A. Grzybowski, The mosaic of surface charge in contact electrification, Science (New York, N.Y.) 333 (6040) (2011) 308–312.
[20] B. Baytekin, H.T. Baytekin, B.A. Grzybowski, What really drives chemical reactions on contact charged surfaces?, J Am. Chem. Soc. 134 (17) (2012) 7223–7226.
[21] M. Kamiyama, M. Maeda, H. Okutani, K. Koyama, H. Matsuda, Y. Sano, Effect of functional groups on the triboelectric charging property of polymer particles, J. Appl. Polym. Sci. 51 (9) (1994) 1667–1671.
[22] S. Trigwell, N. Grable, C.U. Yurteri, R. Sharma, M.K. Mazumder, Effects of surface properties on the tribocharging characteristics of polymer powder as applied to industrial processes, IEEE Trans. Ind. Appl. 39 (1) (2003) 79–86.
[23] R.G. Horn, D.T. Smith, A. Grabbe, Contact electrification induced by monolayer modification of a surface and relation to acid–base interactions, Nature 366 (6454) (1993) 442–443.
[24] K.M. Forward, D.J. Lacks, R.M. Sankaran, Triboelectric charging of granular insulator mixtures due solely to particle−particle interactions, Ind. Eng. Chem. Res. 48 (5) (2009) 2309–2314.
[25] H. Zhao, G.S.P. Castle, I.I. Inculet, A.G. Bailey, Bipolar charging of poly-disperse polymer powders in fluidized beds, IEEE Trans. Ind. Appl. 39 (3) (2003) 612–618.
[26] R.K. Dwari, S.K. Mohanta, B. Rout, R.K. Soni, P.S.R. Reddy, B.K. Mishra, Studies on the effect of electrode plate position and feed temperature on the tribo-electrostatic separation of high ash Indian coking coal, Adv. Powder Technol. 26 (1) (2015) 31–41.
[27] S.K. Mohanta, B. Rout, R.K. Dwari, P.S.R. Reddy, B.K. Mishra, Tribo-electrostatic separation of high ash coking coal washery rejects: Effect of moisture on separation efficiency, Powder Technol. 294 (2016) 292–300.
[28] S. Trigwell, K.B. Tennal, M.K. Mazumder, D.A. Lindquist, Precombustion cleaning of coal by triboelectric separation of minerals, Part. Sci. Technol. 21 (4) (2003) 353–364.
[29] G. Rowley, Quantifying electrostatic interactions in pharmaceutical solid systems, Int. J. Pharm. 227 (1–2) (2001) 47–55.
[30] H. Watanabe, M. Ghadiri, T. Matsuyama, H. Maruyama, S. Matsusaka, M. Ghadiri, T. Matsuyama, Y.L. Ding, K.G. Pitt, H. Maruyama, S. Matsusaka, H. Masuda (Keine Angabe), Triboelectrification of pharmaceutical powders by particle impact, Int. J. Pharmaceut. 334 (1–2) (2007) 149–155.

[31] J. Wong, P.C.L. Kwok, H.-K. Chan, Electrostatics in pharmaceutical solids, Chem. Eng. Sci. 125 (2015) 225–237.
[32] S. Naik, S. Sarkar, B. Hancock, M. Rowland, Y. Abramov, W. Yu, B. Chaudhuri, An experimental and numerical modeling study of tribocharging in pharmaceutical granular mixtures, Powder Technol. 297 (2016) 211–219.
[33] L. Calin, L. Caliap, V. Neamtu, R. Morar, A. Iuga, A. Samuila, L. Dascalescu, Tribocharging of granular plastic mixtures in view of electrostatic separation, IEEE Trans. Ind. Appl. 44 (4) (2008) 1045–1051.
[34] C.-H. Park, H.-S. Jeon, H.-S. Yu, O.-H. Han, J.-K. Park, Application of electrostatic separation to the recycling of plastic wastes: separation of PVC, PET, and ABS, Environ. Sci. Technol. 42 (1) (2008) 249–255.
[35] G. Wu, J. Li, Z. Xu, Triboelectrostatic separation for granular plastic waste recycling: a review, Waste Manage. (New York, N.Y.) 33 (3) (2013) pp. 585–597.
[36] Z. Chen, F. Liu, L. Wang, Y. Li, R. Wang, Z. Chen, Tribocharging properties of wheat bran fragments in air–solid pipe flow, Food Res. Int. 62 (2014) 262–271.
[37] Y. Hemery, X. Rouau, C. Dragan, M. Bilici, R. Beleca, L. Dascalescu, Electrostatic properties of wheat bran and its constitutive layers: Influence of particle size, composition, and moisture content, J. Food Eng. 93 (1) (2009) 114–124.
[38] J. Wang, G. Suo, M. de Wit, R.M. Boom, M.A.I. Schutyser, Dietary fibre enrichment from defatted rice bran by dry fractionation, J. Food Eng. 186 (2016) 50–57.
[39] J. Wang, M. de Wit, R.M. Boom, M.A.I. Schutyser, Charging and separation behavior of gluten–starch mixtures assessed with a custom-built electrostatic separator, Sep. Purif. Technol. 152 (2015) 164–171.
[40] J. Wang, M. de Wit, M.A.I. Schutyser, R.M. Boom, Analysis of electrostatic powder charging for fractionation of foods, Innovative Food Sci. Emerg. Technol. 26 (2014) 360–365.
[41] S. Tabtabaei, M. Jafari, A.R. Rajabzadeh, R.L. Legge, Development and optimization of a triboelectrification bioseparation process for dry fractionation of legume flours, Sep. Purif. Technol. 163 (2016) 48–58.
[42] S. Tabtabaei, M. Jafari, A.R. Rajabzadeh, R.L. Legge, Solvent-free production of protein-enriched fractions from navy bean flour using a triboelectrification-based approach, J. Food Eng. 174 (2016) 21–28.
[43] J. Wang, J. Zhao, M. de Wit, R.M. Boom, M.A.I. Schutyser, Lupine protein enrichment by milling and electrostatic separation, Innovative Food Sci. Emerg. Technol. 33 (2016) 596–602.
[44] S. Tabtabaei, M. Vitelli, A.R. Rajabzadeh, R.L. Legge, Analysis of protein enrichment during single- and multi-stage tribo-electrostatic bioseparation processes for dry fractionation of legume flour, Sep. Purif. Technol. 176 (2017) 48–58.
[45] M.A.I. Schutyser, A.J. van der Goot, The potential of dry fractionation processes for sustainable plant protein production, Trends Food Sci. Technol. 22 (4) (2011) 154–164.
[46] B.A. Kwetkus, Particle Triboelectrifcation and it's use in the Electrostatic Separation Process, Part. Sci. Technol. 16 (1) (1998) 55–68.
[47] E.K. Asare, S. Jaiswal, J. Maley, M. Båga, R. Sammynaiken, B.G. Rossnagel, R.N. Chibbar, Barley grain constituents, starch composition, and structure affect starch in vitro enzymatic hydrolysis, J. Agric. Food Chem. 59 (9) (2011) 4743–4754.
[48] B.V. McCleary, V. Solah, T.S. Gibson, Quantitative measurement of total starch in cereal flours and products, J. Cereal Sci. 20 (1) (1994) 51–58.
[49] E. Scholz, Karl-Fischer-Titration: Methoden zur Wasserbestimmung, Springer, Berlin, Heidelberg, 1984.
[50] H. Masuda, Dry dispersion of fine particles in gaseous phase, Adv. Powder Technol. 20 (2) (2009) 113–122.
[51] H. Edelhoch, Spectroscopic determination of tryptophan and tyrosine in proteins, Biochemistry 6 (7) (1967) 1948–1954.
[52] K. Avila, D. Moxey, A. de Lozar, M. Avila, D. Barkley, B. Hof, The onset of turbulence in pipe flow, Science (New York, N.Y.) 333 (6039) (2011) 192–196.
[53] P.M. Ireland, Triboelectrification of particulate flows on surfaces: Part I — Experiments, Powder Technol. 198 (2) (2010) 189–198.

2.2. Paper II: Effect of particle-wall interaction on triboelectric separation of fine particles in a turbulent flow (Landauer et al., 2019a)

Brief introduction

The influence of particle-wall interaction is examined in this paper. Particle-particle and particle-wall interactions occur if particles are conveyed trough a tube. According to different studies (cf. 1.2.4 and 1.2.6), particle-wall interaction is suggested to be the driving force of triboelectric charging of powder mixtures. Thus, the charging section consisting of Venturi nozzle and charging tube are made of different plastics (PTFE, PVC, POM, PE, PMMA). Moreover, to avoid particle-wall interaction, a boundary-layer control setup consisting of a porous tube is used. The boundary-layer control setup enables to influence the thickness of the boundary layer, and thus the flow conditions. To adjust different boundary-layer thicknesses, the perpendicular flow rate is set to 2.5, 5.0, and 10.0 % of the main flow ($3\,m^3\,h^{-1}$). Computational fluid dynamic (CFD) simulation is used to visualise the flow profile within the charging section for all different setups and to evaluate the possibility of particle-wall interactions. Based on the simulation results, collision numbers are calculated for all experimentally investigated setups (Saffman and Turner, 1956).

Study findings

The use of different wall materials results in no significant differences in selectivity and efficiency of triboelectric separation. Neither an increase nor a decrease of separation properties is found according to the triboelectric series. However, separation efficiency and selectivity slightly decreased when the boundary-layer-control setup is used compared to the plain wall setup. A variation in the perpendicular flow rate has no influence on separation properties. The flow profiles of the boundary-layer-control setup show an increase in the thickness of the laminar sublayer. Thus, particle-wall interactions can be neglected. Particle-collision numbers are calculated from the CFD simulation results to examine the differences between plain wall and boundary-layer-control setup. The boundary-layer scenario with the lowest perpendicular flow rate (2.5 %) shows a slightly lower contact number compared with the plain wall scenario. A further increase in perpendicular flow rate results in a decrease in particle contact number, because boundary-layer-control decreases turbulence dissipation ε. However, by comparing separation properties and contact numbers of plain wall and boundary-layer-control setup, the slight decrease in contact number results in a larger decrease in separation properties, whereas the constant decrease in contact number due to the perpendicular flow rate has no influence on separation properties.

Conclusion

i Wall materials of the charging tube and its position in the empirical triboelectric series have no influence on the separation properties.

ii Correlation of separation properties and contact numbers show no clear dependency, but indicate an influence on triboelectric charging and separation.

iii The influence of particle-wall interactions cannot be excluded, but a major impact on triboelectric charging could be questioned.

Author contributions

Johann Landauer did the conception and design of the study. Johann Landauer and Felicitas Aigner carried out the experimental work. Johann Landauer wrote the manuscript. Michael Kuhn participated to the discussion of the results and to the writing. Petra Först supervised the study.

Advanced Powder Technology 30 (2019) 1099–1107

Contents lists available at ScienceDirect

Advanced Powder Technology

journal homepage: www.elsevier.com/locate/apt

Original Research Paper

Effect of particle-wall interaction on triboelectric separation of fine particles in a turbulent flow

Johann Landauer *, Felicitas Aigner, Michael Kuhn, Petra Foerst

Chair of Process System Engineering, TUM School of Life Sciences Weihenstephan, Technical University of Munich, Germany

ARTICLE INFO

Article history:
Received 21 November 2018
Received in revised form 24 January 2019
Accepted 4 March 2019
Available online 13 March 2019

Keywords:
Triboelectric separation
Particle-particle-interaction
Particle-wall-interaction
Different contact materials
Boundary-layer control

ABSTRACT

Triboelectric separation is an effective way to separate fine powders with particle sizes and densities in the same order of magnitude. Many relevant process variables influence the charging behaviour; however, the corresponding effects on the subsequent separation of particles remain unknown. To utilize triboelectric separation as a powerful tool for fine powder separation, process parameters such as the choice of contact wall materials in the charging region have to be investigated. We report for the first time the influence of the tube's wall material, in which particle charging took place, on triboelectric separation of fine protein-starch mixtures. Different electrically insulating materials along the triboelectric series were tested. No significant influence of the wall material on the separation selectivity and efficiency was found. In addition, particle-wall interaction was inhibited using an experimental setup which allows to control the flow boundary-layer by blowing out air through the tube wall. Also the results obtained by this novel setup showed no significant differences compared to the setup with particle-wall interactions. Additionally, CFD simulations were used to confirm the absence of particle-wall interactions in the boundary-layer control setup. A variation of the boundary-layer thickness leads to a constriction of the particle-containing flow region in the centre of the pipe. Experiments show that this compression of the particle flow zone results in no further increase in selectivity and efficiency of separation. Thus, particle-particle interaction is the prevalent triboelectric charging mechanism of fine powders charged in a turbulent flow regime.

© 2019 The Society of Powder Technology Japan. Published by Elsevier B.V. and The Society of Powder Technology Japan. All rights reserved.

1. Introduction

Contact and subsequent separation of surfaces leads to electrical charge transfer. This phenomenon is called contact charging or triboelectric charging. Triboelectric charging is one of the oldest but still poorly understood phenomena [1]. However, it is prevailing where particles are moved in a gaseous phase such as dust storms [2], volcanic eruptions [3,4], formation of planets [5], fluidized beds [6–8], pneumatic conveying [9,10], powder coating [11], etc. In most industrial applications, triboelectric charging is an undesirable effect as it leads to dust explosion hazards [12]. Surprisingly, triboelectric charging of a dry powder dispersed in a gaseous phase is a promising possibility to separate particles over a large size range from 1 μm to 1 cm due to their ability to charge triboelectrically. Triboelectric separation is predominantly applied to coarse bulk materials larger than 100 μm on lab scale. Nevertheless, the triboelectric effect also opens up new possibilities in the separation of finer powders. The decrease of particle size leads to an increase in specific surface area and thereby the probability of surface contact increases. Furthermore, finer particles have a higher charge to mass ratio, thus separation at lower electric field strengths is feasible [13,14].

To use triboelectric separation as an industrial separation technology, a deeper understanding of the physics of triboelectric charging is necessary for target-orientated plant design. Three different mechanisms of charge transfer – electron, ion, and material transfer – may play a role while focusing on the contact of insulating materials. First, the electron transfer mechanism cannot occur theoretically in insulators due to the large band gab. However, real insulators have defects or 'trap' states in the band gap and electrons can move to lower non-equilibrium states [15]. These non-equilibrium electrons show a high reactivity in redox-reactions [16–18]. Secondly, materials with strongly-bound ions at the surface are balanced with loosely bound counterions. If

* Corresponding author at: Chair of Process Systems Engineering, Gregor-Mendel-Straße 4, 85354 Freising, Germany.
E-mail address: johann.landauer@tum.de (J. Landauer).

https://doi.org/10.1016/j.apt.2019.03.006
0921-8831/© 2019 The Society of Powder Technology Japan. Published by Elsevier B.V. and The Society of Powder Technology Japan. All rights reserved.

contact between these surfaces occurs, loosely bound ions can be transferred and a net charge may appear for each surface [19]. In this case, the humidity at the surface plays a major role [20]. Thirdly, material transfer in form of nanoscale particles can lead to charged surfaces after contact. This material transfer is driven by the inhomogeneous surface at the nano/atomic scale [21,22]. Hence, the incidence of various charging mechanisms reflects that different material characteristics, their combination, and various external factors like humidity influence triboelectric charging [23,24]. The derived physical understanding points up the different behaviour of conductive and insulating materials. To prevent an intermingling of different triboelectric charging mechanisms, only triboelectric charging between insulating material is investigated in this study. The chosen insulating materials are readily available plastic materials with a high potential for an industrial application.

In both cases, and even if particles with identical material collide, bipolar charging will occur. Thus, simple measurement of the particle's net charge does not help in assessing the influence of particle-particle and particle-wall interaction on triboelectric separation. The influence of different parameters on triboelectric charging like conveying techniques such as sliding, bouncing, and fluidisation [25–27], powders of different plastics and different organic materials [28,29], and different particle sizes [30,31] were investigated. With regard to the indeterminate charging mechanism, the monitored influencing factors during triboelectric charging and subsequent separation for insulating organic powders in a turbulent flow regime must be narrowed down to unlock potential fields of application. The wall material can be ordered along the triboelectric series [32,33], which provides only empirical values for the already investigated material combinations. Thus, separation characteristics of binary powder mixtures should be different for varying material combinations, which might result in different amounts of net charge provided that the triboelectric series is the suitable prediction model. However, the general validity of the triboelectric series was already questioned [34,35]. Therefore, two hypotheses that are widely assumed in the literature are explicitly tested in this study:

H1. The tube material has an influence on the charging properties and, thus, on the separation characteristics.

H2. Particle-wall interaction plays an important role in particle charging.

2. Materials and methods

2.1. Materials

Whey protein isolate and barley starch were purchased from Davisco Foods International, USA, and Altia, Finnland, respectively. Whey protein isolate has a protein content of 97.6 wt% dry matter. Barley starch has a protein content below 0.5 wt% and a starch content of 97 wt% dry matter.

To get a narrow particle size distribution, barley starch was classified with a wheel classifier ATP 50, Hosokawa Alpine, Germany at a deflection wheel speed of 10,000 rpm, a mass flow rate of 4.3 kg/h and an air flow rate of 58 kg/h. Whey protein was pre-ground with the same conditions as reported before [14].

Plastics for constructing different charging tubes were purchased from Sahlberg, Germany (Polytetrafluoroethylene, PTFE; Polymethylmethacrylate, PMMA; Polyvinylchloride, PVC; Polyoxymethylene, POM) and Reichelt Chemietechnik, Germany (Polyethylene, PE and porous Polyethylene tube).

2.2. Method

2.2.1. Experimental setup

Fig. 1 shows the experimental setup (modified version of reported setup [14]) consisting of a changeable charging section and a rectangular separation chamber. In the separation chamber the particles adhere on the surfaces of the electrodes according their charge. The fundamental parts of the charging section are a Venturi nozzle to disperse the powder and the charging tube with a diameter of 10 mm and a length of 230 mm. The setup enables the use of different wall materials in the charging section. In the present study, five different insulating materials PTFE, PVC, PMMA, POM, and PE were used. In order to disperse and accelerate the particles, a gas flow rate of 3 m^3/h was chosen. In an additional set of experiments, the tube in the charging section was replaced by a porous PE tube (BLC). An air stream through the porous tube's walls (boundary-layer blowing flow rate) enables boundary-layer control in the charging tube. Different proportions (2.5%, 5%, and 10%) of the total gas flow were radially blowed into the charging tube to keep the particles away from the wall and thus to inhibit particle-wall interactions. The parallel-plate capacitor in the rectangular separation chamber (46 mm × 52 mm × 400 mm) is operated with an electric field strength of 109 V/m. Binary mixtures of protein-starch with protein contents of 15 wt% were used.

2.2.2. Analysis of protein content

The protein content of the separated powders was measured as described before [14]. To evaluate the protein separation efficiency (PSE) indicating the yield of protein depending on the quotient protein purity on the electrode i, $\beta_{i,}$ and the initial protein content β_p is weighted with the and the mass yield w_i (1). The mass of the separated powders was determined by weighing the removed electrodes, thus minimizing the loss of material through further processing steps. Thus, the PSE is equivalent to the quotient of mass of protein on the electrode $m_{i,p}$ to the initial protein mass m_p.

$$PSE_i = \frac{\beta_i}{\beta_P} w_i = \frac{m_{i,p}}{m_p} \tag{1}$$

2.2.3. Particle size analysis

Particle size distributions of the used powders were determined using the laser diffraction spectrometer HELOS, Sympatec, Germany, with the wet dispersing unit CUVETTE. The powder is dispersed in pure ethanol.

2.2.4. Statistics

Mean value was calculated from the results of three independent experiments (n = 3). Error bars indicate the confidence interval using Student's t-test at a significance level $\alpha = 0.05$. Variance of PSE was calculated applying error propagation.

2.2.5. Simulation setup

To describe the differences in flow properties between the normal and the boundary-layer control experimental setup, a CFD simulation was implemented using ANSYS Fluent software (version: 17.0, supplier: Ansys, Inc., Canonsburg, USA). A tetrahedral mesh with a boundary-layer and a hexagonal mesh was used. A standard k-ε turbulence model was applied to simulate the turbulent flow. The Brinkman approach was used to model the perpendicular flow through the porous tube. The mean porosity of the porous tube employed in this study was determined using an X-ray microtomography system (type: XCT-1600HR, supplier: Matrix Technologies, Feldkirchen, Germany) and the image was analysed by Mavi (version: 1.4.1, supplier: Fraunhofer ITWM, Germany). To reduce calculation time a charging setup was symmetrically

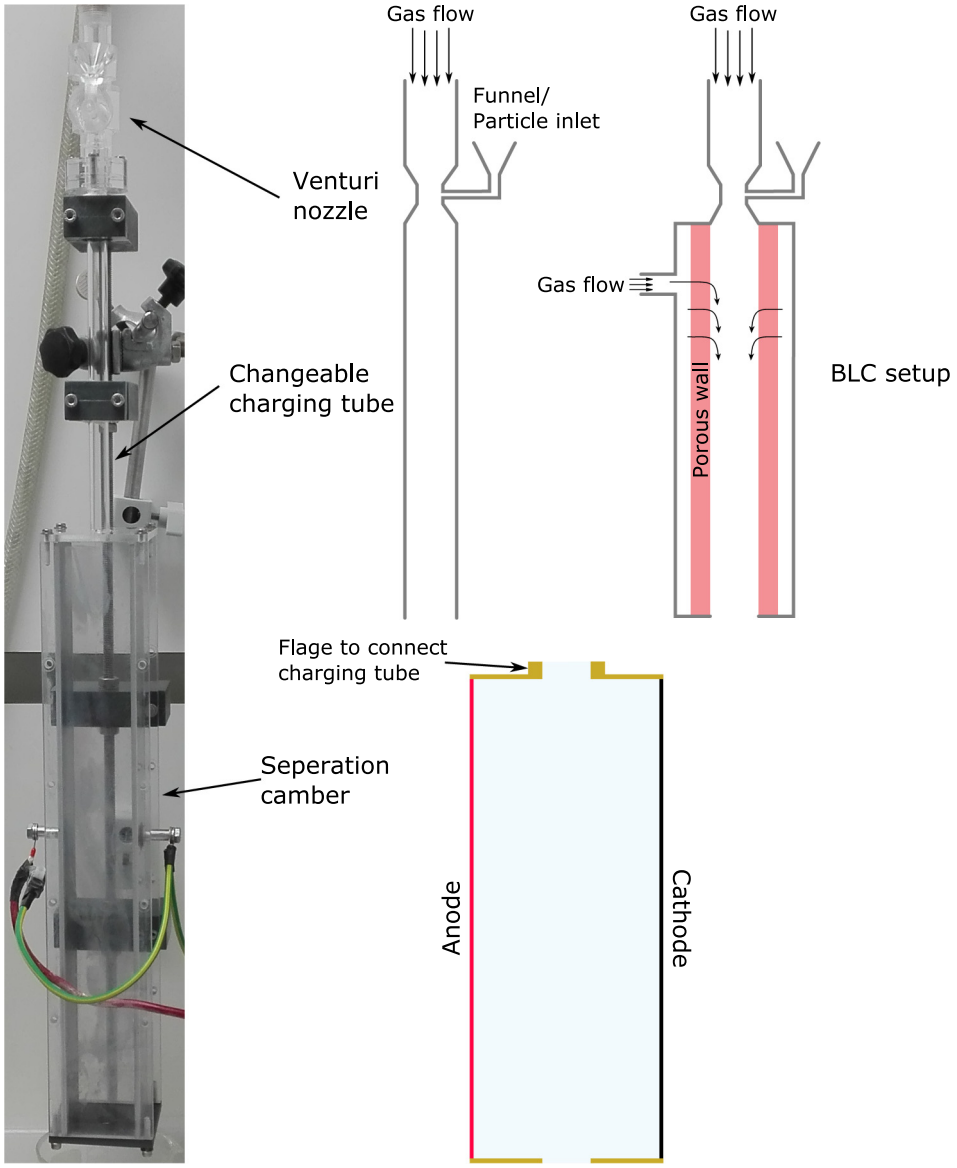

Fig. 1. Photograph (left) and schematic (right) of the experimental setup with charging section and separation chamber. The charging section consists of a funnel placed on the narrowing of a Venturi nozzle and a charging tube. The whole charging section is changeable to enable the use of different wall materials and boundary layer control (BLC).

divided and one half of was simulated using a symmetric boundary condition.

2.2.6. Particle interaction

To gain insight into particle-particle interaction within the charging tube, mean particle concentration $\bar{n}$, residence time t_r, and a collision kernel $\dot{\mathcal{N}}_c$ were calculated using experimental and simulation data. The mean particle concentration $\bar{n}$ was calculated by Eq. (2) as a quotient of number of particles N_p and gas volume $\Omega = \dot{V} t_{exp}$, with the volume flow rate and the test time of each experiment t_{exp}. The number of particles N_p is the true powder volume V_{pow} divided by the average spherical particle diameter $\bar{x}_3$, as shown in Eq. (3).

$$\bar{n} = \frac{N_p}{\Omega}, \tag{2}$$

$$N_p = \frac{6 V_{pow}}{\bar{x}_3^{\,3} \pi}. \tag{3}$$

The collision kernel Γ was estimated using the classical expression of Saffman and Turner [36,37]:

$$\Gamma = 1.294\, \bar{x}_3^{\,3} \left(\frac{\bar{\epsilon}}{\nu}\right)^{\frac{1}{2}}, \tag{4}$$

where $\bar{\epsilon}$ is the mean dissipation rate of turbulence energy and ν is the kinematic viscosity. $\left(\frac{\bar{\epsilon}}{\nu}\right)^{\frac{1}{2}}$ is the inverse of the Kolmogorov time scale. The number of particle-particle collision per unit volume in turbulent flow was modelled by the collision kernel $\dot{\mathcal{N}}_c$:

$$\dot{\mathcal{N}}_c = \Gamma \frac{\bar{n}^2}{2}. \tag{5}$$

Mean residence time of a particle in the charging tube $\bar{t}_r$ was estimated by the mean of velocity $\bar{v}$ of the charging tube for the plain wall setup. For boundary-layer control, the mean velocity was calculated using only the centre part of the velocity field where the majority of particles is expected, assuming particles stay in the main flow starting at the end of the charging setup:

$$\bar{t}_r = \frac{l_t}{\bar{v}}, \tag{6}$$

with the length of the charging tube l_t. Furthermore, $\bar{N}_n$ is the mean number of collisions per unit volume:

$$\bar{N}_n = \dot{\mathcal{N}}_c t_r. \tag{7}$$

3. Results

3.1. Particle size distributions of native and separated powders

Particle size distributions (PSDs) of the native powders and the prepared powder mixtures are shown in Fig. 2 (left). The particle size distribution of protein is monomodal with a mode at 1 μm and a maximum particle size of 20 μm. Starch has a bimodal particle size distribution with peaks at 1 and 20 μm. Both distributions are superposed in a wide range and exhibit the same peak particle size at 1 μm. After preparing the mixture, the bimodal shape of the PSD of starch is no longer pronounced. Fig. 2 (right) shows the particle size distribution of separated powder remaining on the cathode and anode, respectively. Particles separated on the cathode are smaller than on the anode, recognizable by the elevated peak at 1 μm and the lower amount of particles larger than 10 μm. The high peak at 1 μm might indicate a high protein concentration on the cathode. In contrast, larger particles on the anode indicate a higher amount of starch particles. This can be confirmed by the analysis of the chemical powder composition shown in Figs. 3 and 5.

3.2. Influence of different wall materials

3.2.1. Experiments with different wall materials

Fig. 3 shows the protein content of the separated powder on the cathode and the anode after passing through different charging tubes constructed from different insulating materials. The contact materials in the graph are arranged in ascending order of the triboelectric series starting with PTFE on the negative end [32] and ending with PMMA at the positive end. This order was chosen assuming the prediction model of the triboelectric series. The separation in the electric field reveals an insignificant influence of the charging tube materials along the triboelectric series. Only POM and PVC show significant differences. The protein content on the anode is unaffected by the choice of the contact material for the chosen air flow conditions. The experiments show no influence and tendency of the different contact materials on the protein content on cathode and anode.

Fig. 4 shows the PSE for different contact materials. As expected, similar findings with regard to the protein content were made and no clear trend was observed. Experiments using the wall materials POM and PE have significant lower PSEs compared to the other tested insulators. To increase the PSE, the influence of the contact material in the charging tube is insignificant.

3.2.2. Boundary-layer control

The laminar boundary-layer in a turbulent pipe flow was manipulated by boundary-layer blowing (larger boundary-layer) or suction (smaller boundary-layer) [38; pp. 291–295]. Fig. 5 shows the protein content on the cathode and the anode for three

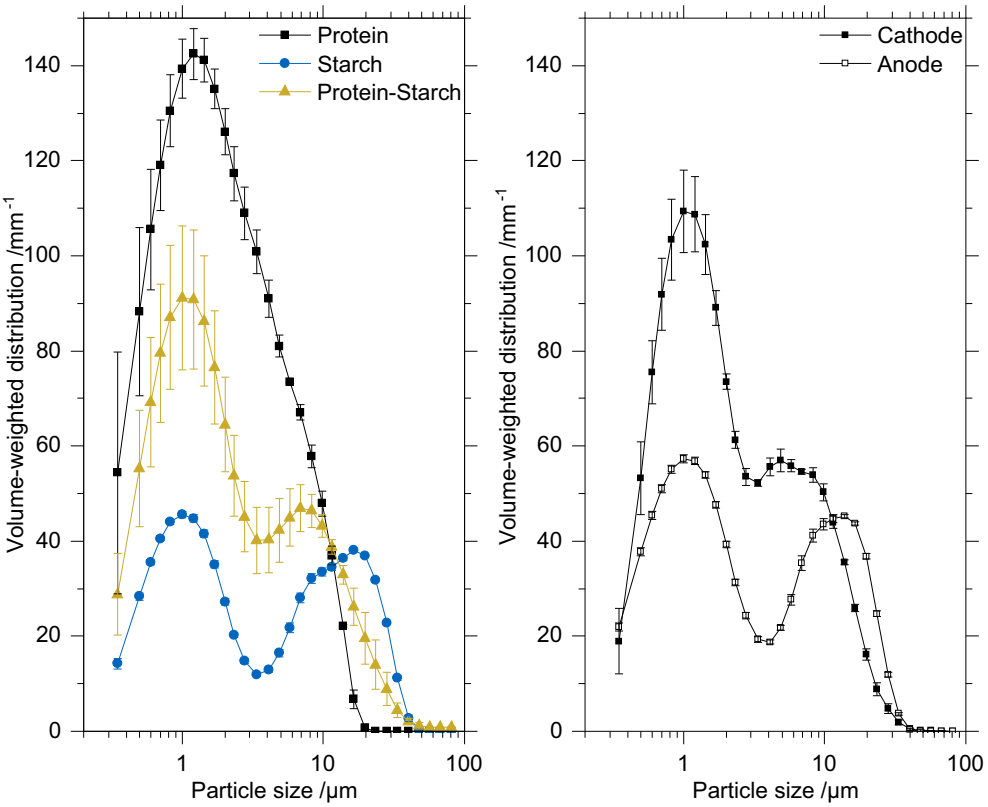

Fig. 2. Volume-weighted particle size distribution of native powder and powder mixtures (left) as well as separated powders on the electrodes (right).

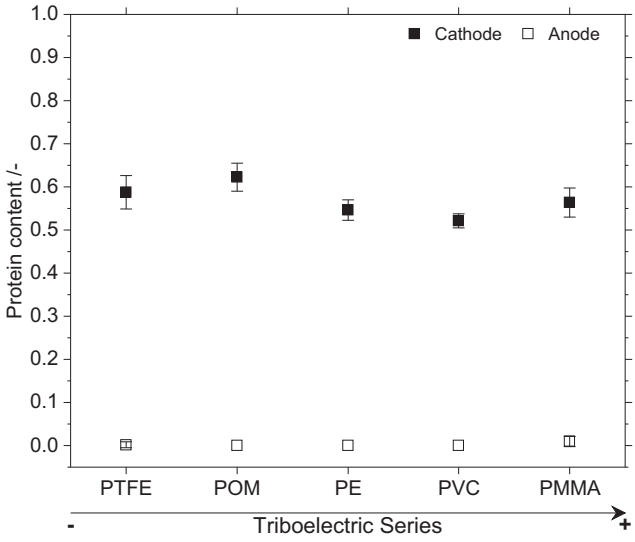

Fig. 3. Protein content of powder mixtures remaining on the cathode and anode after separation in the electric field. PTFE, POM, PE, PVC, and PMMA were used as charging tube materials. The experiments show no differences in protein content on the cathode and anode for all used charging tubes.

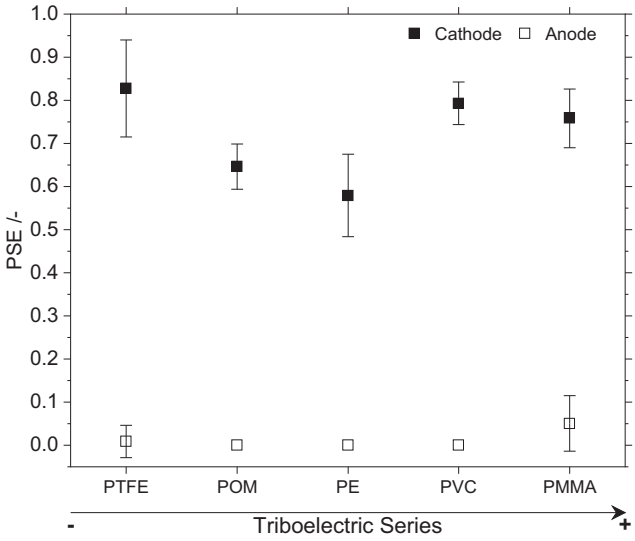

Fig. 4. Protein separation efficiency (PSE) for five different charging tube materials. On the cathode and anode, no significant differences are observed.

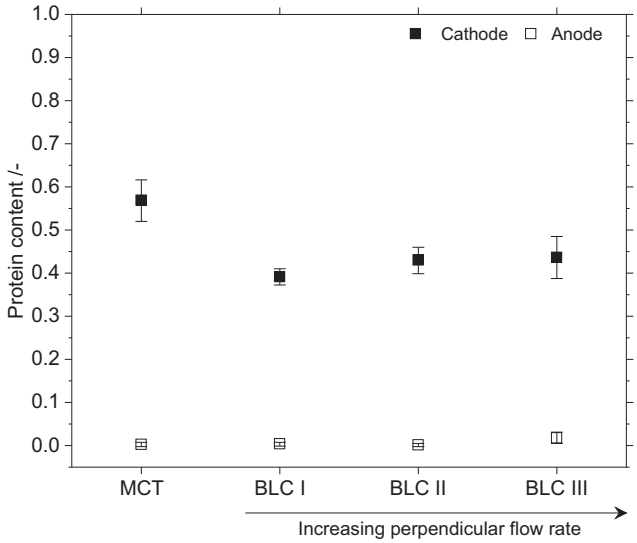

Fig. 5. Protein content on cathode and anode at different boundary layer control settings (BLC) compared to MCT (mean of charging tube experiments).

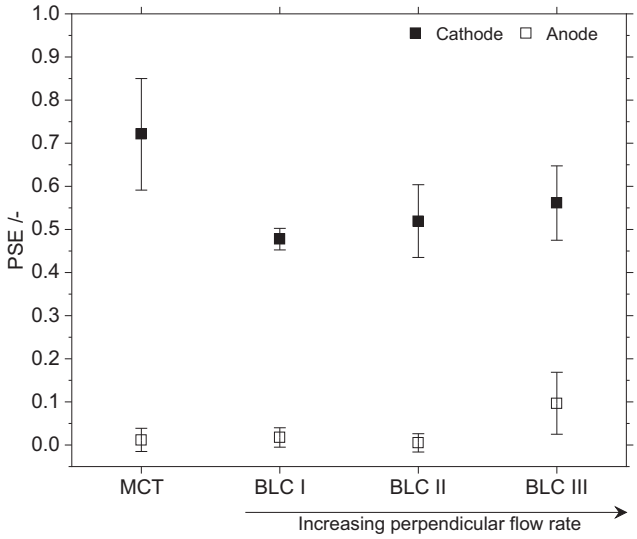

Fig. 6. PSE of boundary layer controlled (BLC) experiments compared to the MCT on cathode and anode.

different boundary-layer thicknesses and the mean of all experiments with different charging tube materials without boundary-layer manipulation (Fig. 3). The perpendicular volumetric flow rate was adjusted to 2.5%, 5%, and 10% of the total flow rate of 3 m^3/h, denoted as boundary-layer control (BLC) I, BLC II, and BLC III, respectively. Boundary-layer blowing leads to a significant decrease of the protein content on the cathode compared to the averaged protein content of all contact materials without boundary-layer control (mean of charging tube experiments, MCT). No differences in the protein content between boundary-layer control and the MCT was measured on the anode. The influence of perpendicular flow rate on the protein content is not significant for both cathode and anode.

In addition, the PSE (Fig. 6) shows a similar behaviour with regard to the protein content. There is a significant decrease in PSE between MCT and BLC I. A variation in the boundary-layer blowing leads to no change in PSE. No significant differences between MCT and BLC II and III is observed, because the variation of the PSE is very high. In contrast, the PSE on the anode remains unaffected.

3.3. CFD simulation

Fig. 7 shows the results of the CFD simulation of the charging tube for different setups, including a plain wall setup and a porous wall with BLC. Gas flow is indicated by streamlines, starting at the gas-inlet (a) and the particle-inlet (b). In the plain wall setup there is a turbulent flow regime within the whole charging and dispersing setup. Streamlines starting at the powder inlet (b) are located in the centre of the tube (top view) and are pulled apart in the upper half of the tube (side view). Several streamlines are very close to the wall. It can be assumed that they follow the streamlines as the particles are very small [39]. Thus, particle-wall interaction is likely to occur. Streamlines starting at the gas-inlet form a turbulent pipe flow with a vortex after the Venturi nozzle.

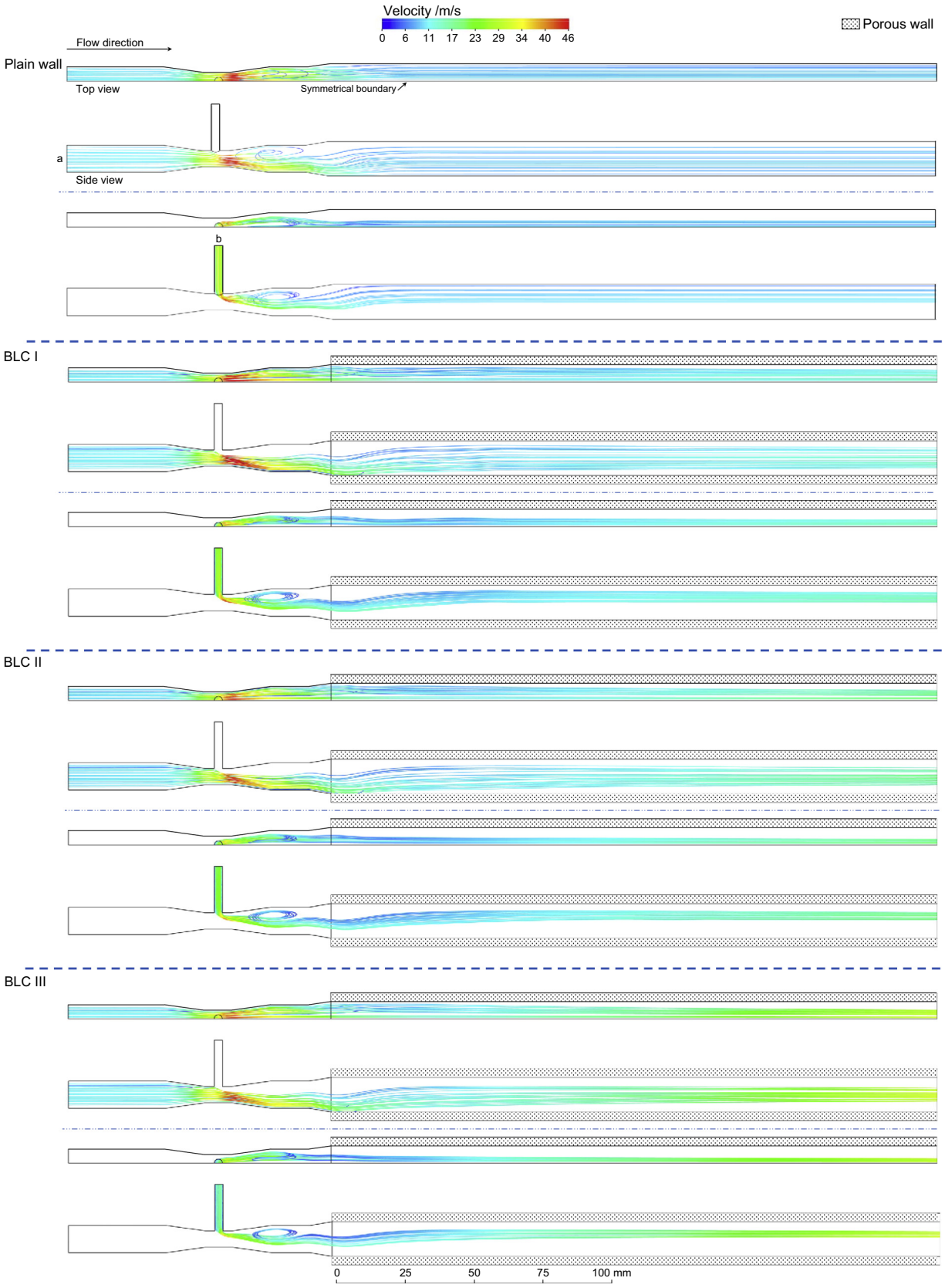

Fig. 7. CFD simulation of plain and boundary layer controlled (BLC) charging setup in top view and side view. Simulation was performed using a symmetrical boundary to divide the charging setup. Streamlines starting from the gas-inlet (a) and the particle-inlet (b) are used to indicate the flow conditions in the charging tube. BLC is shown to be a suitable way to exclude particle-wall interaction and therefore inhibit charging by particle-wall contact.

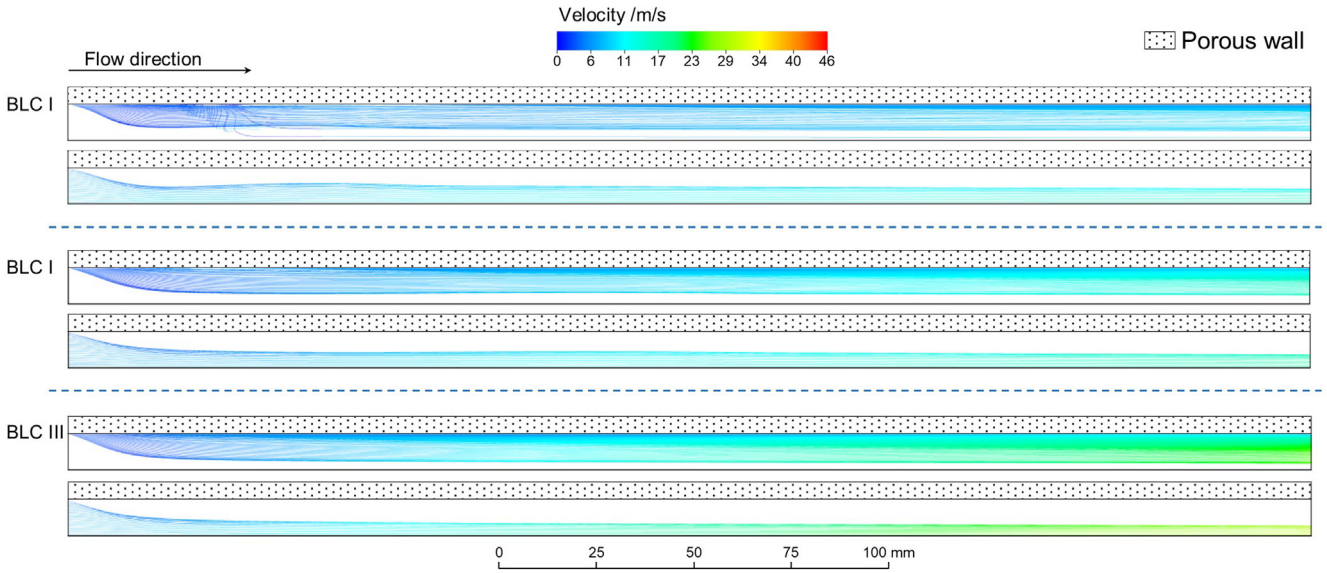

Fig. 8. Streamlines starting at a horizontal plane in the centre of the tube indicate gas flow in the boundary layer controlled section with flow through the porous wall (top) and streamlines of the main flow (bottom). Streamline profiles show opposite profiles of main and perpendicular flow. An increase in perpendicular velocity (boundary layer blowing flow rate) results in an increase in thickness and velocity of the sublayer and, thus, to a compression of the streamlines in the centre of the tube.

The boundary-layer control setup (BLC) shows similar flow characteristics for all perpendicular flow rates. Streamlines starting at the gas-inlet form a turbulent flow throughout the whole investigated setup. The streamlines are compressed towards the tube centre in comparison to the plain setup with an impermeable tube wall. Streamlines starting at the particle-inlet show the same compression pattern and the spacing to the wall is easy to recognize. Hence, particle-wall interaction of the dispersed particles is inhibited. An increase in perpendicular flow rate (boundary-layer blowing flow rate) results in a decrease of gas velocity in the narrowing of the nozzle. Furthermore, streamlines starting at inlet (a) and (b) converge due to an increase in perpendicular flow rate. The gas flow is accelerated along the tube length. CFD simulation of the separation chamber showed similar flow profiles for plain wall and BLC setup. Thus, there are uniform separation conditions for the charged particles in the separation chamber.

To visualise BLC, Fig. 8 shows streamlines starting in a plane perpendicular to the porous wall and at the beginning of the porous tube. The boundary-layer thickness is increasing with increasing perpendicular flow rate. As expected, the boundary-layer thickness also increases along the tube length. A higher perpendicular flow rate leads to an increase in velocity both in the boundary-layer and the main flow. Simultaneously, streamlines of the main flow in the centre of the tube are more compressed with increasing perpendicular flow rate. In conclusion, the BLC setup enables the introduction of a sublayer without particles in order to prevent any particle-wall interaction.

To further elucidate particle-particle interaction for all four investigated flow profiles, the introduced parameters were evaluated; their numerical values are summarized in Table. 1. As visualised in Fig. 8, by increasing the perpendicular flow rate, the velocity of the main flow is increasing. Thus, assuming particles are only in the main flow, the residence time $\bar{t}_r$ of the particles is decreasing. Furthermore, particle concentration $\bar{n}$ is increasing with an increasing perpendicular flow rate, because the effective volume in which particles are dispersed is decreasing. The collision rate per unit volume $\dot{\mathcal{N}}_c$ is also decreasing by narrowing the zone where particles flow. The significant decrease in collision rate of BLC III leads to no decrease in protein content and PSE.

4. Discussion

It has been shown that it is possible to separate organic powders containing different amounts of protein and starch by the triboelectric effect [14]. Since the particle size distributions of protein and starch overlap almost over the whole size range, the decisive separation feature is not the particle size. Particle size distributions on the cathode and anode are similar to the PSDs of native protein and starch powder. This underpins the independence of the triboelectric separation mechanism from the particle size for particles in a size range between 0.1 and 40 μm and lays the focus on the chemical composition and further particle properties.

Table 1
Summary of particle-particle interaction parameters for plain wall and boundary-layer control setup.

	Plain wall	BLC I	BLC II	BLC III
Mean velocity $\bar{v}$ /m/s	10.83	11.62	13.62	17.21
Mean residence time $\bar{t}_r$ /ms	21	20	17	13
Particle concentration $\bar{n}$ /1/m^3	1.02×10^9	1.04×10^9	1.07×10^9	1.13×10^9
Mean dissipation rate of turbulence energy $\bar{\epsilon}$ /m^2/s^3	3.53×10^4	3.11×10^4	2.55×10^4	1.85×10^3
Collision kernel Γ /m^3/s	1.77×10^{-10}	1.66×10^{-10}	1.50×10^{-10}	4.05×10^{-11}
Collision rate $\dot{\mathcal{N}}$ /1/(s m^3)	9.13×10^7	9.02×10^7	9.61×10^7	2.58×10^7
Collison number $\bar{N}_n$ /1/m^3	1.94×10^6	1.79×10^6	1.45×10^6	3.45×10^5

The process of triboelectric separation is split into a charging and a separation part. It is necessary to increase the triboelectric charging of the particles to improve triboelectric separation. In order to find a suitable material combination between protein, starch, and the charging tube, different material combinations were tested. Hence, five different plastic tubes along the triboelectric series were chosen. No significant differences in protein separation efficiency between the used wall materials were observed. Assuming that a large number of particle-wall collisions occur and the triboelectric series of the contact material should have an influence on triboelectric charging, there should be a continuous decrease of protein content from PTFE to PMMA along the triboelectric series. This decrease should be also reflected in the corresponding distance in the triboelectric series between, e.g., protein and PTFE as well as protein and PMMA, because a lower charging of the protein particles might be assumed. However, the PSE shows neither a continuous decrease along the triboelectric series nor any other clear tendency (only PE and POM differ significantly from PTFE, PVC, and PMMA). Due to the fact that no trend in selectivity and efficiency along the triboelectric series was found, it is concluded that the triboelectric series do not describe the manifold influence parameters on triboelectric separation like humidity [24,40], elastic moduli [21], surface morphology [34] or surface ions [19]. Thus, H1 (contact material has an influence on particle charging and subsequent separation) cannot be supported by the results. These findings are in contrast with several studies addressing the influence of the wall materials in triboelectric charging [41–44]. Particles sliding down a gutter might have a higher interaction rate compared to particles blown though a tube in a turbulent flow regime [26,45]. This might reduce the influence of the wall material on particle charging with the presented setup. Furthermore, different gas flow rates in the charging tube have no influence on the separation of starch and protein [14]. It must be noted that the triboelectric series is an empirical order of materials, only tested for binary contact. Thus, the universality of the triboelectric series can be questioned [34,35]. It might be unimportant what material the charging tube is made of in order to separate fine powders in a turbulent flow regime.

The findings of this study encourage the focus on the influence of particle-particle interaction. To investigate the influence of the particle-particle interaction without particle-wall interaction, a boundary-layer control setup was implemented. CFD simulations of the experimental setup show no particle-wall interaction, as indicated by streamlines. The separation selectivity (protein content) reveals significant differences compared to mean of charging tubes (MCT) but same findings in all BLC conditions. The PSE only demonstrates significant differences between BLC I and MCT and therefore underline the subordinate role of particle-wall interaction. Thus, particle-particle interaction is suggested to be the main charging mechanism in a turbulent flow regime and H2 can be rejected. Although particle-wall interaction has an influence and might play a subordinate role. Indeed, CFD simulations show that streamlines are very close to the wall, but they are most concentrated in the centre of the tube. This might underline the subordinate role of particle-wall interaction without boundary-layer control.

Furthermore, the decrease in both protein content and PSE might be the consequence of the changed particle-particle interaction parameters (Table. 1). The higher particle concentration in the narrowed main flow for BLC experiments cannot balance the shorter residence time of the particles induced by the perpendicular flow leading to a decrease in the collision rate which is linked to a decrease in the collision number. Surprisingly, the increase of flow through the wall has no influence on the charging and subsequent separation of the used powder even though the area, where particles flow, is narrowed. Thus, the decrease in the collision rate could not describe the whole charging process, because the difference between plain wall and BLC I setup shows only slight differences. However, the collision number might show that the collision frequency is sufficient for triboelectric charging. Further studies using CFD-DEM simulations might be necessary to investigate this interaction.

5. Conclusion

Triboelectric separation of fine organic powders below 40 μm at turbulent flow conditions was investigated in relation to different wall materials of an insulating charging tube. Furthermore, charging with only particle-particle interaction was applied. First, the use of different wall materials resulted in no significant differences in selectivity and efficiency in triboelectric separation. In a further step, particle-wall interaction was inhibited and only particle–particle interaction enabled triboelectric particle charging. Slight differences in separation selectivity were determined, implicating a subordinate role of particle-wall interactions. CFD simulation studies confirmed the exclusion of particle-wall interactions in case of the used BLC setup. A further increase in perpendicular flow rate leads to a compression of the area through which particles flow and caused no improvement in selectivity and efficiency. In summary, particle-particle interaction was found to be the principal charging mechanism for fine powders at turbulent flow conditions.

Acknowledgements

This research did not receive any specific grant from funding agencies in the public, commercial, or not-for-profit sectors. The authors would like to thank Stefan Schmideder for the help performing X-ray microtomography pictures, Christoph Metzger for the fruitful discussions, and Heiko Briesen for the possibility to carry out this study.

References

[1] P. Iversen, D.J. Lacks, A life of its own: the tenuous connection between Thales of Miletus and the study of electrostatic charging, J. Electrostat. 70 (2012) 309–311, https://doi.org/10.1016/j.elstat.2012.03.002.
[2] W.M. Farrell, Electric and magnetic signatures of dust devils from the 2000–2001 MATADOR desert tests, J. Geophys. Res. 109 (2004) 5427, https://doi.org/10.1029/2003JE002088.
[3] Y. Tanaka, T. Miura, T. Koyaguchi, Measurements of electric charge distribution in volcanic plumes at Sakurajima Volcano Japan, Bull. Volcanol. 64 (2002) 75–93, https://doi.org/10.1007/s00445-001-0182-1.
[4] J. Méndez Harper, J. Dufek, The effects of dynamics on the triboelectrification of volcanic ash, J. Geophys. Res. Atmos. 121 (2016) 8209–8228, https://doi.org/10.1002/2015JD024275.
[5] V. Lee, S.R. Waitukaitis, M.Z. Miskin, H.M. Jaeger, Direct observation of particle interactions and clustering in charged granular streams, Nat. Phys. 11 (2015) 733–737, https://doi.org/10.1038/nphys3396.
[6] A.G. Bailey, Electrostatic phenomena during powder handling, Powder Technol. 37 (1984) 71–85, https://doi.org/10.1016/0032-5910(84)80007-8.
[7] P. Mehrani, M. Murtomaa, D.J. Lacks, An overview of advances in understanding electrostatic charge buildup in gas-solid fluidized beds, J. Electrostat. 87 (2017) 64–78, https://doi.org/10.1016/j.elstat.2017.03.005.
[8] F. Fotovat, X.T. Bi, J.R. Grace, Electrostatics in gas-solid fluidized beds: a review, Chem. Eng. Sci. 173 (2017) 303–334, https://doi.org/10.1016/j.ces.2017.08.001.
[9] P. Bunchatheeravate, J. Curtis, Y. Fujii, S. Matsusaka, Prediction of particle charging in a dilute pneumatic conveying system, AChE J 59 (2013) 2308–2316, https://doi.org/10.1002/aic.14025.
[10] H. Grosshans, M.V. Papalexandris, Large Eddy simulation of triboelectric charging in pneumatic powder transport, Powder Technol. 301 (2016) 1008–1015, https://doi.org/10.1016/j.powtec.2016.07.031.
[11] W. Kleber, B. Makin, Triboelektric powder coating: a practical approach for industiral use, Part. Sci. Technol. 16 (1998) 43–53, https://doi.org/10.1080/02726359808906783.
[12] M. Glor, Ignition hazard due to static electricity in particulate processes, Powder Technol. 135–136 (2003) 223–233, https://doi.org/10.1016/j.powtec.2003.08.017.

[13] T. Matsuyama, H. Yamamoto, Maximum electrostatic charge of powder in pipe flow, Adv. Powder Technol. 21 (2010) 350–355, https://doi.org/10.1016/j.apt.2010.03.009.
[14] J. Landauer, P. Foerst, Triboelectric separation of a starch-protein mixture – impact of electric field strength and flow rate, Adv. Powder Technol. 29 (2018) 117–123, https://doi.org/10.1016/j.apt.2017.10.018.
[15] J. Lowell, W.S. Truscott, Triboelectrification of identical insulators. I. An experimental investigation, J. Phys. D Appl. Phys. 19 (1986) 1273–1280, https://doi.org/10.1088/0022-3727/19/7/017.
[16] C. Liu, A.J. Bard, Electrostatic electrochemistry at insulators, Nat. Mater. 7 (2008) 505–509, https://doi.org/10.1038/nmat2160.
[17] C.-Y. Liu, A.J. Bard, Chemical redox reactions induced by cryptoelectrons on a PMMA surface, J. Am. Chem. Soc. 131 (2009) 6397–6401, https://doi.org/10.1021/ja806785x.
[18] S. Piperno, H. Cohen, T. Bendikov, M. Lahav, I. Lubomirsky, The absence of redox reactions for palladium(II) and copper(II) on electrostatically charged Teflon: relevance to the concept of "cryptoelectrons", Angew. Chem. Int. Ed Engl. 50 (2011) 5654–5657, https://doi.org/10.1002/anie.201101203.
[19] L.S. McCarty, G.M. Whitesides, Electrostatic charging due to separation of ions at interfaces: contact electrification of ionic electrets, Angew. Chem. Int. Ed Engl. 47 (2008) 2188–2207, https://doi.org/10.1002/anie.200701812.
[20] T.R.D. Ducati, L.H. Simoes, F. Galembeck, Charge partitioning at gas-solid interfaces: humidity causes electricity buildup on metals, Langmuir 26 (2010) 13763–13766, https://doi.org/10.1021/la102494k.
[21] H.T. Baytekin, B. Baytekin, J.T. Incorvati, B.A. Grzybowski, Material transfer and polarity reversal in contact charging, Angew. Chem. 124 (2012) 4927–4931, https://doi.org/10.1002/ange.201200057.
[22] H.T. Baytekin, A.Z. Patashinski, M. Branicki, B. Baytekin, S. Soh, B.A. Grzybowski, The mosaic of surface charge in contact electrification, Science 333 (2011) 308–312, https://doi.org/10.1126/science.1201512.
[23] J. Kolehmainen, P. Sippola, O. Raitanen, A. Ozel, C.M. Boyce, P. Saarenrinne, S. Sundaresan, Effect of humidity on triboelectric charging in a vertically vibrated granular bed: experiments and modeling, Chem. Eng. Sci. 173 (2017) 363–373, https://doi.org/10.1016/j.ces.2017.08.006.
[24] A. Schella, S. Herminghaus, M. Schröter, Influence of humidity on tribo-electric charging and segregation in shaken granular media, Soft Matter 13 (2017) 394–401, https://doi.org/10.1039/c6sm02041k.
[25] H. Masuda, S. Matsusaka, S. Akiba, H. Shimomura, Electrification of fine particles in gas-solids pipe flow [Translated]†, KONA 16 (1998) 216–222. https://doi.org/10.14356/kona.1998024.
[26] P.M. Ireland, Triboelectrification of particulate flows on surfaces: Part I — Experiments, Powder Technol. 198 (2010) 189–198, https://doi.org/10.1016/j.powtec.2009.11.017.
[27] K.M. Forward, D.J. Lacks, R.M. Sankaran, Triboelectric charging of granular insulator mixtures due solely to particle−particle interactions, Ind. Eng. Chem. Res. 48 (2009) 2309–2314, https://doi.org/10.1021/ie8004786.
[28] E. Németh, V. Albrecht, G. Schubert, F. Simon, Polymer tribo-electric charging: dependence on thermodynamic surface properties and relative humidity, J. Electrostat. 58 (2003) 3–16, https://doi.org/10.1016/S0304-3886(02)00137-7.
[29] J. Wang, G. Suo, M. de Wit, R.M. Boom, M.A.I. Schutyser, Dietary fibre enrichment from defatted rice bran by dry fractionation, J. Food Eng. 186 (2016) 50–57, https://doi.org/10.1016/j.jfoodeng.2016.04.012.
[30] D.J. Lacks, A. Levandovsky, Effect of particle size distribution on the polarity of triboelectric charging in granular insulator systems, J. Electrostat. 65 (2007) 107–112, https://doi.org/10.1016/j.elstat.2006.07.010.
[31] R. Mukherjee, V. Gupta, S. Naik, S. Sarkar, V. Sharma, P. Peri, B. Chaudhuri, Effects of particle size on the triboelectrification phenomenon in pharmaceutical excipients: experiments and multi-scale modeling, Asian J. Pharm. Sci. 11 (2016) 603–617, https://doi.org/10.1016/j.ajps.2016.04.006.
[32] A.F. Diaz, R.M. Felix-Navarro, A semi-quantitative tribo-electric series for polymeric materials: the influence of chemical structure and properties, J. Electrostat. 62 (2004) 277–290, https://doi.org/10.1016/j.elstat.2004.05.005.
[33] J. Lowell, A.C. Rose-Innes, Contact electrification, Adv. Phys. 29 (1980) 947–1023, https://doi.org/10.1080/00018738000101466.
[34] A.E. Wang, P.S. Gil, M. Holonga, Z. Yavuz, H.T. Baytekin, R.M. Sankaran, D.J. Lacks, Dependence of triboelectric charging behavior on material microstructure, Phys. Rev. Mater. 1 (2017), https://doi.org/10.1103/PhysRevMaterials. 1.035605.
[35] M.M. Apodaca, P.J. Wesson, K.J.M. Bishop, M.A. Ratner, B.A. Grzybowski, Contact electrification between identical materials, Angew. Chem. Int. Ed Engl. 49 (2010) 946–949, https://doi.org/10.1002/anie.200905281.
[36] P.G. Saffman, J.S. Turner, On the collision of drops in turbulent clouds, J. Fluid Mech. 1 (1956) 16, https://doi.org/10.1017/S0022112056000020.
[37] L.-P. Wang, A.S. Wexler, Y. Zhou, On the collision rate of small particles in isotropic turbulence. I. Zero-inertia case, Phys. Fluids 10 (1998) 266–276, https://doi.org/10.1063/1.869565.
[38] H. Schlichting, K. Gersten, Boundary-Layer Theory, Springer Berlin Heidelberg, Berlin, Heidelberg, 2017.
[39] J.A. Pita, S. Sundaresan, Developing flow of a gas-particle mixture in a vertical riser, AIChE J. 39 (1993) 541–552, https://doi.org/10.1002/aic.690390402.
[40] T. Shinbrot, M. Rutala, H. Herrmann, Surface contact charging, Phys. Rev. E 96 (2017) 16, https://doi.org/10.1103/PhysRevE.96.032912.
[41] Hiroaki Masuda, Shuji Matsusaka, Shinji Nagatani, Measurements of powder flow rate in gas-solids pipe flow based on the static electrification of particles, Adv. Powder Technol. 5 (3) (1994) 241–254, https://doi.org/10.1163/156855294X00320.
[42] H. Masuda, S. Matsusaka, H. Shimomura, Measurement of mass flow rate of polymer powder based on static electrification of particles, Adv. Powder Technol. 9 (1998) 169–179, https://doi.org/10.1016/S0921-8831(08)60585-3.
[43] S. Matsusaka, M. Oki, H. Masuda, Control of electrostatic charge on particles by impact charging, Adv. Powder Technol. 18 (2007) 229–244, https://doi.org/10.1163/156855207780208673.
[44] J. Pérez-Vaquero, M.A.S. Quintanilla, A. Castellanos, Electric charge limits on settled powders, J. Appl. Phys. 119 (2016) 223302, https://doi.org/10.1063/1.4953649.
[45] J. Wang, M. de Wit, R.M. Boom, M.A.I. Schutyser, Charging and separation behavior of gluten–starch mixtures assessed with a custom-built electrostatic separator, Sep. Purif. Technol. 152 (2015) 164–171, https://doi.org/10.1016/j.seppur.2015.08.025.

2.3. Paper III: Influence of particle contact number on triboelectric separation selectivity (Landauer and Foerst, 2019b)

Brief introduction

To separate starch and protein from different botanical origins using triboelectric separation, the initial powder consumption might influence the separation performance. Thus, the initial powder consumption of binary starch protein mixtures is varied and triboelectric separation experiments were carried out using the previously described setup (Landauer et al., 2019a). Since protein and starch have slightly different particle size distributions, the particle size distribution of the initial powder mixture containing 15, 30, and 45 wt. % protein is decreasing with increasing protein content. For all separation experiments, the same amount of powder (2.5 g) is used. Thus, the particle number is increasing by increasing the initial protein content. For the different initial protein contents the particle-particle interaction rates are calculated according to Saffman and Turner (1956).

Study findings

An increase in initial protein content from 15 to 45 wt. % results in an increase in separation selectivity from 60 to 80 wt. % for all investigated plain walls on the cathode. On the anode separation selectivity decreased slightly by increasing the initial protein content. The highest measured protein content is 10 wt. %. No clear tendency according to the empirical triboelectric series is determined. However, boundary-layer-control scenario in the charging tube shows for an initial protein content of 45 wt. % the same separation selectivity as the plain wall scenario. In addition, the increase in contact number of the particles, influenced by flow condition and particle numbers, leads to an increase in separation selectivity. The increase in separation selectivity seems to be linear in a contact number range of 1×10^8 to 5×10^8.

Conclusion

i An increase in initial protein content results in higher separation selectivity.

ii Particle-wall interaction has no influence on separation selectivity for higher initial protein contents.

iii Particle contact number decisively influences triboelectric separation and results in a linear increase in separation selectivity within the investigated range.

Author contributions

Johann Landauer did the conception and design of the study, the experimental work, and wrote the manuscript. Petra Foerst participated to the writing and supervised the work.

processes

MDPI

Article

Influence of Particle Contact Number on Triboelectric Separation Selectivity

Johann Landauer * and Petra Foerst

Chair of Process Systems Engineering, TUM School of Life Sciences Weihenstephan, Technical University of Munich, Gregor-Mendel-Straße 4, 85354 Freising, Germany; petra.foerst@tum.de

* Correspondence: johann.landauer@tum.de; Tel.: +49-8161-71-5172

Received: 22 August 2019; Accepted: 29 September 2019; Published: 9 October 2019

Abstract: Triboelectric separation is a promising technology to separate fine powders. To enable triboelectric separation for its application in industry, the impact of the process and product parameters must be examined. In this study, with regards to different wall materials in the charging step (PTFE, POM, PE, PVC, and PMMA), the influence of the powder composition of a binary starch-protein mixture with a protein content of 15 wt. %, 30 wt. % and 45 wt. % was studied. By increasing the protein content in the feed, the separation selectivity increased. No dependency of the empirical triboelectric series was determined for all powder compositions. The variation in the protein content of the initial powder and turbulent flow profiles results in a variation in the contact number of particles calculated. An increase in the contact number of particles leads to an increase in the protein content separated on the cathode, whereas the protein content on the anode is only slightly affected. These findings underpin the assumption that particle-particle interaction plays a decisive role in triboelectric charging of fine powders.

Keywords: triboelectric charging; triboelectric separation; particle-particle interaction; powder composition; contact number

1. Introduction

Triboelectric charging occurs when two surfaces come in contact and are then separated [1]. This phenomenon is called contact, surface or triboelectric charging [2,3]. While triboelectric charging is the most common expression, the subword "tribo" can be misleading as no friction is necessary to obtain charged surfaces [4]. Nevertheless, when the simplest triboelectric experiment with a balloon rubbed on hair is performed, both surfaces get charged. However, in this example, rubbing increases the number of contacts between balloon and hair and, thus, ensures sufficient contact between surfaces. This insight can be transferred to the triboelectric charging of dry powders. By dispersing powder in a gas stream high numbers of particle-particle and particle-wall collisions happen. This high interaction rate of dispersed and moved particles can be the manipulated variable for triboelectric separation of powders, since the mechanism of triboelectric charging is still unknown [5].

Triboelectric charging occurs in almost every system involving moving particles: in pneumatic conveying [6,7], fluidized beds [8], dry powder mixing [9], dust storms [10,11], or even during the formation of planets in the orbit [12] In most cases, the triboelectric charging of powders is undesirable. However, this effect can be employed as a novel separation tool for fine and dry powders [13–18]. The net amount of charge at the surface of one particle acts as a separation feature. Factors influencing triboelectric charging and separation are the chemical composition of the particles [19,20], functional groups determining surface chemistry [21], particle properties such as size, shape, and surface roughness [22–27], and electrical properties of particles as well as surrounding walls [28,29]. Furthermore, environmental conditions influence charge transfer.

Humidity [30], external electrical fields [31], and the magnitude of the contact momentum [32,33] are vital in preventing or enabling triboelectric charging. To date, the actual charging mechanisms are only partly understood [5]. Based on this background, the characterisation of influencing factors is necessary and provides an opportunity to gain further knowledge about triboelectric charging. Hence, different influencing factors must be examined for using triboelectric separation for fine powders based on their different charging properties. Hitherto, only a few studies addressed the effect of powder composition on triboelectric charging. For pharmaceutical powder mixtures, an increase in drug polymer showed a decrease in the charge to mass ratio [34]. A variation of the mixing ratio of lactose and glucose results in a twice change of sign and a charge to mass ratio of the powder. These experiments were performed for sliding particles [35].

To investigate the influence of particle-particle and particle-wall interactions on triboelectric separation, the impact of both collision types must be studied. The influence of the wall material plays a subordinated role, which was demonstrated in [36]. Particle-particle interactions might be the dominant mechanism to generate triboelectric charge in pneumatic conveyed binary particulate systems. In a binary mixture, primarily charging between different materials occurs. A single contact between two particle surfaces suffices to generate charge [29,37] or to dissipate charge [38].

Since the charging mechanism is still unknown [5] and particle-wall interaction has a subordinate role on triboelectric charging [36], it is assumed that particle-particle interactions are the main drivers of triboelectric separation. Therefore, a variation of powder composition and flow profiles are used to identify the influence of particle-particle contact numbers on triboelectric separation of fine organic powders. In this study it is hypothesised that higher particle-particle contact numbers induced by a variation of the initial powder composition and flow profiles in a turbulent flow regime improve triboelectric separation selectivity fine organic binary powder mixtures.

2. Materials and Methods

2.1. Materials

Whey protein isolate and barley starch are used as model particles and were purchased form Davisco Foods International, USA, and Altia, Finland, respectively. Whey protein isolate has a protein content of 97.6 wt. %. Barley starch has a protein content below 0.5 wt. % and starch content of 97.0 wt. %. Barley starch was classified using a wheel classifier ATP 50, Hosokawa Alpine, Germany at a deflection wheel speed of 10,000 rpm, a mass flow of 4.3 kg h^{-1}, and an air flow rate of 58 kg h^{-1}. Whey protein was ground with the same conditions as shown in [36].

2.2. Methods

2.2.1. Experimental Setup

The simple experimental setup demonstrated by Landauer et al. [36,39] was used, which consists of an exchangeable charging section and a rectangular separation chamber. A scheme of the setup is shown in Figure 1. In the charging section, a Venturi nozzle facilitates the dispersion of powders added to the gas flow. 2.5 g of powder are added manually to the gas flow during 300 ± 10 s. Since the constant feed time a continuous mass flow can be assumed. The charging tube dimensions are 10 mm in diameter and 230 mm in length. The setup enables the use of different charging sections. Five different insulators (Polytetrafluoroethylene PTFE, Polyvinylchloride PVC, Polymethylmethacrylate PMMA, Polyoxymethylene POM, and Polyethylene PE) were used as wall materials of the charging tube. To disperse and accelerate the particles, a gas flow rate of 3 m^3 h^{-1} was chosen. Further experimental setup of the charging tube involving a porous PE tube is used to facilitate air boundary-layer control (BLC) [40]. To prevent particle–wall interactions, different volume ratios (2.5% BLC I and 5% BLC II) of the total gas flow were radially inserted in the charging tube. An electrical field strength of 109 V/m was applied to the parallel-plate capacitor in the rectangular separation chamber

(46 mm × 52 mm × 400 mm). Binary protein-starch mixtures with protein contents of 15 wt. %, 30 wt. %, and 45 wt. % were used for the experiments. To determine the separation selectivity, the protein content on the anode and the cathode was measured by the absorption of protein at 280 nm on each electrode [36,39].

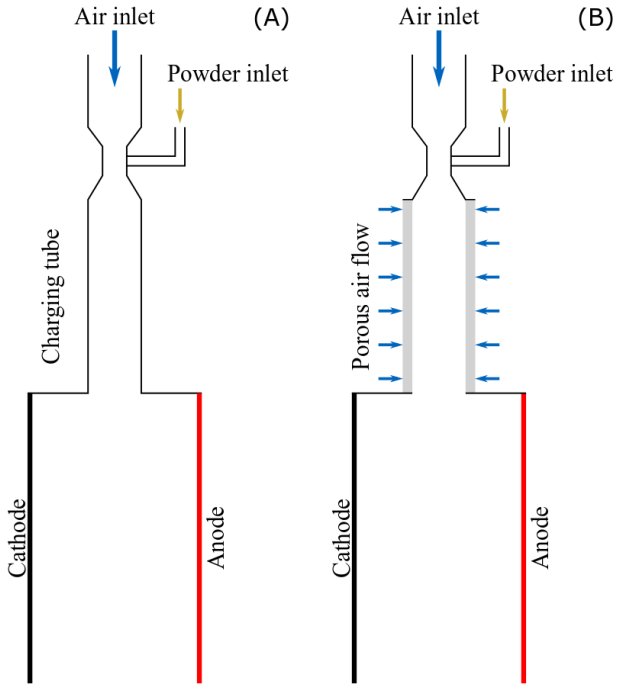

Figure 1. Scheme of the used dispersing, charging and separation setup with plain wall (**A**) and porous tube to adjust boundary-layer control (**B**). After the charging tube, particles are separated in a homogenous electrical field and particles are precipitated on the electrodes.

Triboelectric charging may occur when surfaces get into contact and are subsequently separated. Therefore, it is impossible to use uncharged particles to carry out experiments or to determine the charge of the particles before the experiments in a non-invasive manner. For the used powder containing starch and protein particles below 40 µm, the determination or even estimation of the charge of single particles is very challenging [41] and an interconnection of both experiments without altering the separation characteristics seems to be impossible. Thus, powder preparation and all experiments were carried out according to the same protocol to induce reproducible charge until the start of the experiment.

2.2.2. Particle Analysis

Particle size analysis for initial powders and the powder deposits on the electrodes were performed using the laser diffraction system (HELOS, Sympatec, Germany) with a measuring range of 0.25 µm to 87.5 µm and the wet dispersing unit QUIXEL. Ethanol was used as dispersion medium. The true density of each powder is evaluated using a gas pycnometer (Accupyc 1330, Micromeritics Instrument Corp., Norcross, GA, USA). Scanning electron microscopy (SEM) images of separated powders were recorded at an acceleration voltage of 5 kV (JSM-IT100, JEOL Ltd., Tokyo, Japan).

2.2.3. Particle Interaction Parameter

According to the particle size and flow conditions, the contact number of particles in a fluid can be estimated [42,43]. The encounter frequency γ of two particles with the diameters x_i and x_j in turbulent flow with the turbulence eddy dissipation rate ϵ and the viscosity of the fluid ν can be estimated according to Saffman and Turner [44], as follows:

$$\gamma = \frac{1.3}{8} \sqrt{\frac{\epsilon}{\nu}} (x_i + x_j)^3. \quad (1)$$

The contact of particles x in a binary powder mixture can occur between particles of different material and of different sizes. The turbulence eddy dissipation rate ϵ is taken from the results of the CFD study carried out in [36]. Furthermore, different powder mixtures vary in the protein to starch ratio and have a different number of particles for each species in the same size range. Thus, the encounter frequency must be scaled by the particle number in order to obtain a contact number depending on the particle size and the initial powder composition. The contact number Γ of each powder is calculated by the encounter frequency γ, scaled with the particle number of each size range c_i, c_j, and the mean interaction time Δt equivalent to the residence time of a particle in the charging tube [45]:

$$\Gamma = \frac{1.3}{8} \sqrt{\frac{\epsilon}{\nu}} \, \Delta t \, \sum_{i=1}^{n} \sum_{j=1}^{n} (x_i + x_j)^3 \, c_i \, c_j. \quad (2)$$

The particle number of each size range c_i, c_j is calculated using the measured particle size distribution and the true density of each powder. The size ranges i, j were taken from the used laser-diffraction system, whereby $n = 31$ classes are equally distributed on a logarithmic (base 10) scale.

Besides flow conditions, particle concentration, and particle size the charge of particles influences the contact number. Due to the charge, attractive and repulsive forces can result in segregation or agglomeration of particles, respectively, and therefore reduced contact numbers of particles. To understand the segregation or agglomeration of particles caused by triboelectric charging, several experimental and simulative studies were carried out [46–49]. However, in order to be able to apply the suggested models for calculating the contact number by electrostatic forces, the particle size-dependent charge distribution must be known, or the segregation or agglomeration within the charging section has to be determined. So far, the particle size-dependent charge distribution was not determined for such fine particles and seems to be challenging [41]. The determination of the segregation or agglomeration of particles within the charging tube for particles below 40 µm and flow velocity of $10\,\mathrm{m\,s^{-1}}$ is also challenging. In addition, agglomeration of particles due to electrostatic force is only investigated for very low gas velocities [47], and no agglomeration of particles was found in within same experimental conditions [50]. Therefore, electrostatic interaction is excluded for the estimation of contact number. Furthermore, a sensitivity analysis of the used equation to calculate the contact number is shown in Figure S1 (Supplementary Materials).

The calculation of the contact numbers of particles describes the initial and absolutely necessary step in triboelectric charging—the contact of two surfaces. However, triboelectric charging is a very complex phenomenon [5] and further factors like different materials, humidity, etc. play a decisive role. Since all experimental conditions are the same for each experiment, all random and unknown factors of triboelectric charging might be constant within this study. Hence, the contact numbers of particles are used to examine the influence of particle-particle-contacts and to cave out an influence parameter to engineer triboelectric charging.

2.2.4. Statistics

For all experiments the mean value was calculated from the results of three independent experiments ($n = 3$). The variance of the experiments are indicated by error bars. The error bars are calculated using Student's t-test at a significance level of $\alpha = 0.05$.

3. Results

3.1. Particle Size Distribution and SEM of Separated Powders

Figure 2 shows the particle size distribution of the raw materials, prepared powder mixtures (A), and separated powders on the cathode and anode (B). The protein powder has a monomodal particle

size distribution between 0.2 µm to 20 µm with a maximum value at 1 µm. The starch powder has a bimodal distribution with local maxima at 1 µm and 20 µm and a maximum particle size of 40 µm. Mixtures with initial protein contents of 15 wt. %, 30 wt. %, and 45 wt. % show similar particle size distributions with maximum values at 1 µm and 7 µm, because the particle size distributions of starch and protein overlap in almost the whole width. The particle size distribution could not be closed for all measured powders, because the used measuring range has enable both a detection of the largest and finest particles. Thus, particle sizes below 0.25 µm were neglected, since a dry dispersion of particles below 0.25 µm seems to be very unlikely. The particle size distributions of the separated powder show significantly different patterns on the cathode and the anode. On the anode, the particle size distributions show an approximately identical evolution for each initial protein content featuring almost the same peaks as starch, but with increased peak height. Therefore, the starch concentration on the anode is concluded to be high. In contrast, the particle size distributions of powders on the cathode bear a resemblance to the particle size distribution of the initial protein-starch mixture. Triboelectric separation leads to an increase in peak height at 1 µm and a flattening of the peak at larger particle sizes forming almost a monomodal distribution. Different initial protein contents lead to different peak heights at 1 µm; however, the shape of the particle size distributions above 4 µm is similar. The peak height is identical for the initial protein content of 30 wt. % and 45 wt. %, while both higher compared to 15 wt. %. Thus, separation efficiency depends on the initial protein content.

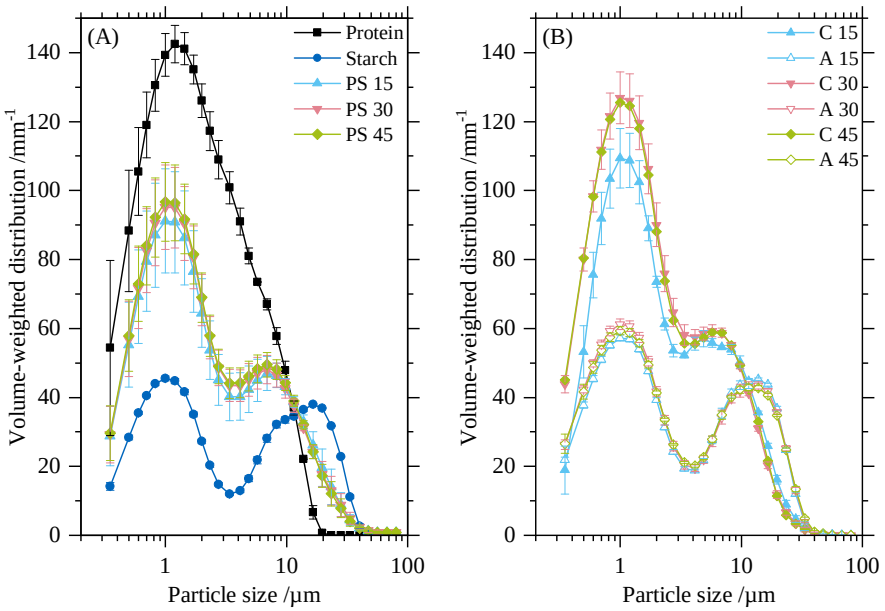

Figure 2. Particle size distributions of native powders, powder mixtures (**A**) and powders collected after separation (**B**) on cathode C (closed symbol) and anode A (open symbol). PVC was used as wall material in the charging tube. Despite varying protein content, initial powder mixtures have no different particle size distributions. On the cathode, an initially higher protein content results in finer powder. No such difference is visible on the anode.

Figure 3 shows SEM images of separated powders collected on the cathode (A) and anode (B) with an initial protein content of 30 wt. %. Small and rugged protein particles are clearly visible on the cathode. Protein particles tend to agglomerate among themselves forming larger structures. Only very few starch particles, identifiable by their round morphology and smooth surface, are detected on the cathode. On the contrary, starch particles of several sizes are found in very high incidence on the anode and very small protein particles are adsorbed on the surface of the starch particles. Thus, a complete separation of the powder mixture in starch and protein could not be achieved.

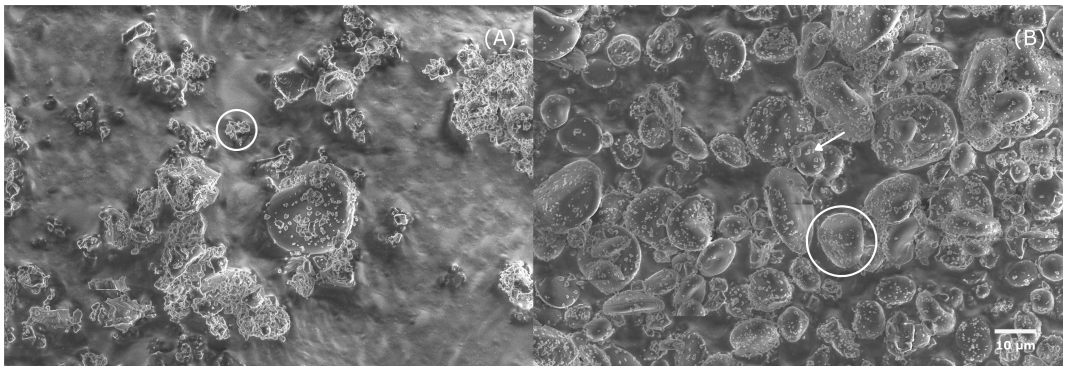

Figure 3. SEM images of separated powders on the cathode (**A**) and anode (**B**) with PVC as charging tube material. On the cathode, small and rugged protein particles (circle left) represent the main fraction. Smooth starch particles (circle right) predominate the population on the anode, while small protein particles adhere on the surface of large starch particles (arrow).

3.2. Influence on Separation Selectivity

Figure 4 shows the protein content indicating the separation selectivity on the cathode and anode after triboelectric separation. The protein content of the powder mixture was incrementally increased from 15 wt. % to 30 wt. % and 45 wt. %. Different wall materials were used to determine the combined influence of the particle-wall interaction and powder composition. For all employed wall materials, the increase in the initial protein content from 15 wt. % to 30 wt. % causes a significant increase in the protein content on the cathode, while the protein content on the anode remains unaffected. Such low protein contents on the anode indicate a very high starch content of up to 100 wt. %. Further increase in the initial protein content to 45 wt. % does not lead to an increase in the protein content on the cathode in combination with any of the tested contact materials. Thus, an increase in selectivity is observed only for PE and PVC. The tube materials POM and PMMA show no increase in selectivity above 30% protein content. In contrast, the protein content on the anode increases slightly when the initial protein content increases from 30 wt. % to 45 wt. % for all materials except PE. In summary, different wall materials have an impact on the selectivity at different initial protein contents; however, this impact cannot be explained on the basis of the empirical triboelectric series.

To test the influence of particle-wall interactions on triboelectric charging, wall contact was prevented by a boundary-layer control setup. A porous tube was applied with two different gas flow rates perpendicular to the particle stream [36]. The protein content on the cathode increases with the incremental increase in the initial protein content from 15 wt. % to 45 wt. %. The significant difference between 15 wt. % and 45 wt. % is in contrast to the plain wall setup. At the initial protein content of 15 wt. %, however, no significant differences between all BLC conditions are visible at the initial protein content of 15 wt. %. BLC I and BLC II show a small difference at 30 wt. %. At the highest initial protein content, no difference between BLC I, II and most of the plain wall setups was detected. On the anode, the protein content of BLC I and II increases as the initial protein content increases. Furthermore, only slight differences between the experimental setups were observed at 30 wt. %.

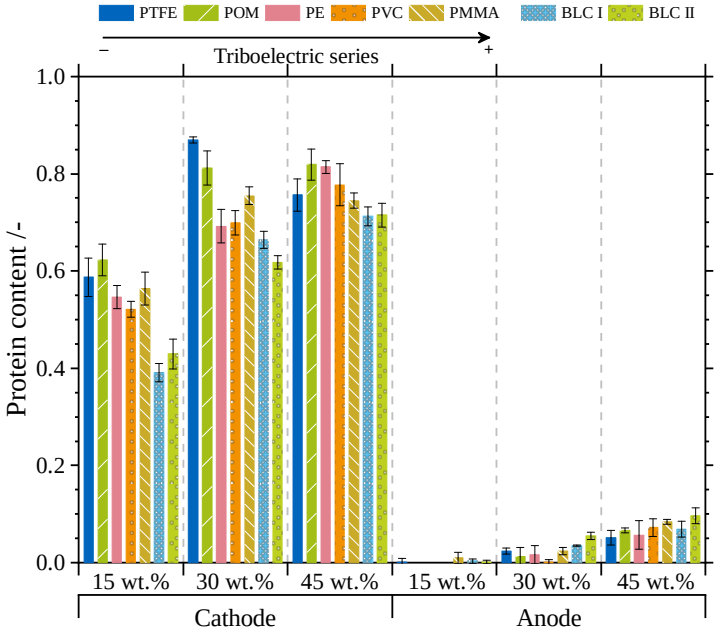

Figure 4. Protein content on the cathode and anode of powders with an initial protein content of 15 wt. %, 30 wt. % and 45 wt. %. Bars indicate different contact materials along with the triboelectric series and setup without wall interaction (BLC I & II). An increase in initial protein content leads to a significant increase in protein content on the cathode and anode. Different contact materials do not affect the protein content on each electrode. Results for 15 wt. % were taken from a previous study [36].

3.3. Particle Interaction

3.3.1. Contact Number Distribution Depending on Particle Size

Figure 5 shows the contact number distribution of protein (A) and starch (B) particles. The used values to calculate the contact numbers are summarised in Table 1. Protein particles show a high contact number for small particles. The contact number decreases as the particle size increases. The protein-protein contact number is always higher than the protein-starch contact number. An increase in protein content leads to an increase in the contact number for protein-protein and protein-starch. Starch particles show a high contact number for particles between 7 µm to 40 µm. The contact number between starch-protein increases by decreasing starch content in the initial powder mixture. These findings result from the increase in protein particle number because protein particles are a slightly finer than starch particles. The contact number between starch particles is almost the same for all investigated powder mixtures and always lower than the contact number between protein-starch. By comparing starch-starch and protein-protein contacts, the contact number of protein-protein interaction is always higher than that of starch-starch interaction. In summary, the variation in initial powder composition leads to different contact between the dispersed powders and thus might provide the first indication to the different separation selectivity (cf. Figure 4).

Table 1. Parameters used to calculate contact numbers of particles.

	Mean of Plain Wall	**BLC I**	**BLC II**
ϵ /m^2 s^{-3}	3.53×10^4	3.11×10^4	2.55×10^4
ν /m^2 s^{-1}		1.33×10^{-5}	
ρ_{Protein} /kg m^{-3}		1330	
ρ_{Starch} /kg m^{-3}		1520	

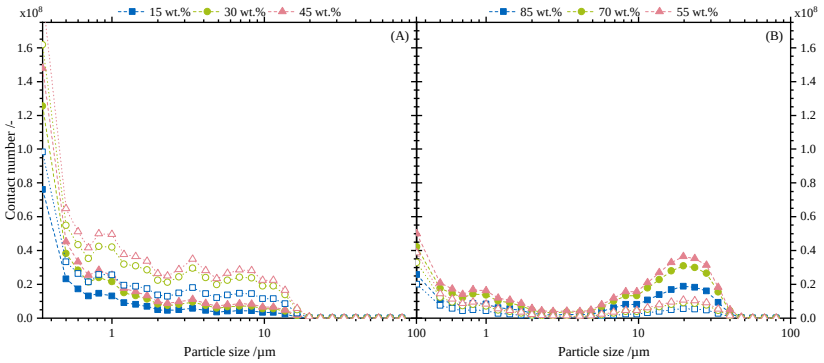

Figure 5. Contact number distribution of protein (**A**) and starch (**B**) particles. Closed symbols indicate the interaction with different materials, whereas open symbols show interaction with the same material. Protein shows a higher contact number for small particles. A higher initial protein content leads to higher contact numbers.

3.3.2. Separation Selectivity and Contact Numbers

A variation in the flow conditions leads to a change in the turbulence eddy dissipation rate, which plays a vital role in the contact number (Equation (1)). The experiments carried out with a plain wall, BLC I, and II have slightly different flow profiles. Thus, both a variation in the flow properties and that in the initial powder composition (cf. Figure 5) result in different contact numbers. As triboelectric or contact charging occurs, only a single contact suffices to attain a charged surface of a particle [29,37]. A collision of contrary charged particles of course results in charge annihilation. Based on this understanding, Figure 6 shows the protein content on the anode and cathode with respect to the contact number. The protein content on the cathode (closed symbols) shows a significant increase by increasing the contact number of particles. Lower contact numbers result in protein contents between 0.4 and 0.6, whereas higher contact numbers have protein contents of approximately 0.8. An increase in the protein content on the anode (open symbols) is also caused by an increase in the contact number. However, the increase in the protein content on the anode is considerably less compared to that on the cathode. For low contact numbers that have no protein can be detected on the anode, whereas for higher contact numbers, the maximum protein content reaches a value of 0.1. In summary, contact number affects the protein content on the anode and the cathode, while the protein content on the cathode is strongly affected and that on the anode is slightly affected.

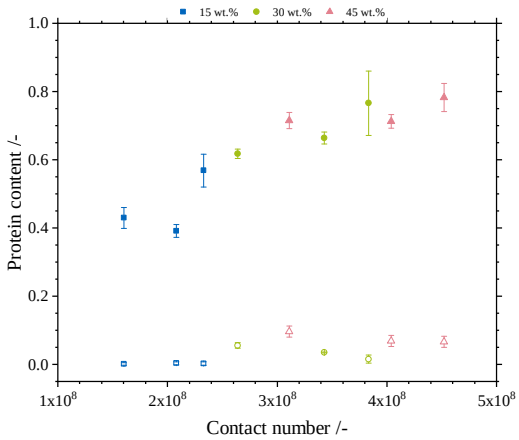

Figure 6. Protein content of separated powders on the cathode (closed symbols) and on the anode (open symbols). To improve clarity, the average protein content is plotted for all plain wall measurements. An increase in contact number results in a significant increase in protein content on the cathode. The protein content on the anode increases slightly with the increase in contact number.

4. Discussion

Triboelectric separation is a suitable technique used to separate powders containing different ratios of protein and starch [36,39,51–54]. The separation feature is not the particle size, as the particle size distributions of protein and starch overlap almost in the whole. Furthermore, there is no apparent dependency on the particle size during and after separation [50]. Powders containing different initial protein contents have similar particle size distributions before separation. After separation, the particle size distribution of the powders collected on the anode commonly shows the same evolution independent of the initial protein content. This underpins the independence of triboelectric separation from the particle size in a size range of 0.1 µm to 40 µm and puts the focus on the chemical composition [21] as well as further particle properties such as morphology and roughness as separation feature [25,27]. These results are in contrast with findings of the bipolar charging of single component powders claiming that small particles are always charged negatively [22,55–57].Furthermore, there are different charge distributions for positively and negatively charged particles [41]. The particle size distributions of powders collected on the cathode after separation feature higher peaks at 1 µm for initial protein contents of 30 wt. % and 45 wt. % compared to 15 wt. % (Figure 2). This increase can be associated with the increase in the protein content for higher initial protein concentrations. In contrast, the particle size distributions remain similar, implying an increase in the protein content on the anode with the stepwise increase in the initial protein content (Figure 4). However, comparing the particle size distribution of the pristine starch powder and the powder collected on the anode, a clear increase in the peak value of both peaks is visible, which might correspond to agglomerated particles on the electrodes, because no agglomeration was found for dispersed particles [50].

The separation selectivity shows a dependence on the initial protein content (Figure 4). For all plain wall setups and BLC setups, the protein content on the cathode increases with an increase in the initial protein content. Furthermore, all plain wall setups show no dependence on the triboelectric series of the wall materials. These findings correspond to the previous study [36]. As triboelectric charging can only occur if particles get into contact and are subsequently separated, the interactions of particles in the charging tube play a decisive role. Therefore, according to Saffman and Turner [44], an interaction parameter Γ of particles in a turbulent flow is calculated. In a binary powder mixture, a particle can collide with a particle of the same origin or with a particle of the other origin assuming that the particle-wall interaction plays a subordinated role. In addition to the origin of particles, the particle size affects the contact number of particles (Equation (2), Figure 5). Starch particles collide more frequently with protein particles, whereas protein particles collide more frequently among themselves. These findings indicate the influence of the pristine particle sizes as well as the initial protein content on triboelectric charging. Next to particle size and mixture composition, the flow properties in the charging tube also have an impact on the contact number. As Figure 6 shows, the contact number affects triboelectric separation properties which are in direct relation with triboelectric charging. The increase in the protein content on the cathode is accompanied by an almost linear increase along the particle-particle contact number. Since higher contact numbers of particles result in higher protein contents on the cathode, the protein content on the anode might decrease; however, on the anode the protein content is slightly increasing with increasing contact number. These findings might correlate with the increased interaction beneath protein particles (Figure 5). The increase of protein content on the anode due to higher contact numbers is huge compared with the increase of protein content on the anode. Therefore it is concluded, the increase in contact numbers of particles results in superior separation selectivity of fine organic powders. Thus, particle-particle interaction in the charging step of triboelectric separation is the decisive interaction parameter and can be used to enlarge or adjust triboelectric separation properties. Hence, the hypothesis that higher particle-particle contact numbers induced by a variation of the initial powder composition and turbulent flow profiles improves triboelectric separation selectivity is confirmed; however the calculation of the contact numbers of particles showed that powder composition mainly influence contact numbers and, thus, separation selectivity.

5. Conclusions

This study examines the influence of protein content in a binary powder mixture and flow properties on separation selectivity of triboelectric charging. The particle size distributions of initial and separated powder on the cathode showed an increase of fine particles with increasing initial protein content; however, the particle size distributions on the anode were unaffected by the initial protein content. These findings match with the separation selectivity. Thus, higher proportions of protein in the initial powder result in an increase of the protein content on both cathode and anode. Different wall materials along the empirical triboelectric series show no influence on the separation selectivity. A variation in the powder mixture and flow profile induce different contact numbers. An increase in the contact number results in an increase in the protein content. To put all in a nutshell, triboelectric charging and, thus, the separation selectivity of a binary powder mixture in turbulent flow can be influenced by the contact number of the particles. To adjust the contact number of particles, both particle size and turbulence eddy dissipation can be used. Thus, the contact number is a good parameter to improve triboelectric separation selectivity.

Supplementary Materials: The following are available online at http://www.mdpi.com/2227-9717/7/10/716/s1. Figure S1: Sensitivity analysis of Equation (2) to estimate the influence of turbulence eddy dissipation rate and protein content in the initial powder (from 0.99 to 0.01) on the contact number. Contact numbers and turbulent eddy dissipation rates used in this study are highlighted.

Author Contributions: J.L. did the conception and design of the study, the experimental work, and wrote the manuscript. P.F. participated to the writing and supervised the work.

Funding: This research received no external funding.

Acknowledgments: The authors would like to thank Stefan Schmideder for the fruitful discussion of contact number calculation and Heiko Briesen for the possibility to carry out this study.

Conflicts of Interest: The authors declare no conflict of interest.

Abbreviations

The following abbreviations are used in this manuscript:

BLC Bondary-layer control

References

1. Lacks, D.J.; Mohan Sankaran, R. Contact electrification of insulating materials. *J. Phys. D Appl. Phys.* **2011**, *44*, 453001.[CrossRef]
2. Matsusaka, S.; Masuda, H. Electrostatics of particles. *Adv. Powder Technol.* **2003**, *14*, 143–166.[CrossRef]
3. Matsusaka, S.; Maruyama, H.; Matsuyama, T.; Ghadiri, M. Triboelectric charging of powders: A review. *Chem. Eng. Sci.* **2010**, *65*, 5781–5807.[CrossRef]
4. Baytekin, H.T.; Patashinski, A.Z.; Branicki, M.; Baytekin, B.; Soh, S.; Grzybowski, B.A. The mosaic of surface charge in contact electrification. *Science* **2011**, *333*, 308–312.[CrossRef] [PubMed]
5. Lacks, D.J.; Shinbrot, T. Long-standing and unresolved issues in triboelectric charging. *Nat. Rev. Chem.* **2019**, *3*, 465–476.[CrossRef]
6. Grosshans, H.; Papalexandris, M.V. Large Eddy simulation of triboelectric charging in pneumatic powder transport. *Powder Technol.* **2016**, *301*, 1008–1015.[CrossRef]
7. Bunchatheeravate, P.; Curtis, J.; Fujii, Y.; Matsusaka, S. Prediction of particle charging in a dilute pneumatic conveying system. *AChE J.* **2013**, *59*, 2308–2316.[CrossRef]
8. Fotovat, F.; Bi, X.T.; Grace, J.R. Electrostatics in gas-solid fluidized beds: A review. *Chem. Eng. Sci.* **2017**, *173*, 303–334.[CrossRef]
9. Naik, S.; Mukherjee, R.; Chaudhuri, B. Triboelectrification: A review of experimental and mechanistic modeling approaches with a special focus on pharmaceutical powders. *Int. J. Pharm.* **2016**, *510*, 375–385.[CrossRef] [PubMed]

10. Mareev, E.A.; Dementyeva, S.O. The role of turbulence in thunderstorm, snowstorm, and dust storm electrification. *J. Geophys. Res. Atmos.* **2017**, *122*, 6976–6988.[CrossRef]
11. Forward, K.M.; Lacks, D.J.; Sankaran, R.M. Particle-size dependent bipolar charging of Martian regolith simulant. *Geophys. Res. Lett.* **2009**, *36*, 139.[CrossRef]
12. Lee, V.; Waitukaitis, S.R.; Miskin, M.Z.; Jaeger, H.M. Direct observation of particle interactions and clustering in charged granular streams. *Nat. Phys.* **2015**, *11*, 733–737.[CrossRef]
13. Dwari, R.K.; Mohanta, S.K.; Rout, B.; Soni, R.K.; Reddy, P.; Mishra, B.K. Studies on the effect of electrode plate position and feed temperature on the tribo-electrostatic separation of high ash Indian coking coal. *Adv. Powder Technol.* **2015**, *26*, 31–41.[CrossRef]
14. Mohanta, S.K.; Rout, B.; Dwari, R.K.; Reddy, P.; Mishra, B.K. Tribo-electrostatic separation of high ash coking coal washery rejects: Effect of moisture on separation efficiency. *Powder Technol.* **2016**, *294*, 292–300.[CrossRef]
15. Bouhamri, N.; Zelmat, M.E.; Tilmatine, A. Micronized plastic waste recycling using two-disc tribo-electrostatic separation process. *Adv. Powder Technol.* **2019**, *30*, 625–631.[CrossRef]
16. Messafeur, R.; Mahi, I.; Ouiddir, R.; Medles, K.; Dascalescu, L.; Tilmatine, A. Tribo-electrostatic separation of a quaternary granular mixture of plastics. *Part. Sci. Technol.* **2019**, *37*, 760–765.[CrossRef]
17. Xing, Q.; de Wit, M.; Kyriakopoulou, K.; Boom, R.M.; Schutyser, M.A. Protein enrichment of defatted soybean flour by fine milling and electrostatic separation. *Innov. Food Sci. Emerg. Technol.* **2018**, *50*, 42–49.[CrossRef]
18. Chen, Z.; Liu, F.; Wang, L.; Li, Y.; Wang, R.; Chen, Z. Tribocharging properties of wheat bran fragments in air–solid pipe flow. *Food Res. Int.* **2014**, *62*, 262–271.[CrossRef]
19. Albrecht, V.; Janke, A.; Drechsler, A.; Schubert, G.; Németh, E.; Simon, F. Visualization of Charge Domains on Polymer Surfaces. In *Characterization of Polymer Surfaces and Thin Films*; Progress in Colloid and Polymer Science; Grundke, K., Stamm, M., Adler, H.J., Eds.; Springer: Berlin/Heidelberg, Germany, 2006; Volume 132, pp. 48–53.
20. Harper, W.R. The Volta Effect as a Cause of Static Electrification. *Proc. R. Soc. A Math. Phys. Eng. Sci.* **1951**, *205*, 83–103.[CrossRef]
21. Kamiyama, M.; Maeda, M.; Okutani, H.; Koyama, K.; Matsuda, H.; Sano, Y. Effect of functional groups on the triboelectric charging property of polymer particles. *J. Appl. Polym. Sci.* **1994**, *51*, 1667–1671.[CrossRef]
22. Forward, K.M.; Lacks, D.J.; Sankaran, R.M. Triboelectric Charging of Granular Insulator Mixtures Due Solely to Particle—Particle Interactions. *Ind. Eng. Chem. Res.* **2009**, *48*, 2309–2314.[CrossRef]
23. Trigwell, S.; Grable, N.; Yurteri, C.U.; Sharma, R.; Mazumder, M.K. Effects of surface properties on the tribocharging characteristics of polymer powder as applied to industrial processes. *IEEE Trans. Ind. Appl.* **2003**, *39*, 79–86.[CrossRef]
24. Schönert, K.; Eichas, K.; Niermöller, F. Charge distribution and state of agglomeration after tribocharging fine particulate materials. *Powder Technol.* **1996**, *86*, 41–47.[CrossRef]
25. Atroune, S.; Tilmatine, A.; Alkama, R.; Samuila, A.; Dascalescu, L. Comparative Experimental Study of Triboelectric Charging of Two Size Classes of Granular Plastics. *Part. Sci. Technol.* **2015**, *33*, 652–658.[CrossRef]
26. Lacks, D.J.; Levandovsky, A. Effect of particle size distribution on the polarity of triboelectric charging in granular insulator systems. *J. Electrost.* **2007**, *65*, 107–112.[CrossRef]
27. Mukherjee, R.; Gupta, V.; Naik, S.; Sarkar, S.; Sharma, V.; Peri, P.; Chaudhuri, B. Effects of particle size on the triboelectrification phenomenon in pharmaceutical excipients: Experiments and multi-scale modeling. *Asian J. Pharm. Sci.* **2016**, *11*, 603–617.[CrossRef]
28. Sakaguchi, M.; Shimada, S.; Kashiwabara, H. Mechanoions produced by mechanical fracture of solid polymer. 6. A generation mechanism of triboelectricity due to the reaction of mechanoradicals with mechanoanions on the friction surface. *Macromolecules* **1990**, *23*, 5038–5040.[CrossRef]
29. Horn, R.G.; Smith, D.T.; Grabbe, A. Contact electrification induced by monolayer modification of a surface and relation to acid–base interactions. *Nature* **1993**, *366*, 442–443.[CrossRef]
30. Kolehmainen, J.; Sippola, P.; Raitanen, O.; Ozel, A.; Boyce, C.M.; Saarenrinne, P.; Sundaresan, S. Effect of humidity on triboelectric charging in a vertically vibrated granular bed: Experiments and modeling. *Chem. Eng. Sci.* **2017**, *173*, 363–373.[CrossRef]
31. Wistuba, H. The effect of an external electric field on the operation of an aluminium oxide–cast iron sliding contact joint. *Wear* **1997**, *208*, 113–117.[CrossRef]

32. Watanabe, H.; Ghadiri, M.; Matsuyama, T.; Maruyama, H.; Matsusaka, S.; Ghadiri, M.; Matsuyama, T.; Ding, Y.L.; Pitt, K.G.; Maruyama, H.; et al. Triboelectrification of pharmaceutical powders by particle impact. *Int. J. Pharm.* **2007**, *334*, 149–155.[CrossRef] [PubMed]
33. Ireland, P.M. Impact tribocharging of soft elastic spheres. *Powder Technol.* **2019**, *348*, 70–79.[CrossRef]
34. Ghori, M.U.; Supuk, E.; Conway, B.R. Tribo-electric charging and adhesion of cellulose ethers and their mixtures with flurbiprofen. *Eur. J. Pharm. Sci.* **2014**, *65*, 1–8.[CrossRef] [PubMed]
35. Murtomaa, M.; Laine, E. Electrostatic measurements on lactose–glucose mixtures. *J. Electrost.* **2000**, *48*, 155–162.[CrossRef]
36. Landauer, J.; Aigner, F.; Kuhn, M.; Foerst, P. Effect of particle-wall interaction on triboelectric separation of fine particles in a turbulent flow. *Adv. Powder Technol.* **2019**, *30*, 1099–1107.[CrossRef]
37. Horn, R.G.; Smith, D.T. Contact electrification and adhesion between dissimilar materials. *Science* **1992**, *256*, 362–364.[CrossRef] [PubMed]
38. Haeberle, J.; Schella, A.; Sperl, M.; Schröter, M.; Born, P. Double origin of stochastic granular tribocharging. *Soft Matter* **2018**, *14*, 4987–4995.[CrossRef] [PubMed]
39. Landauer, J.; Foerst, P. Triboelectric separation of a starch-protein mixture – Impact of electric field strength and flow rate. *Adv. Powder Technol.* **2018**, *29*, 117–123.[CrossRef]
40. Schlichting, H.; Gersten, K. *Boundary-Layer Theory*; Springer: Berlin/Heidelberg, Germay, 2017.[CrossRef]
41. Landauer, J.; Tauwald, S.M.; Foerst, P. A Simple\textmu-PTV Setup to Estimate Single-Particle Charge of Triboelectrically Charged Particles. *Front. Chem.* **2019**, *7*, 1.[CrossRef]
42. Meyer, C.J.; Deglon, D.A. Particle collision modeling—A review. *Miner. Eng.* **2011**, *24*, 719–730.[CrossRef]
43. Schmideder, S.; Kirse, C.; Hofinger, J.; Rollié, S.; Briesen, H. Modeling the Separation of Microorganisms in Bioprocesses by Flotation. *Processes* **2018**, *6*, 184.[CrossRef]
44. Saffman, P.G.; Turner, J.S. On the collision of drops in turbulent clouds. *J. Fluid Mech.* **1956**, *1*, 16.[CrossRef]
45. Smoluchowski, M. Versuch einer mathematischen Theorie der Koagulationskinetik kolloider Lösungen. *Z. Phys. Chem. (Leipzig)* **1917**, *92*, 129–168. [CrossRef]
46. Kolehmainen, J.; Ozel, A.; Boyce, C.M.; Sundaresan, S. Triboelectric charging of monodisperse particles in fluidized beds. *AIChE J.* **2017**, *63*, 1872–1891.[CrossRef]
47. Kolehmainen, J.; Ozel, A.; Gu, Y.; Shinbrot, T.; Sundaresan, S. Effects of Polarization on Particle-Laden Flows. *Phys. Rev. Lett.* **2018**, *121*, 124503.[CrossRef] [PubMed]
48. Schella, A.; Herminghaus, S.; Schröter, M. Influence of humidity on tribo-electric charging and segregation in shaken granular media. *Soft Matter* **2017**, *13*, 394–401.[CrossRef] [PubMed]
49. Schella, A.; Weis, S.; Schröter, M. Charging changes contact composition in binary sphere packings. *Phys. Rev. E* **2017**, *95*, 062903.[CrossRef] [PubMed]
50. Landauer, J.; Foerst, P. Influence of Particle Charge and Size Distribution on Triboelectric Separation—New Evidence Revealed by In Situ Particle Size Measurements. *Processes* **2019**, *7*, 381.[CrossRef]
51. Tabtabaei, S.; Jafari, M.; Rajabzadeh, A.R.; Legge, R.L. Solvent-free production of protein-enriched fractions from navy bean flour using a triboelectrification-based approach. *J. Food Eng.* **2016**, *174*, 21–28.[CrossRef]
52. Tabtabaei, S.; Jafari, M.; Rajabzadeh, A.R.; Legge, R.L. Development and optimization of a triboelectrification bioseparation process for dry fractionation of legume flours. *Sep. Purif. Technol.* **2016**, *163*, 48–58.[CrossRef]
53. Wang, J.; de Wit, M.; Boom, R.M.; Schutyser, M.A. Charging and separation behavior of gluten–starch mixtures assessed with a custom-built electrostatic separator. *Sep. Purif. Technol.* **2015**, *152*, 164–171.[CrossRef]
54. Wang, J.; de Wit, M.; Schutyser, M.A.; Boom, R.M. Analysis of electrostatic powder charging for fractionation of foods. *Innov. Food Sci. Emerg. Technol.* **2014**, *26*, 360–365.[CrossRef]
55. Inculet, I.I.; Peter Castle, G.S.; Aartsen, G. Generation of bipolar electric fields during industrial handling of powders. *Chem. Eng. Sci.* **2006**, *61*, 2249–2253.[CrossRef]

56. Zhao, H.; Castle, G.; Inculet, I.I.; Bailey, A.G. Bipolar charging of poly-disperse polymer powders in fluidized beds. *IEEE Trans. Ind. Appl.* **2003**, *39*, 612–618.[CrossRef]
57. Sowinski, A.; Miller, L.; Mehrani, P. Investigation of electrostatic charge distribution in gas–solid fluidized beds. *Chem. Eng. Sci.* **2010**, *65*, 2771–2781.[CrossRef]

© 2019 by the authors. Licensee MDPI, Basel, Switzerland. This article is an open access article distributed under the terms and conditions of the Creative Commons Attribution (CC BY) license (http://creativecommons.org/licenses/by/4.0/).

2.4. Paper IV: A Simple µ-PTV Setup to Estimate Single-Particle Charge of Triboelectrically Charged Particles (Landauer et al., 2019b)

Brief introduction

For the separation of fine organic powders triboelectric charging and subsequent separation is a suitable tool. The measurement of single particle charge of particles in a range between 1 µm and 100 µm can be valuable in order to estimate the possibility for triboelectric separation and for the process design of a triboelectric separation system. Therefore, a measurement setup suiting to the separation setup (Landauer et al., 2019a; Landauer and Foerst, 2018) is designed. The charge measurement system is based on visualising the trajectories of charged particles in a homogenous electrical field. The trajectories are visualised using a µ-PTV (micro-particle-tracking velocimetry) setup. The µ-PTV setup consists of a separation chamber where charged particles are conveyed through a homogenous electrical field, a laser to illuminate the particles, and a high-speed camera placed perpendicular to the laser. The setup is designed for turbulent and laminar flow conditions in the charging tube and separation/recording chamber, respectively. The trajectories recorded with the high-speed camera are evaluated by image analysis and regression analysis using the equations of motion for particles deflected in an electrical field according to their charges. The obtained charge distribution is examined using starch from different botanical origin (barley, corn, potato) and whey protein as well as starch-protein mixtures.

Study findings

The designed setup enables the simultaneous estimation of negatively and positively charged particles. The calculated particle charge of different powders show different patterns. All starch powders have a monomodal charge distribution for negatively charged particles and a multimodal distribution for positively charged particles. Peak maxima of the positive charge distribution differ according to their botanical origin. Whey protein powder show the same charge distribution for positively and negatively charged particles. All investigated powders have a different particle morphology. Thus, particle morphology might play a decisive role for particle charging. Charge distribution of starch-protein mixtures show similar pattern as charge distribution of pure starch. Negatively charged particles have a monomodal distribution, whereas positively charged distributions have a trimodal distribution. It is obvious that the addition of protein powder to starch powder influences the charge distribution. Thus, chemical composition of the powder mixture plays a decisive role in triboelectric charging of binary powder mixtures.

Conclusion

i Particle charge distribution of particles between 1 µm and 100 µm can be estimated by a µ-PTV setup.

ii Positive and negative charge distributions showed same and different patterns for protein and starches, respectively.

iii Starch-protein mixtures had different charge distributions compared to pure starch powders.

iv Particle morphology has an influence on particle charge distribution.

Author contributions

Johann Landauer did the conception and design of the study and wrote the manuscript. Sandra Tauwald did the experimental works. Petra Foerst participated to the writing and supervised the work.

frontiers in Chemistry

ORIGINAL RESEARCH
published: 07 May 2019
doi: 10.3389/fchem.2019.00323

A Simple μ-PTV Setup to Estimate Single-Particle Charge of Triboelectrically Charged Particles

Johann Landauer, Sandra Melina Tauwald and Petra Foerst*

Chair of Process Systems Engineering, TUM School of Life Sciences Weihenstephan, Technical University of Munich, Freising, Germany

Triboelectric separation is a useful phenomenon that can be used to separate fine powders. To design technical devices or evaluate the potential of powders to be triboelectrically separated, knowledge about the charge distribution on a single-particle level has to be obtained. To estimate the single-particle charge distribution in an application-oriented way, a simple μ-PTV system was developed. The designed setup consists of a dispersing and a charging unit using a Venturi nozzle and a tube, respectively, followed by a separation chamber. In the separation chamber, a homogenous electrical field leads to a deflection of the particles according to their individual charge. The trajectories of the particles are captured on single frames using microscope optics and a high-speed camera with a defined exposure time. The particles are illuminated using a laser beam combined with a cylindrical lens. The captured images enable simultaneous measurement of positively and negatively charged particles. The charge is calculated assuming a mean particle mass derived from the mean particle size. Initial experiments were carried out using starch of different botanical origins and protein powder. Single-component experiments with starch powders show very different charge distributions for positively and negatively charged particles, whereas protein powder shows bipolar charging. Different starch-protein mixtures show similar patterns for positive and negative charge distributions.

Keywords: triboelectric charging, triboelectric separation, singe-particle charge, charge distribution, charge measurement setup

OPEN ACCESS

Edited by:
Jose Luis Sanchez, University of Zaragoza, Spain

Reviewed by:
Peter Matthew Ireland, University of Newcastle, Australia
Juraj Kosek, University of West Bohemia, Czechia

****Correspondence:***
Johann Landauer
johann.landauer@tum.de

Specialty section:
This article was submitted to Chemical Engineering, a section of the journal Frontiers in Chemistry

Received: *25 January 2019*
Accepted: *23 April 2019*
Published: *07 May 2019*

Citation:
Landauer J, Tauwald SM and Foerst P (2019) A Simple μ-PTV Setup to Estimate Single-Particle Charge of Triboelectrically Charged Particles. Front. Chem. 7:323. doi: 10.3389/fchem.2019.00323

1. INTRODUCTION

Triboelectric charging occurs everywhere in nature from child rubbing a balloon on their hair to industrial powder handling. In particulate systems, triboelectric charging is predominately described as a problem, rather than an opportunity. Nevertheless, triboelectric charging is an exciting but so far not completely understood phenomenon. It has been investigated in many fields of research, such as contact electrification in dust devils (Farrell, 2004; Mareev and Dementyeva, 2017), in clouds after volcanic eruptions (Anderson et al., 1965; Mather and Harrison, 2006), in the formation of planets (Yair et al., 2008; Wang et al., 2017), and in almost every application dealing with fine and dry powders. Commonly, triboelectric charging is seen as a problem in industrial applications if particles are to be moved because charged particles tend to agglomerate and adhere on surfaces (Wong et al., 2015). Dry powder mixing (Ghori et al., 2014), pneumatic conveying (Bunchatheeravate et al., 2013; Korevaar et al., 2014; Grosshans and Papalexandris, 2016), and

fluidised beds (Fotovat et al., 2017; Kolehmainen et al., 2017; Mehrani et al., 2017; Peltonen et al., 2018) are especially vulnerable steps in powder processing. In contrast, triboelectric charging of particles and surfaces is a desirable effect in electrophotography (Schein, 1999), nanogenerators (Wang, 2013; Jiang et al., 2018), and particle separation (Eichas and Schönert, 1992; Wu et al., 2013; Wang et al., 2015; Tabtabaei et al., 2016; Landauer and Foerst, 2018; Landauer et al., 2019).

In all cases, prediction of the triboelectric charging ability and characterization of charged particles is a necessary prerequisite for designing processes. Several approaches to measuring the charge of particles are known in literature. One simple charge-measuring setup is a Faraday cage or cup; when charged particles are put into a metal cup that is insulated on the outer wall, the electrical charge of the particles can drain and is measured. In the inductive one, particles flow through a conducting tube and the induced current can be measured. If both the charge of the Faraday cup and the mass of the particles is measured, the charge-to-mass ratio can be calculated. As it is a cumulative method, the measurement of bipolar charged particles is only possible with difficulty. For different applications, Faraday cups are designed to enable the measurement of fine powders or in a flow-through type (Matsuyama and Yamamoto, 1994; Watanabe et al., 2007). Faraday cups have been used in numerous studies to evaluate the charge-to-mass ratio (Zhao et al., 2002; Saini et al., 2008; Ducati et al., 2010; Ireland, 2010; Hussain et al., 2013; Pérez-Vaquero et al., 2016; Schella et al., 2017). Therefore, if particles are charged in a bipolar manner, the actual charge of a single particle is not determinable. Kelvin probe force microscopy is suitable for measuring surface charges. The charge present on a surface can be measured in high-resolution, but only in a small area (Nonnenmacher et al., 1991; Baytekin et al., 2012; Burgo et al., 2013; Mirkowska et al., 2014). However, Kelvin probe microscopy is an important method for illuminating the ongoing micro processes in triboelectric charging such as the *mosaic charged surfaces* (Baytekin et al., 2011), but only small surface sections can be characterized and the charging process can only happen in a standardized way. If the charge of a single particle must be evaluated, techniques inspired by characterization of particle movement or flow visualization can be used. In all cases, charged particles in motion are deflected in an electrical field depending on the ratio of mass to charge. In a pulsed electrical field, the frequency of the oscillating particle corresponds to the charge of the particle. The motion is measured by laser doppler velocimetry (Mazumder et al., 1991; Baron et al., 2011; Alois et al., 2017). In homogenous electrical fields, the charge-induced motion of particles can be visualized by consecutive images (Shin and Lee, 2002; Chull Ahn et al., 2004). The advantage of a particle-based charge measurement is the ability to calculate the charge distribution in a powder.

If particles are charged due to motion, a statistical contact probability between particles and the particle-wall has to be assumed, and the charge of all particles should be distributed. Furthermore, this distribution is also influenced by the colliding surface of the particles, potentially leading to eradication or single-sided increase of the particle charge after a bipolar charging step (Grosshans and Papalexandris, 2017). For large homogenous particles, charging and discharging is described by a combination of two different normal distributions (Haeberle et al., 2018). Conveyed particles also showed weight-normal distributions for chard silica and glassy carbon particles. An increase in gas velocity leads to a broadening of the charge distribution (Chull Ahn et al., 2004). Both cases show ideal particulate systems with probably very similar surface properties of individual particles. However, if triboelectric charging is to be used as a tailor-made tool to separate fine powders at a microscale size due to their triboelectric changing ability, a process-oriented measurement setup is needed to evaluate the possibility of powders for separation, as well as to design technical devices that incorporate the influences of different particle morphologies.

To gain a deeper insight into the charging mechanism and subsequent separation properties of powders of organic origin, a new measurement setup was designed. In order facilitate good comparability, the particle-charge measurement setup should have a similar design to earlier the described separation setups (Wang et al., 2014, 2015; Landauer and Foerst, 2018; Landauer et al., 2019). Furthermore, simultaneous measurement of a large number of positively and negatively charged particles is necessary. The designed setup should establish a basis for investigating the charge distribution of organic powders and their mixtures to evaluate the ability for separation. Starch granules from different botanical origin such as potato or corn, show dissimilar granular morphologies (Jane et al., 1994; Singh et al., 2003). Therefore, if particle morphology influences the triboelectric charging ability, the charge distribution of starch granules from different botanical origin might show different patterns. Consequently, binary mixtures of starch from different origins and proteins might show different charge distributions, as well as the influence of particle morphology upon triboelectric charging and subsequent separation.

2. MATERIALS AND METHODS

2.1. Materials

Whey protein isolate with a protein content of 97.6 wt.% dry matter was purchased from Davisco Foods International, USA. Barley starch was purchased from Altia, Finland, with protein content below 0.5 wt.% and a starch content of 97 wt.% dry matter. Corn and potato starch were purchased with an analytical grade from Merck, Germany.

2.2. Methods

2.2.1. Particle Charging

To measure the charge of single particles on the micrometer scale, a micro particle tracking velocimetry (μ-PTV) setup was developed. **Figure 1** shows the experimental setup. The principle design is similar to the laboratory-scale separation unit shown in Landauer and Foerst (2018) and Landauer et al. (2019). Approximately 10 mg of powder is dispersed in a nitrogen stream using a Venturi nozzle and conveyed through a tube (Polymethylmethacrylat) with an inner diameter of 3 mm and a length of 139 mm. Such a small amount of powder does not strongly affect the homogeneity of the electrical field and the particle concentration in the measuring area is low. Hence,

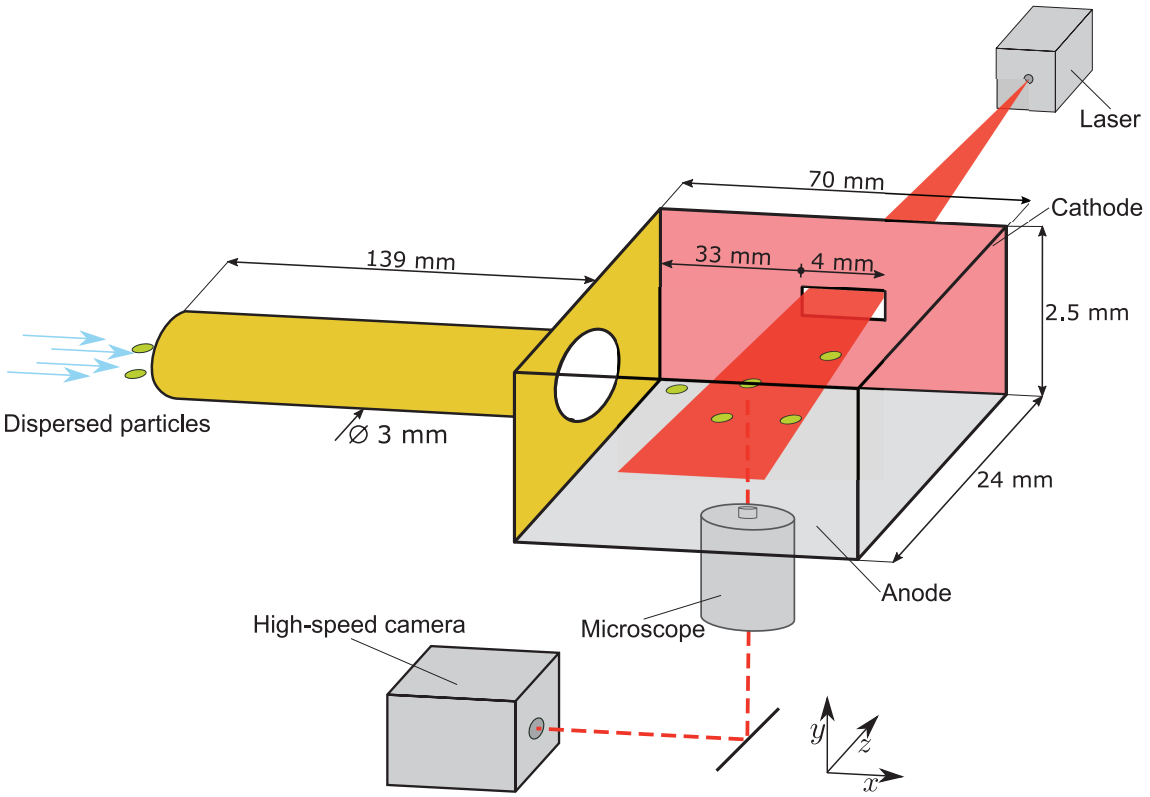

FIGURE 1 | Experimental setup of the charging tube and the separation chamber and the micro particle tracking velocimetry (μ-PTV) setup to estimate the subsequent single-particle charge. The μ-PTV setup consists of a microscope with a high-speed camera and a sliced laser.

particle collisions that would be seen on the deviation of the path, can be excluded. The volumetric flow rate was adjusted to $\dot{V} = 0.8\,\mathrm{m^3\,h^{-1}}$. For all investigated powders, the charging conditions and the pretreatment were equal and thus differences in the charge distribution due to the setup and environmental conditions can be excluded.

2.2.2. Particle Separation and μ-PTV

In the separation chamber, a homogeneous electrical field is applied perpendicular to the particle flow direction. To track the particle motion within the electrical field, a μ-PTV system is applied in the separation chamber. Therefore, the flow conditions in the separation chamber are adjusted to laminar flow (Re = 1,013). A He-Ne laser beam (Head 633-5P, Linos, Germany) with a diameter of 0.8 mm and a wavelength of $\lambda = 632.8\,\mathrm{nm}$ diverged by a cylindrical lens to a light sheet enters the separation chamber through a small slot in one electrode, which is in the same plane as the center of the tube. In order to track the particles, a high-speed camera (Phantom Miro 310, Vision Research, USA) with a frame rate of 3.200 Hz and an exposure time of 40 µs is used in combination with an inverse microscope (DM IRB, Leica Microsystems, Germany) at a magnification of 25x. The electrical field strength was set to $227\,\mathrm{kV\,m^{-1}}$. The middle region of the separation chamber was chosen as measuring area for the particles in order to avoid a non-homogenous electrical field. The relative permittivity of the used particles and gas are in the same range. Therefore, no influence of dielectrophoretic forces can be assumed. The resulting images show the trajectories of charged particles in the electrical field of the separation chamber.

Figure 2 shows a schematic representation of the images received in the μ-PTV setup. The transparent green path was recorded with the camera. Within the homogeneous electrical field between the cathode and the anode, charged particles have a constant velocity $\vec{v_0}$ along the abscissa and an accelerated motion $\vec{v_{el}}$ along the ordinate. The resulting change of site $\frac{\partial \vec{r}}{\partial t}$ (1) yields a parabolic trajectory $\vec{r(t)}$ (3). The acceleration $\vec{a_{el}}$ of a particle of mass m carrying the charge q is induced by the electrical field strength $\vec{E}$ as the ratio of the voltage U and the distance of the electrodes d_p (2).

$$\frac{\partial \vec{r}}{\partial t} = \begin{pmatrix} \frac{\partial x}{\partial t} \\ \frac{\partial y}{\partial t} \end{pmatrix} = \begin{pmatrix} v_0 \\ \frac{\partial v_{el}}{\partial t} \end{pmatrix} = \begin{pmatrix} v_0 \\ a_{el} t \end{pmatrix} \tag{1}$$

$$\vec{a_{el}} = \frac{Uq}{\vec{d_p} \overline{m}} \tag{2}$$

$$\vec{r}(t) = \begin{pmatrix} v_0 t \\ \frac{U}{2 \overline{m} d_p} q t^2 + y_0 \end{pmatrix} \tag{3}$$

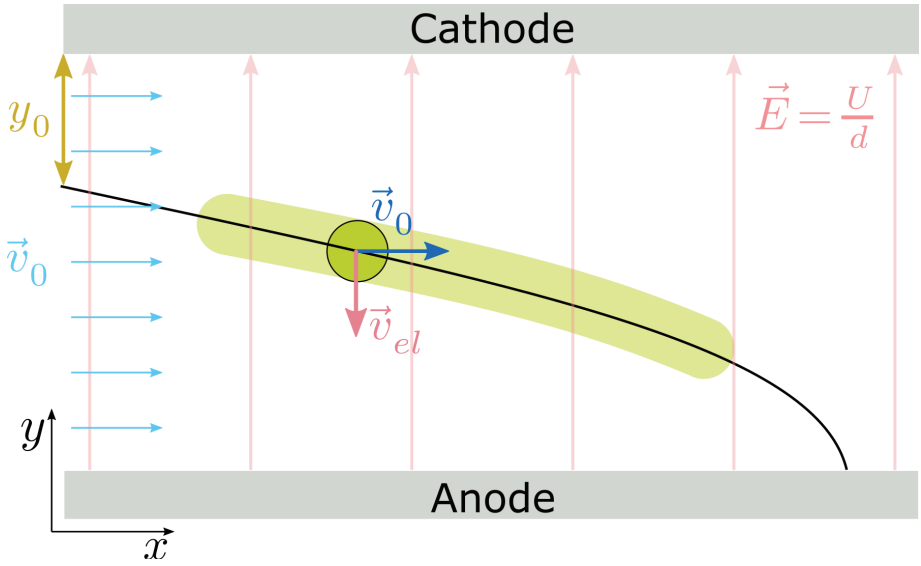

FIGURE 2 | Scheme representing the evaluation from the images received in the μ-PTV setup including a charged particle (green) and the calculated trajectory of a single particle according Equation (3) with the recorded trajectory (transparent green) due to the adjusted exposure time. The black line indicates the resulting trajectory of a charged particle in the homogeneous electrical field $\vec{E}$ at a constant gas velocity $\vec{v_0}$. Velocity vectors attaching on the center of a particle indicate the motion in two spatial directions.

To calculate the charge of each particle image processing of the images showing the path lines is used. First, to reduce *salt and pepper noise*, a linear median filter is used; Gaussian smoothing with $\sigma = 1.5$ is then employed to reduce further noise. Subsequently, the images are binarised using *adaptive thresholding*. These images are transformed into a skeleton and the resulting path lines are fitted to Equation (3) using the method of least squares (**Figure 2**, black line). The mass of one particle is calculated using the mean particle size and density. On raw images, no particles with a clearly detectable contour were visible, because only path lines were recorded. This contour is sharp. Therefore, it was impossible to calculate particle size based on the recorded path lines. Image processing is automated using MATLAB (MathWork, USA) in order to analyse high numbers of particles. Error bars of the charge distributions due to the variability of the particle size distribution were calculated according the standard derivation of the particle size distribution.

2.2.3. Flow Simulation

In order to verify the assumption that turbulent flow dominates in the charging tube and laminar flow in the separation chamber, a CFD study using ANSYS Fluent, (ANSYS, Inc., USA) was carried out. In the CFD study the half of the symmetric geometry was simulated using a standard k-ϵ model with a standard wall function.

2.2.4. Particle Characterization

To measure the particle size distribution of the powders, a laser diffraction system HELOS (Sympatec, Germany) with the RHODOS dispersing unit is used. True density is evaluated using a gas pycnometer (Accupyc 1330, Micromeritics Instrument Corp., USA). Scanning electron microscope (SEM) images were created using a JEOL JSM-IT100 (Japan) with a secondary electron detector at an acceleration voltage of 5 kV.

3. RESULTS

3.1. Velocity and Turbulence Profile

Figure 3A shows the velocity profile and **Figure 3** the turbulence intensity **B** $u' = \sqrt{\frac{2}{3}k}$ calculated by the turbulence kinetic energy k. High turbulence intensities u' indicate high Reynolds numbers, so direct effects of viscosity are negligibly small (Pope, 2000). The velocity profile in the charging tube shows slight differences between *inlet* and *outlet* of the tube, which is recorded six times the diameter after/before the inlet/outlet of the charging tube. In the center of the tube a gas velocity of 38 m s^{-1} is determined and high turbulence intensity is calculated. In contrast, the gas velocity in the separation chamber and especially at the inlet, middle, and outlet is 5 m s^{-1}. This substantiates the assumption that there is a homogenous gas velocity [see **Figure 2** and Equation (1)]. Drag force perpendicular to the flow direction could be excluded according to a Stokes number estimation.

3.2. Particle Characterization

Figure 4A shows the particle size distribution of the fine powders. Particle sizes of barley and corn starch are narrowly distributed between 4 and 40 μm. In contrast, potato starch and whey protein show a broader particle size distribution. **Figure 4B** shows the particle size distribution of starch-protein mixtures containing 15 wt.% protein. **Table 1** shows a summary of the mean particle sizes, which were used to calculate the mean mass and the standard deviation of each particle size distribution. All distributions show a narrow size range. **Table 1** summarizes the

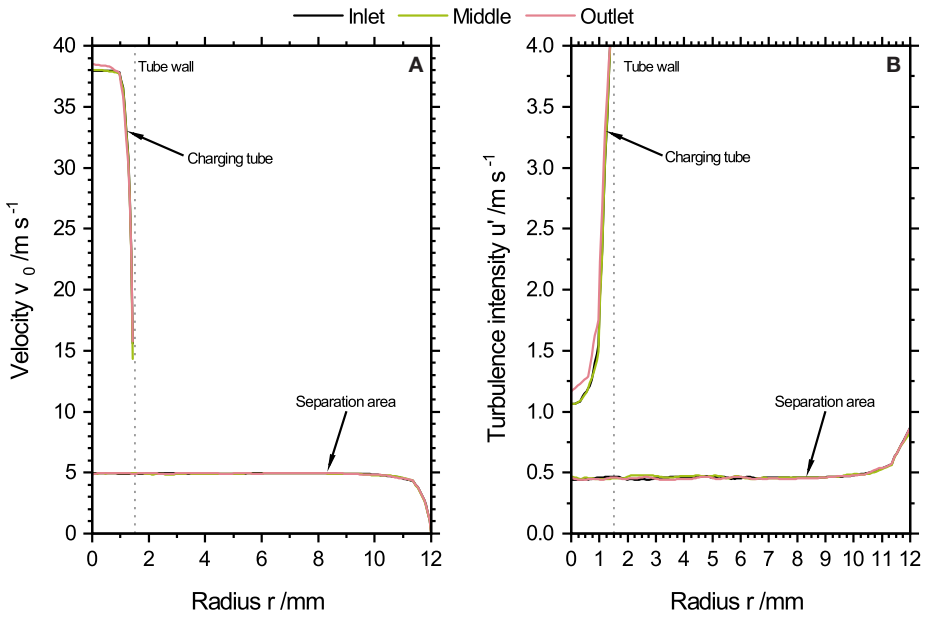

FIGURE 3 | Velocity **(A)** and turbulence intensity **(B)** profile of the flow in the charging tube and the separation chamber. In the charging tube, high velocities and turbulence intensities were detected. In the separation/measuring chamber, moderate velocities and turbulence intensities were found. In the tube, a slight difference in the flow profiles between start (after six times the tube diameter after the beginning of the tube) and end (before six times the tube diameter of the end of the tube) is visible. In the measuring zone (positions are set due to the position of the gap for the laser (**Figure 1**), no differences were found.

mean particle size and the standard deviation of the particle size distribution indicating the width of the distribution. Based on the standard deviation of the particle size distribution, the variation of the mean mass used for the estimation of the particle charge is approximately 4 times the mean. The mean mass $\overline{m}$ of an individual particle is calculated from the mean particle size $x_{50,3}$ and the true density under the assumption of spherical particles. The mean mass $\overline{m}$ of the individual particles is necessary to fit the recorded trajectories with Equation (3).

3.3. Charge Distribution of Raw Powder

Figure 5 shows the charge distribution of both positively and negatively charged barley starch particles. Positively charged particles show a trimodal charge distribution with peaks from 10^{-2} to 5×10^{-1} nC, 2 to 2×10^{1} nC, and 2×10^{2} to 3×10^{4} nC. Positively charged barley starch particles show a monomodal charge distribution with a very wide range of charges from 10^{-3} to 10^{3} nC. The maximum of the relative frequency is located at 4 nC. The charge range of the negatively charged particles is smaller than that for positive ones.

Error bars indicate the variance of particle charge due to the variance in the particle size distribution (cf. **Table 1**). In order to improve readability of the figure in all further charge distributions show no error bars. For all investigated powders the charge distributions including error bars are shown in **Figure 1S** to point out that the charge distributions have a variance.

Different findings were obtained by analysing the charge distribution of protein powder shown in **Figure 6**. Positively and negatively charged particles show the same charge distribution with a mean charge of 50 nC. Furthermore, the span of the charge distribution has a narrow size range from 10^{-1} to 10^{4} nC.

Figure 7 shows a compilation of the charge distributions for all used raw powders. Negatively charged particles show a broad overlap and the monomodal distributions have the same shape. Potato starch particles have the highest charge and only a small number of particles possess a low negative charge (**Table 2**). Corn starch and protein particles have similar distributions for negatively charged particles. Barley starch particles show the smallest negative charge. By contrast, positively charged particles show completely different charge distributions. Particles of different origins do not overlap in a wide charge range. Besides barley starch, potato and corn starch also have trimodal and bimodal charge distributions, respectively. The highest positive charge is observed for potato starch followed by corn starch, barley starch, and protein. Corn, barley starch, and protein are on the same order of magnitude (**Table 2**). Thus, positively charged particles show a broad charge range depending on the used powder, whereas for negatively charged particles, a congruence in the charge distribution of all investigated powders can be observed.

Table 2 summarizes the means of each charge distribution, the difference of the means, and number of the measured particles. For raw powders, the mean of charge for positively and negatively charged particles are on almost the same order of magnitude. Differences in the mean are positive for all raw materials, indicating that positively charged particles carry a higher charge. Furthermore, this observation is underlined by comparing the numbers of simultaneously measured positively and negatively charged particles. Negatively charged particles

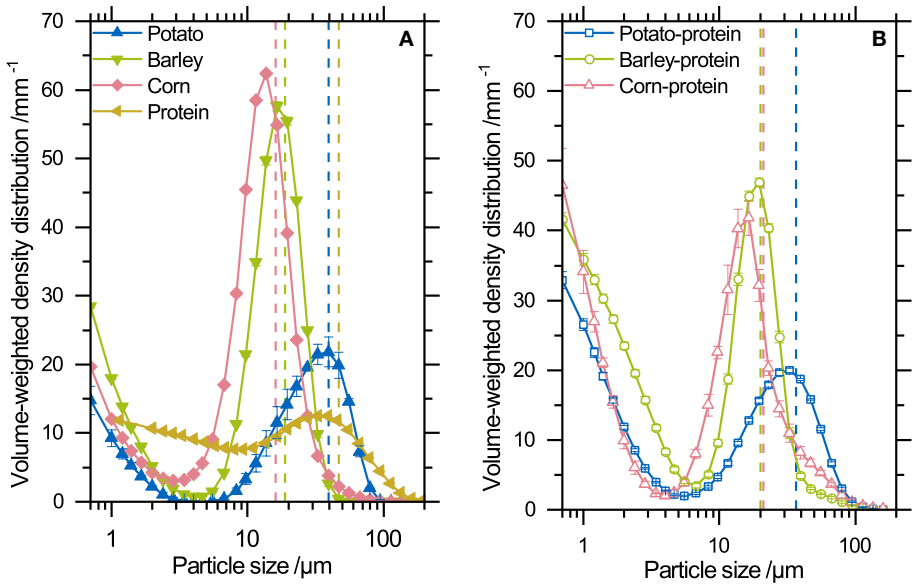

FIGURE 4 | (A) Particle size distributions of the tested powders: potato, barley, and corn starch and whey protein. Each mean particle size $x_{50,3}$ is indicated by dashed lines. **(B)** Particle size distribution of starch-protein mixtures containing 15 wt.% whey protein and potato, barley, and corn starch, respectively. Mean particle sizes are indicated by dashed lines.

TABLE 1 | Summary of the mean particle size and the related standard deviation of the particle size distribution.

	Mean particle size /µm	Standard deviation /µm
Potato	39.5	10.7
Barley	18.9	6.5
Corn	15.9	6.2
Protein	46.8	16.8
Potato-Protein	36.6	15.7
Barley-Protein	20.4	11.0
Corn-Protein	21.1	11.2

possess an average percentage of the measured particle number of (87 ± 4) % and are thus attracted to the anode. Consequently, positively charged particles have an amount of (13 ± 4) %. Until now, the charge distributions of the four different raw powders exhibited similar findings for positively and negatively charged particles. The negatively charged particles showed a uniform monomodal charge distribution with broad overlaps, whereas positive charge was distributed unevenly over a wide range. The difference in the mean charge is always positive and the proportions of positively and negatively charged particles is uniform for all materials.

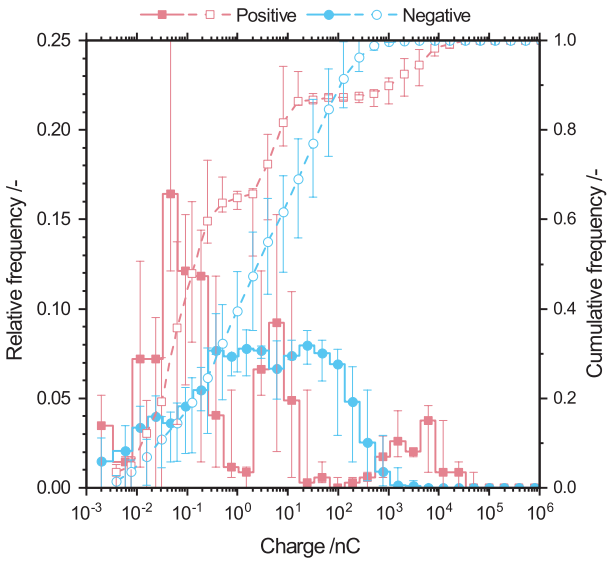

FIGURE 5 | Relative and cumulative frequency distribution of positively and negatively charged barley starch particles. Positively charged particles show a trimodal distribution whereas negatively charged particles show a broad monomodal charge distribution. The charge of each particle was accumulated using a geometric series of basis 2. Error bars indicating the variation of charge due to the particle size distribution.

3.4. Charge Distribution of Powder Mixtures

Figure 8 shows the charge distribution of starch-protein mixtures containing 15 wt.% protein and starch from different origins. Negatively charged particles have monomodal distributions. The corn-protein mixture charge distribution has the highest negative mean charge; by contrast, barley-protein mixture has the lowest. These findings are differ from those for the mean charges of raw

powders. Potato starch has the highest negative charge (**Table 2**). Charging of binary powders leads to an increase of negative charge, as indicated by an increase in the mean charge. As expected from the raw powder, barley starch has the highest number of weakly charged particles. Highly charged particles from raw potato starch (between -10^2 and -10^4 nC) are not visible in charging experiments using the starch-protein mixture. Corn starch-protein mixtures show a decrease in the relative frequency of particles with a charge between to -10^2nC and an increase in those with a charge between -10^2 and -10^4 nC.

Positively charged particles in **Figure 8** exhibit different shapes of charge distributions compared to negatively charged ones. Starch-protein mixtures prepared with potato and barley starch had bimodal charge distributions with peaks approximately at the same positive charges of 1 and 10^2 nC. By contrast, corn starch-protein mixtures have a trimodal charge distribution. Two peaks in potato and barley starch-protein mixtures are at approximately the same charge. The third peak is located at 2×10^4 nC. The positive net charge for starch-protein mixtures increases

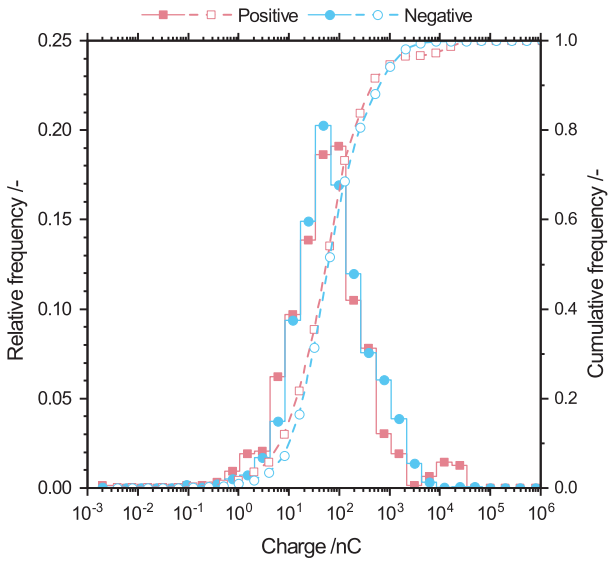

FIGURE 6 | Relative and cumulative frequency distribution of positively and negatively charged whey protein particles. Such particles show the same monomodal charge distribution with a mean charge of 50 nC.

TABLE 2 | Summary of the first moment $M_{1,0}$ of each charge distribution and the difference of the first moments $\Delta M_{1,0}$, indicating the net charge and the charge difference between positively and negatively charged particles, respectively. Furthermore, the numbers of particles evaluated to calculate the positive and negative charge distributions are displayed.

	$M_{1,0}$ /nC	$\Delta M_{1,0}$ /nC	Particle number /-	Total particle number/-
Potato	4.61×10^4	4.33×10^4	300	3,874
	-2.86×10^3		3,574	
Barley	6.69×10^2	6.23×10^2	347	2,430
	-4.51×10^1		2,083	
Corn	9.19×10^2	7.16×10^2	94	792
	-2.03×10^2		698	
Protein	6.68×10^2	3.47×10^2	628	2,957
	-3.21×10^2		2,329	
Potato-Protein	2.65×10^3	2.12×10^3	94	792
	-5.34×10^2		698	
Barley-Protein	3.72×10^3	3.46×10^3	300	3,181
	-2.62×10^2		2,881	
Corn-Protein	7.04×10^4	6.67×10^4	626	4,381
	-3.67×10^3		3,755	

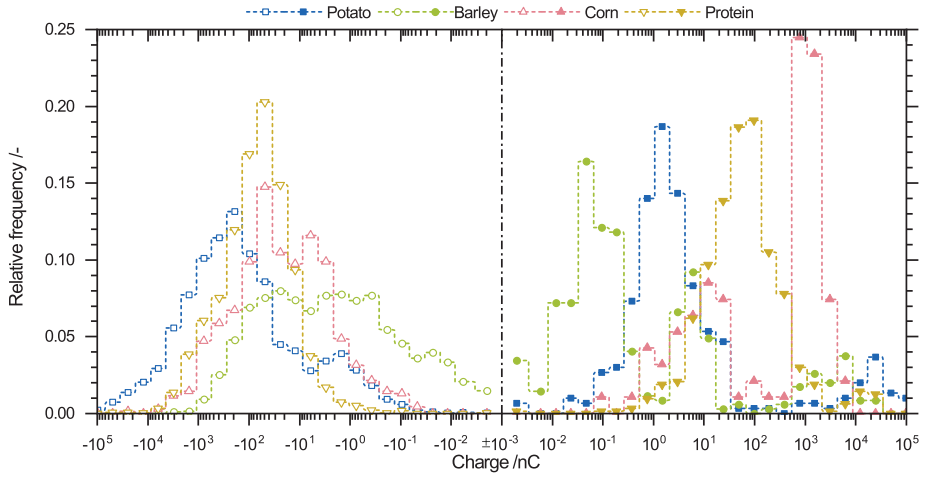

FIGURE 7 | Charge distribution of potato, barley, and corn starch, as well as whey protein powder. After triboelectric charging negatively (open symbols) and positively (closed symbols) charged particles were found. Negatively charged particles show similar monomodal charge distributions, whereas positively charged particles show multimodal distributions.

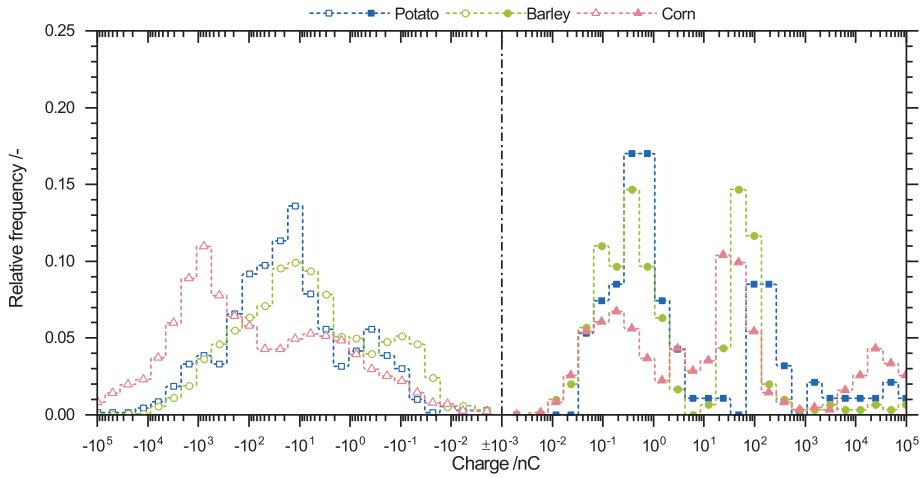

FIGURE 8 | Relative frequency densities of positively and negatively charged particles originating from starch-protein mixtures containing 15 wt.% protein and potato, barley, and corn starch. Negatively charged particles have a wide monomodal charge distribution, whereas positively charged particles show a trimodal distribution.

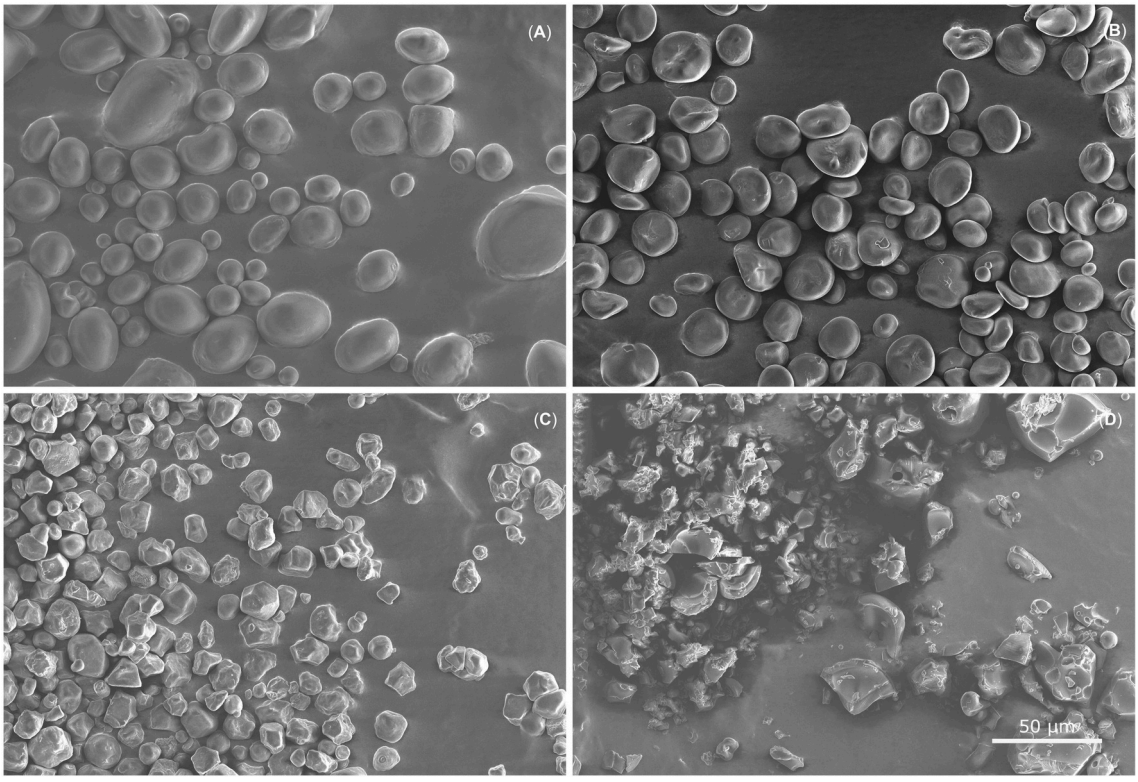

FIGURE 9 | Scanning electron microscope images show raw powders of potato starch **(A)**, barley starch **(B)**, corn starch **(C)**, and protein **(D)**. Different particle morphologies between the different starch powders are clearly visible. Potato starch particles are both round and elliptical with a very smooth surface, whereas barley starch consists of round and lenticular particles with fine cracks on the smooth surfaces. Corn starch forms polyhedral particles with rough surfaces. Protein shows no principal particle morphology and different surface roughnesses are visible.

from potato to barley to corn starch. The new peak at 10^2 nC occurs where raw protein powder has its peak (**Figure 7**). This may indicate that protein as well as starch are positively charged.

Comparison of the charge distributions of binary mixtures of starch and protein an raw powders show that negatively and positively charged particles behave similarly. Negatively charged particles in both cases have monomodal and widely

overlapping charge distributions. Positively charged particles form multimodal distributions. However, powder mixtures show uniform modes for all different starch particles, which may indicate the influence of protein particles on the amount of charge exchange onto positively charged particles.

4. DISCUSSION

The guiding principle of the triboelectric effect is that if two surfaces come into contact and are separated subsequently, opposite charges remains on each surface. Thus, bipolar charging occurs. To examine triboelectric surface charging of fine powders with mean particle sizes between 20 and 40 µm (**Figure 4**), a novel experimental setup was established. This setup enables simultaneous measurement of the charges of positively and negatively charged particles; hence, a charge distribution for both positively and negatively charged particles can be calculated. However, some assumptions were made to calculate the charge of each particle. In order to calculate the mass of each particle, the mean of the volume-size distribution was used, which might lead to either an overestimation or underestimation of the particle's net charge. To remedy this inaccuracy, further work on optical resolution and illumination must be done. By improving the experimental setup to subsequently estimate the particle size and charge of each single particle, the direct correlation between size and charge can be evaluated. This might lead to deeper insights into the dependency of charge and particle size.

Experiments show completely different distribution patterns for positively and negatively charged particles. Negatively charged particles have monomodal charge distributions whereas positive ones show multimodal distributions. All pure-starch powders showed different charge distributions for positively and negatively charged particles. The empirical findings of monomodal and multimodal charge distributions are not deducible from previous studies. Thus, the setup allows to show another mosaic stone of triboelectric charging. In order to gain a deeper understanding of this pattern further studies are needed. It is well-known that, for bimodal powders, smaller particles become predominantly negatively and larger particles positively charged if both are present and particle-wall interaction is excluded (Lacks and Levandovsky, 2007). A decrease in mean particle size might accordingly lead to an increase in negative charge, but potato starch particles with the highest mean particle size show the highest negative charge (**Table 2**). However, it cannot be ruled out that other particle characteristics, such as morphology and crystallinity may influence triboelectric charging. SEM images (**Figure 9**) show different morphologies of the used pure-starch powders. It is well-known that starch from different botanical origins have different particle morphologies (Jane et al., 1994; Singh et al., 2003). The difference in morphology is influenced by the chemical structure of the monomers (amylose, amylopectin) forming the particles and their crystalline structure which molds the architecture and the surface properties of starch particles (Tang et al., 2006). This morphological difference might lead to different charge distributions. In comparison to starch particles, protein particles show bipolar charging (**Figure 6**); here, no clear difference in morphology is visible, as it is usual for powders performed by grinding agglomerates. Besides the morphological differences the between different powders, for every powder different particle sizes are present so an influence of the particle size could not be excluded.

For powder mixtures containing starch and protein, the same findings were made (**Figure 8**). The negative charge distribution is monomodal whereas the positive is trimodal. However, comparing powder mixtures with pure powders, same peaks are only visible for barley. Hence, binary powder mixtures lead to uniform charge distributions. The partially uniform distributions for both negatively and positively charged particles might suggest independence from the initial particle morphology, as shown for pure powders. Thus, the differences in the triboelectric charging abilities between starch and protein are more pronounced than the inhomogeneities of starch particles different botanical origins (**Figure 9**). However, an increase in the charge of the binary mixtures is not observed for all powder mixtures as should be expected (**Table 2**) (Forward et al., 2009). It is likely that the triboelectric charging properties of pure powders and binary mixtures are more complex and comprise different factors such as the chemical composition or morphology of the surfaces.

The experimental conditions for all carried out experiments were identical. All investigated powders had the same pretreatment, charging (turbulence intensity, flow rate, particle concentration), and environmental conditions. Thus, the influence of well-known influencing factors like humidity, particle interaction parameters, distinction between particle-particle and particle-wall interaction (Landauer et al., 2019), and reaching the saturation of charge on the particles were deliberately excluded in the proposed discussion. Since triboelectric charging is a surface phenomenon, it is assumed that the differences in morphology and composition of the surface influence the triboelectric charging and thus lead to differences in charge distributions. However, the setup enables to investigate these well-known influencing factors in further studies to gain a deeper insight in triboelectric charging.

5. CONCLUSION

In the present study, a novel measurement setup is presented to evaluate the charge of single particles in a size range between 1 and 100 μm. The setup based on a μ-PTV configuration enables each particle to be tracked and to have its associated charge calculated by the mean mass of the initial particle size distribution. The particles are dispersed in the gas phase for charge estimation; thus, this method can be adjusted to estimate the charge of all particles dispersed in the gas phase. However, uncertainties in the evaluation arise due to the unknown relationship between the recorded trajectory and the exact particle size or mass. To overcome the deficiency of this setup, the velocity in the measuring area has to be reduced but simultaneously the turbulence intensity, which ensures a high particle-particle interaction rate, should be kept constant. For all calculations, the mean particle mass

assuming a homogeneous true density of the used powders was employed. Nevertheless, the novel measurement setup enables the charge distributions of triboelectrically charged powders to be calculated.

Charge distributions of large portions of all investigated triboelectrically charged powders showed the same pattern. Negatively charged particles have a monomodal distribution whereas positively charged ones have a multimodal one. These findings were the same for both raw powders and starch-protein mixtures. Comparing different raw starch powders, different triboelectric charging properties are visible. It is assumed that different particle morphologies may be the reason, because all further influence parameters were the same for performed experiments. Analysis of the starch-protein mixtures exhibits no such tendency of different particle morphologies. It is likely that particle-particle interaction of particles of different botanical origin mask the impact of particle morphologies and sizes. The developed setup to estimate the single particle charge can be a valuable tool to gain a deeper understanding of triboelectric charging. In further studies the setup can help to investigate several questions in triboelectric charging like influence of interaction rate, charging time or saturation of charge.

AUTHOR CONTRIBUTIONS

JL did the conception and design of the study and wrote the manuscript. ST did the experimental works. PF participated to the writing and supervised the work.

ACKNOWLEDGMENTS

The authors would like to thank Cornelia Eder for the fruitful discussion by creating the experimental setup, and Heiko Briesen for the opportunity to carry out this work.

SUPPLEMENTARY MATERIAL

The Supplementary Material for this article can be found online at: https://www.frontiersin.org/articles/10.3389/fchem.2019.00323/full#supplementary-material

REFERENCES

Alois, S., Merrison, J., Iversen, J. J., and Sesterhenn, J. (2017). Contact electrification in aerosolized monodispersed silica microspheres quantified using laser based velocimetry. *J. Aerosol Sci.* 106, 1–10. doi: 10.1016/j.jaerosci.2016.12.003

Anderson, R., Gathman, S., Hughes, J., Björnsson, S., Jónasson, S., Blanchard, D. C., et al. (1965). Electricity in volcanic clouds: investigations show that lightning can result from charge-separation processes in a volcanic crater. *Science* 148, 1179–1189. doi: 10.1126/science.148.3674.1179

Baron, P. A., Mazumder, M. K., Cheng, Y.-S., and Peters, T. M. (2011). "Real-time techniques for aerodynamic size measurement," in *Aerosol Measurement, Vol. 36*, eds P. Kulkarni, P. A. Baron, and K. Willeke (Hoboken, NJ: John Wiley & Sons, Inc.), 313–338.

Baytekin, H. T., Baytekin, B., Incorvati, J. T., and Grzybowski, B. A. (2012). Material transfer and polarity reversal in contact charging. *Angew. Chem.* 124, 4927–4931. doi: 10.1002/ange.201200057

Baytekin, H. T., Patashinski, A. Z., Branicki, M., Baytekin, B., Soh, S., and Grzybowski, B. A. (2011). The mosaic of surface charge in contact electrification. *Science* 333, 308–312. doi: 10.1126/science.1201512

Bunchatheeravate, P., Curtis, J., Fujii, Y., and Matsusaka, S. (2013). Prediction of particle charging in a dilute pneumatic conveying system. *AChE J.* 59, 2308–2316. doi: 10.1002/aic.14025

Burgo, T. A. L., Silva, C. A., Balestrin, L. B. S., and Galembeck, F. (2013). Friction coefficient dependence on electrostatic tribocharging. *Sci. Rep.* 3:2384 doi: 10.1038/srep02384

Chull Ahn, Y., Hyun Kim, D. O., Chan Kim, S., Gene Hwang, E. U., Geon Lee, C., Tae Kim, G. I., et al. (2004). Measurement and control of triboelectrically charged silica and glassy carbon particles. *Part. Sci. Technol.* 22, 305–320. doi: 10.1080/02726350490501727

Ducati, T. R. D., Simoes, L. H., and Galembeck, F. (2010). Charge partitioning at gas-solid interfaces: humidity causes electricity buildup on metals. *Langmuir* 26, 13763–13766. doi: 10.1021/la102494k

Eichas, K., and Schönert, K. (1992). Trennung feinkörniger zweikomponentiger mischungen im elektrostatischen feld nach triboaufladung. *Chem. Ing. Tech.* 64:840. doi: 10.1002/cite.3306409104

Farrell, W. M. (2004). Electric and magnetic signatures of dust devils from the 2000–2001 matador desert tests. *J. Geophys. Res.* 109:5427. doi: 10.1029/2003JE002088

Forward, K. M., Lacks, D. J., and Sankaran, R. M. (2009). Triboelectric charging of granular insulator mixtures due solely to particle−particle interactions. *Indus. Eng. Chem. Res.* 48, 2309–2314. doi: 10.1021/ie8004786

Fotovat, F., Bi, X. T., and Grace, J. R. (2017). Electrostatics in gas-solid fluidized beds: a review. *Chem. Eng. Sci.* 173, 303–334. doi: 10.1016/j.ces.2017.08.001

Ghori, M. U., Supuk, E., and Conway, B. R. (2014). Tribo-electric charging and adhesion of cellulose ethers and their mixtures with flurbiprofen. *Eur. J. Pharm. Sci.* 65, 1–8. doi: 10.1016/j.ejps.2014.08.010

Grosshans, H., and Papalexandris, M. V. (2016). Large eddy simulation of triboelectric charging in pneumatic powder transport. *Powder Technol.* 301, 1008–1015. doi: 10.1016/j.powtec.2016.07.031

Grosshans, H., and Papalexandris, M. V. (2017). A model for the non-uniform contact charging of particles. *Powder Technol.* 305, 518–527. doi: 10.1016/j.powtec.2016.10.024

Haeberle, J., Schella, A., Sperl, M., Schröter, M., and Born, P. (2018). Double origin of stochastic granular tribocharging. *Soft Matter* 14, 4987–4995. doi: 10.1039/C8SM00603B

Hussain, T., Kaialy, W., Deng, T., Bradley, M. S. A., Nokhodchi, A., and Armour-Chelu, D. (2013). A novel sensing technique for measurement of magnitude and polarity of electrostatic charge distribution across individual particles. *Int. J. Pharm.* 441, 781–789. doi: 10.1016/j.ijpharm.2012.10.002

Ireland, P. M. (2010). Triboelectrification of particulate flows on surfaces: part I — experiments. *Powder Technol.* 198, 189–198. doi: 10.1016/j.powtec.2009.11.017

Jane, J.-l., Kasemsuwan, T., Leas, S., Zobel, H., and Robyt, J. F. (1994). Anthology of starch granule morphology by scanning electron microscopy. *Starch - Stärke* 46, 121–129. doi: 10.1002/star.19940460402

Jiang, W., Li, H., Liu, Z., Li, Z., Tian, J., Shi, B., et al. (2018). Fully bioabsorbable natural-materials-based triboelectric nanogenerators. *Adv. Mater.* 30:e1801895. doi: 10.1002/adma.201801895

Kolehmainen, J., Ozel, A., Boyce, C. M., and Sundaresan, S. (2017). Triboelectric charging of monodisperse particles in fluidized beds. *AIChE J.* 63, 1872–1891. doi: 10.1002/aic.15541

Korevaar, M. W., Padding, J. T., van der Hoef, M. A., and Kuipers, J. A. M. (2014). Integrated DEM–CFD modeling of the contact charging of pneumatically conveyed powders. *Powder Technol.* 258, 144–156. doi: 10.1016/j.powtec.2014.03.020

Lacks, D. J., and Levandovsky, A. (2007). Effect of particle size distribution on the polarity of triboelectric charging in granular insulator systems. *J. Electrostat.* 65, 107–112. doi: 10.1016/j.elstat.2006.07.010

Landauer, J., Aigner, F., Kuhn, M., and Foerst, P. (2019). Effect of particle-wall interaction on triboelectric separation of fine particles in a turbulent flow. *Adv. Powder Technol.* 30, 1099–1107. doi: 10.1016/j.apt.2019.03.006

Landauer, J., and Foerst, P. (2018). Triboelectric separation of a starch-protein mixture – impact of electric field strength and flow rate. *Adv. Powder Technol.* 29, 117–123. doi: 10.1016/j.apt.2017.10.018

Mareev, E. A., and Dementyeva, S. O. (2017). The role of turbulence in thunderstorm, snowstorm, and dust storm electrification. *J. Geophys. Res.* 122, 6976–6988. doi: 10.1002/2016JD026150

Mather, T. A., and Harrison, R. G. (2006). Electrification of volcanic plumes. *Surveys Geophys.* 27, 387–432. doi: 10.1007/s10712-006-9007-2

Matsuyama, T., and Yamamoto, H. (1994). Charge transfer between a polymer particle and a metal plate due to impact. *IEEE Trans. Indus. Appl.* 30, 602–607. doi: 10.1109/28.293706

Mazumder, M. K., Ware, R. E., Yokoyama, T., Rubin, B. J., and Kamp, D. (1991). Measurement of particle size and electrostatic charge distributions on toners using e-spart analyzer. *IEEE Trans. Indus. Appl.* 27, 611–619. doi: 10.1109/28.85472

Mehrani, P., Murtomaa, M., and Lacks, D. J. (2017). An overview of advances in understanding electrostatic charge buildup in gas-solid fluidized beds. *J. Electrostat.* 87, 64–78. doi: 10.1016/j.elstat.2017.03.005

Mirkowska, M., Kratzer, M., Teichert, C., and Flachberger, H. (2014). Atomic force microscopy as a tool to explore triboelectrostatic phenomena in mineral processing. *Chem. Ing. Tech.* 86, 857–864. doi: 10.1002/cite.201400027

Nonnenmacher, M., O'Boyle, M. P., and Wickramasinghe, H. K. (1991). Kelvin probe force microscopy. *Appl. Phys. Lett.* 58:2921. doi: 10.1063/1.105227

Peltonen, J., Murtomaa, M., and Salonen, J. (2018). Measuring electrostatic charging of powders on-line during surface adhesion. *J. Electrostat.* 93, 53–57. doi: 10.1016/j.elstat.2018.03.007

Pérez-Vaquero, J., Quintanilla, M. A. S., and Castellanos, A. (2016). Electric charge limits on settled powders. *J. Appl. Phys.* 119:223302. doi: 10.1063/1.4953649

Pope, S. B. (ed.). (2000). *Turbulent Flows*. Cambridge: Cambridge University Press.

Saini, D., Trigwell, S., Srirama, P. K., Sims, R. A., Sharma, R., Biris, A. S., et al. (2008). Portable free-fall electrostatic separator for beneficiation of charged particulate materials. *Part. Sci. Technol.* 26, 349–360. doi: 10.1080/02726350802084200

Schein, L. B. (1999). Recent advances in our understanding of toner charging. *J. Electrostat.* 46, 29–36. doi: 10.1016/S0304-3886(98)00056-4

Schella, A., Herminghaus, S., and Schröter, M. (2017). Influence of humidity on tribo-electric charging and segregation in shaken granular media. *Soft Matter* 13, 394–401. doi: 10.1039/C6SM02041K

Shin, J.-H., and Lee, J.-K. (2002). Pvc separation and flow visualization of triboeletrostatically charged plastic particles using fluidized bed tribocharger. *Geosyst. Eng.* 5, 25–30. doi: 10.1080/12269328.2002.10541184

Singh, N., Singh, J., Kaur, L., Singh Sodhi, N., and Singh Gill, B. (2003). Morphological, thermal and rheological properties of starches from different botanical sources. *Food Chem.* 81, 219–231. doi: 10.1016/S0308-8146(02)00416-8

Tabtabaei, S., Jafari, M., Rajabzadeh, A. R., and Legge, R. L. (2016). Solvent-free production of protein-enriched fractions from navy bean flour using a triboelectrification-based approach. *J. Food Eng.* 174, 21–28. doi: 10.1016/j.jfoodeng.2015.11.010

Tang, H., Mitsunaga, T., and Kawamura, Y. (2006). Molecular arrangement in blocklets and starch granule architecture. *Carbohydr. Polym.* 63, 555–560. doi: 10.1016/j.carbpol.2005.10.016

Wang, A. E., Gil, P. S., Holonga, M., Yavuz, Z., Baytekin, H. T., Sankaran, R. M., et al. (2017). Dependence of triboelectric charging behavior on material microstructure. *Phys. Rev. Mater.* 1:035605. doi: 10.1103/PhysRevMaterials.1.035605

Wang, J., de Wit, M., Boom, R. M., and Schutyser, M. A. (2015). Charging and separation behavior of gluten–starch mixtures assessed with a custom-built electrostatic separator. *Separ. Purif. Technol.* 152, 164–171. doi: 10.1016/j.seppur.2015.08.025

Wang, J., de Wit, M., Schutyser, M. A., and Boom, R. M. (2014). Analysis of electrostatic powder charging for fractionation of foods. *Innov. Food Sci. Emerg. Technol.* 26, 360–365. doi: 10.1016/j.ifset.2014.06.011

Wang, Z. L. (2013). Triboelectric nanogenerators as new energy technology for self-powered systems and as active mechanical and chemical sensors. *ACS Nano* 7, 9533–9557. doi: 10.1021/nn404614z

Watanabe, H., Ghadiri, M., Matsuyama, T., Maruyama, H., Matsusaka, S., Ghadiri, M., et al. (2007). Triboelectrification of pharmaceutical powders by particle impact. *Int. J. Pharm.* 334, 149–155. doi: 10.1016/j.ijpharm.2006.11.005

Wong, J., Kwok, P. C. L., and Chan, H.-K. (2015). Electrostatics in pharmaceutical solids. *Chem. Eng. Sci.* 125, 225–237. doi: 10.1016/j.ces.2014.05.037

Wu, G., Li, J., and Xu, Z. (2013). Triboelectrostatic separation for granular plastic waste recycling: a review. *Waste Manage.* 33, 585–597. doi: 10.1016/j.wasman.2012.10.014

Yair, Y., Fischer, G., Simões, F., Renno, N., and Zarka, P. (2008). Updated review of planetary atmospheric electricity. *Space Sci. Rev.* 137, 29–49. doi: 10.1007/s11214-008-9349-9

Zhao, H., Castle, G., and Inculet, I. I. (2002). The measurement of bipolar charge in polydisperse powders using a vertical array of faraday pail sensors. *J. Electrostat.* 55, 261–278. doi: 10.1016/S0304-3886(01)00209-1

Conflict of Interest Statement: The authors declare that the research was conducted in the absence of any commercial or financial relationships that could be construed as a potential conflict of interest.

Copyright © 2019 Landauer, Tauwald and Foerst. This is an open-access article distributed under the terms of the Creative Commons Attribution License (CC BY). The use, distribution or reproduction in other forums is permitted, provided the original author(s) and the copyright owner(s) are credited and that the original publication in this journal is cited, in accordance with accepted academic practice. No use, distribution or reproduction is permitted which does not comply with these terms.

2.5. Paper V: Influence of Particle Charge and Size Distribution on Triboelectric Separation – New Evidence Revealed by In Situ Particle Size Measurements (Landauer and Foerst, 2019a)

Brief introduction

It is assumed that particle size has an influence on triboelectric charging. Hitherto, the influence of particle size is examined with spherical particles of two different sizes. Since starch-protein mixtures can be separated in an electrical field, bipolar charging takes place and particle size has only a subordinate role for the polarity of charge; however, the particle size might influence the net charge. The amount of net charge influences the separation position in the separation section. If particle size distribution of starch or protein influences the net charge, particle size distribution might vary along the electrodes. To measure the particle size distribution along the electrodes, the separation chamber was modified to be installed in a laser-diffraction spectrometer. This enables an in-situ determination of the particle size distribution during the separation. Furthermore, agglomeration tendency along the charging tube is investigated using in-situ particle size analysis. To estimate the charge of one particle, which is necessary to be separated in the measuring section, a CFD simulation was carried out. Furthermore, the results of particles size distributions are related to spatially resolved measurements of powder height and protein content along the electrodes.

Study findings

During the charging process no agglomeration occurred. Thus, the separation efficiency and selectivity might not decrease by partial dispersing properties. Particle size distributions near the cathode and the anode are strongly effected by the initial protein content, because a higher amount of finer protein particles (15 wt. % and 30 wt. %) leads to finer particle size distribution on both electrodes. Particle size distributions differ along the electrodes indicting a dependence of particle charge and particle size. The estimation of particle charge by CFD simulation showed that large charge differences were required to separate particles in the different measuring regions. This wide range of particle charges could be also expected due to the roughly homogenous powder height on the cathode and the steep decrease of powder height on the anode. Furthermore, the protein content is decreasing along the cathode.

Conclusion

i No correlation of particle size and charge were detected.

ii A high range of particle charges is formed due to triboelectric charging.

iii Triboelectric separation of binary powder mixtures has a high complexity and particle size might play a minor role.

Author contributions

Johann Landauer did the conception and design of the study, the experimental work, and wrote the manuscript. Petra Foerst participated to the writing and supervised the work.

processes

MDPI

Article

Influence of Particle Charge and Size Distribution on Triboelectric Separation—New Evidence Revealed by In Situ Particle Size Measurements

Johann Landauer * and Petra Foerst

Chair of Process Systems Engineering, TUM School of Life Sciences Weihenstephan, Technical University of Munich, Gregor-Mendel-Straße 4, 85354 Freising, Germany; petra.foerst@tum.de

* Correspondence: johann.landauer@tum.de; Tel.: +49-8161-71-5172

Received: 20 May 2019; Accepted: 15 June 2019; Published: 19 June 2019

Abstract: Triboelectric charging is a potentially suitable tool for separating fine dry powders, but the charging process is not yet completely understood. Although physical descriptions of triboelectric charging have been proposed, these proposals generally assume the standard conditions of particles and surfaces without considering dispersity. To better understand the influence of particle charge on particle size distribution, we determined the in situ particle size in a protein–starch mixture injected into a separation chamber. The particle size distribution of the mixture was determined near the electrodes at different distances from the separation chamber inlet. The particle size decreased along both electrodes, indicating a higher protein than starch content near the electrodes. Moreover, the height distribution of the powder deposition and protein content along the electrodes were determined in further experiments, and the minimum charge of a particle that ensures its separation in a given region of the separation chamber was determined in a computational fluid dynamics simulation. According to the results, the charge on the particles is distributed and apparently independent of particle size.

Keywords: triboelectric separation; particle size distribution; particle charge; binary mixture; in situ particle size measurement; charge estimation

1. Introduction

Electrostatic effects were first recognized by the ancient Greek philosophers, who generated electricity by rubbing amber with fur. Thales of Miletus is often called the discoverer of the triboelectric effect [1,2]; however, this ancient observation has not been completely understood. Triboelectric charging of conductive materials is described by work function [3,4]. At conductor–insulator and insulator–insulator contacts, triboelectric charging has been described with "effective work function" [5,6], electron transfer [7], ion transfer [8,9], and material transfer [10,11]. Furthermore, contact charging is affected by environmental conditions such as humidity [12–14] and physical impact [15–17].

Triboelectric charging is undesired in process engineering because it interferes with pneumatic conveying [18,19], fluidized beds [20,21], mixing [22,23], and tablet pressing [24]. Moreover, it is a surface effect, indicating that particle surface plays a critical role. The known factors affecting triboelectric charging are particle area (indicated by particle size) [25–30], surface roughness [31–33], chemical composition [34], and elasticity (indicated by contact area) [35–38]; however, most experimental studies assumed uniform particles or contact surfaces. In most applications, the particles are not monodispersed and have no defined surface; however, the particles are dispersed in size, surface area, elasticity, crystallinity, and morphology.

To use triboelectric charging and subsequent separation as a tool to separate particles due to their chemical composition, surface morphology, crystallinity, or particle morphology, it is necessary to

understand the influence of particle size distribution or powder composition as well as the influence of non-ideal conditions. All these factors show the necessity of triboelectric separation experiments with real, but defined, powders (like starch and protein) in order to use triboelectric separation to enrich, e.g., protein in lupine flour [39] and to take into account further influencing factors. Furthermore, the use of a starch–protein mixture as a model substrate for triboelectric charging is anticipated to have a possible application to enrich protein out of cereals or legumes. This ability of triboelectric separation has been demonstrated [39–46].

Hitherto, lots of studies have been carried out with well-defined particles or with inhomogeneous and undefined organic systems. Supplementary to these findings, real powders with a defined chemical composition and dispersity in particle size should be investigated. The discussion of influencing factors, such as particle morphology or further particle properties, suggest that particle surface charge is affected by the particle size distribution, in turn influencing the triboelectric charging effect. As the particle charge strongly affects the subsequent separation step, particles with different charges become separated at different regions on the electrodes, depending on the flow profile in the separation chamber and the electric field strength. Therefore, we hypothesize that if particle size (as a proxy of surface area) influences the charging and the subsequent separation properties, then particles of different sizes will be separated at different regions on the electrodes.

2. Materials and Methods

2.1. Materials

Whey protein isolate (Davisco Foods International, Le Sueur, MN, USA) with a protein content of 97.6 wt % was ground as that described in Landauer et al. [47]. Barley starch (Altia, Finland) with a starch content of 97.0 wt % was narrowed in particle size distribution in a wheel classifier (ATP 50, Hosokawa Alpine, Augsburg, Germany) under the conditions described in Landauer et al. [47].

2.2. Methods

2.2.1. Separation Setup

The simple experimental setup, originally demonstrated by Landauer et al. [47,48], comprises of an exchangeable charging section and a rectangular separation chamber. The dispersion of powders added to the gas flow is facilitated by a Venturi nozzle. The charging tube (of diameter 10 mm and length 230 mm) was composed of polytetrafluoroethylene (PTFE). An electrical field strength of 109 V/m was applied to the parallel-plate capacitor in a rectangular separation chamber (46 mm × 52 mm × 400 mm). The protein contents of the binary protein–starch mixtures were varied as 15, 35, and 45 wt %, and were determined as described in [48]. Briefly, the powder was dispersed in NaCl buffer (pH 7, 0.15 M) and the protein concentration was photometrically determined at 280 nm. To measure the protein content along the electrodes, the powder was sampled in three colored areas (see Figure 1a).

The amount of particles separated along the electrodes was determined by measuring the height of the separated powder. The measuring points are shown in Figure 1a and marked with gray circles. The powder deposition height was measured homogenously along each electrode in order to get a topography. Note that the powder height was determined using a micrometer screw (according to DIN 863-1:2017-02). The mean was calculated from the results of three independent separation experiments (n = 3). Error bars indicate the confidence intervals of the Student's t-test with an α = 0.05 significance level.

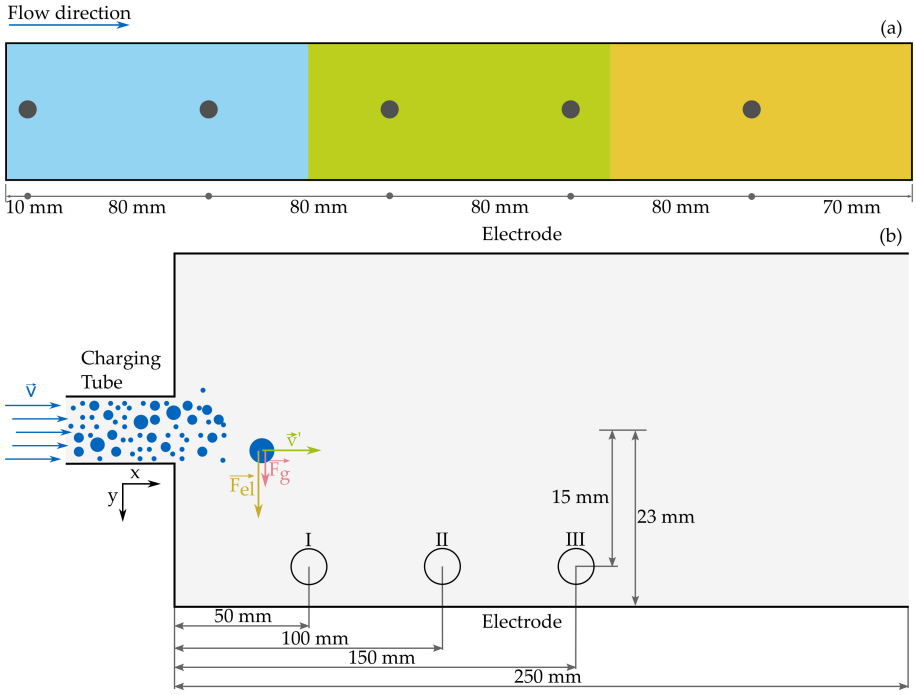

Figure 1. (**a**) Schematic of the sampling points along the electrodes. The powder deposition height on the electrode was measured at the points marked by gray circles. Colored areas mark the areas of powder sampling along the electrode. (**b**) Schematic of the separation chamber and the charging tube. The in situ particle size near the electrodes was measured at positions I, II, and III. Measurements near the anode and cathode were enabled by switching the polarity of the electrical field. The electric force F_{el} and weight force F_g acting on each particle in the separation chamber are visualized.

2.2.2. In Situ Particle Size Analysis

To investigate whether the particles agglomerate along the charging tube, we analyzed the in situ particle size distributions along the charging tube. For this purpose, parts of the charging and separation setup were installed in the measuring gap of a HELOS laser diffraction system (Sympatec, Clausthal-Zellerfeld, Germany). The charging and dispersing setup has been described in previous studies [47,48]. In the charging section, the particle size distributions were determined at the outlet of the Venturi nozzle (inlet of the charging section) and at the outlet of the charging tube. In the separation chamber, the particle size distribution was measured as a function of length. The schematic in Figure 1b shows the measuring positions I, II, and III along the electrodes in the separation chamber. The measuring points were chosen to be close to the electrodes and in the first half of the separation chamber. Due to the triboelectric separation, the particle concentration is decreasing along the separation chamber. Thus, the particle concentration, which is required to determine the particle size distribution, was not accessible. The particle size distributions on the anode and the cathode were obtained by switching the polarity of the electrical field with an electrical field strength of 217.4 kV/m. The mean of six independent separation experiments ($n = 6$) was calculated and the error is indicated by the confidence intervals of the Student's t-test with an $\alpha = 0.05$ significance level using error bars.

2.2.3. Flow Simulation and Estimation of the Particle Charge

The change in cross section between the charging tube and the separation chamber is very rigorous. The flow profile in the separation chamber, which might affect the separation characteristics and the particle size distribution along the electrodes (Figure 1b), was investigated in a computational fluid dynamics (CFD) simulation (ANSYS Fluent, version: 17.0, supplier: Ansys, Inc., Canonsburg, PA,

USA) of a realizable k–ε model. The particle motion in the separation chamber was visualized by tracking particles in the flow simulation. The inserted spherical particles followed a Weibull size distribution with a minimum, mean, and maximum (measured in the initial particle size distribution) of 1, 16, and 40 µm, respectively. The powder density was considered as the mean of the true density (1465 kg/m^3), which was measured by a gas pycnometer (Accupyc 1330, Micromeritics Instrument Corp., Norcross, GA, USA). The minimum charge at which the particle will be deflected in the measuring region was determined by simulating the in situ particle size distribution at different gravity levels (emulating different particle charges). The Coulomb force aligns with the weight force, as shown in Figure 1b. The absolute value of the charge q of the particles is estimated as follows:

$$q = \frac{x_3}{6E}\pi\rho_s g(n-1) \quad (1)$$

where x is the mean particle size, ρ_s is the true density, $\vec{E}$ is the electrical field, $\vec{g}$ is gravity, and the scaling factor n is the increase in particle charge. The scaling factor in the simulation was varied between 1 and 44. Note that the polarity of the charge depends on the electrical field's polarity.

3. Results

3.1. Particle Size Distribution

3.1.1. Agglomeration within the Charging Tube

Figure 2 shows the volume–weight density distributions at the Venturi nozzle outlet (panel a) and at the outlet of the charging tube (panel b) in the 15 and 30 wt % powders. In both particle size distributions, the particle size decreased with increasing initial protein content. The particle size distributions were similar at the outlets of the nozzle and the charging tube. The mean particle size (peak position) and the maximum particle size are the same at the tube inlet and the tube outlet. By comparing the distribution of finer particles, an increase in finer particles is visible. Thus, a dispersion along the charging tube is measured. The reason for this dispersion could be the high particle–particle collision number within the charging tube, due to the high turbulence [47]. The results in Figure 2 indicate breaking up particle agglomerates of fine particles during the charging step that could promote electrostatic separation. Contrarily, no electrostatic agglomeration that could impair electrostatic separation is observed.

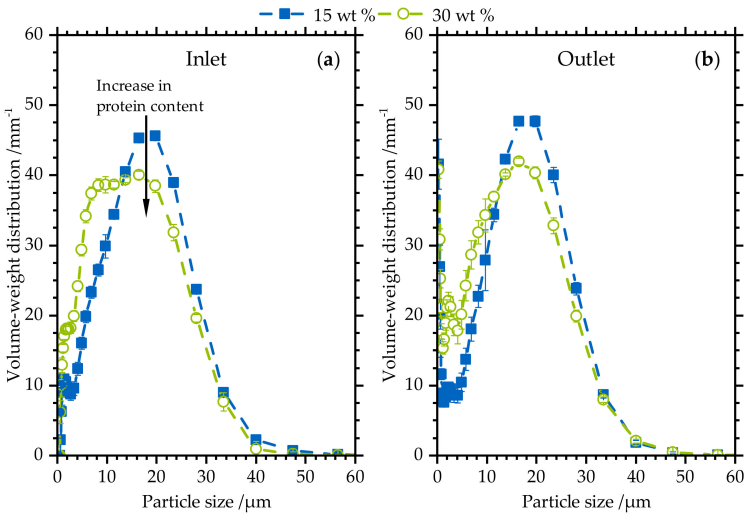

Figure 2. Volume–weight density distribution at (**a**) the Venturi nozzle outlet and (**b**) the outlet of the charging tube. Increasing the initial protein content (from 15 to 30 wt %) refined the particle size distribution. The distributions at the nozzle and tube ends are not obviously different.

3.1.2. Particle Size Distribution along the Electrodes

Figure 3 shows the volume–weight density distributions of the powder close to the cathode (a) and the anode (b) in measuring regions I, II, and III (Figure 1b). Increasing the initial protein content refined the particle size distributions at both the cathode and anode, as evidenced by the higher peak at ~6 µm in the 30 wt % compared to the 15 wt % distribution. This higher peak indicates a higher amount of finer protein particles (cf. Figure 2). In the sample with an initial protein content of 15 wt %, the particle size decreased along the investigated regions I, II, and III (note the lower peak height at 16 µm than that at 6 µm). This stepwise decrease in particle size was observed along both the cathode and the anode, as well as in the sample with higher initial protein content (30 wt %). The peak increases from 15 to 30 wt % are more clearly observed at 6 µm compared to 16 µm because increasing the protein content increases the amount of smaller particles. Comparing the particle size distributions at the cathode and the anode, the particles were finer on the cathode regardless of the initial protein content. These results suggest a higher protein content on the cathode (cf. Figure 2). The protein content of the separated powder on the cathode and the anode is approximately 80 and 2.5 wt %, respectively. Thus, protein is enriched on the cathode and starch is enriched on the anode [47,48]. However, the enhancement of finer protein particles near the cathode cannot be correlated with the protein content because the used protein powder is finer than the starch powder. Nevertheless, the particle size distributions at each measuring position in the separation chamber depended on the initial protein content. Thus, the particle size is influenced by the polarity of the electric field, the distance from the charging tube outlet, and (most strongly) the initial protein content. The region in which the particles separate plays a subordinate role on the particle size distribution. Furthermore, the particle size distributions on the anode and cathode resembled the initial distributions determined at the outlets of the Venturi nozzle and the tube.

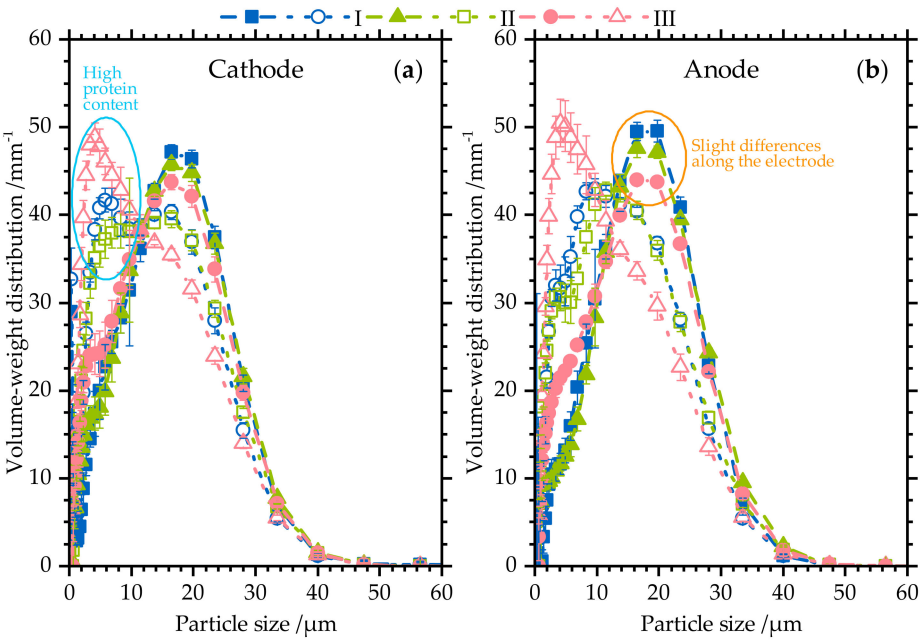

Figure 3. Volume–weight density distributions recorded near the cathode (**a**) and the anode (**b**) in regions I, II, and III. Closed and open symbols denote initial protein contents of 15 and 30 wt %, respectively. Increasing the initial protein content reduces the particle size at both anode and cathode. The particle size distributions differ in the three measuring regions.

3.2. Powder on the Electrodes

3.2.1. Powder Height

Figure 4 shows the powder height along the cathode and the anode. On the cathode, the distribution of powder was approximately homogeneous along the electrode. The powder height varied most extensively at the second measuring point, and was least variable at the first and fourth measuring points. This significant but extremely low variation should not be overinterpreted; however, the powder height severely decreased along the anode. The powder height was constant at the first two measuring points, and then dropped to zero over the next two measurement points. Thus, the powder heights on the cathode and the anode exhibited very different profiles, suggesting different charges of the particles separated on the two electrodes. In particular, the negatively charged particles exhibited a higher net charge than the positively charged particles.

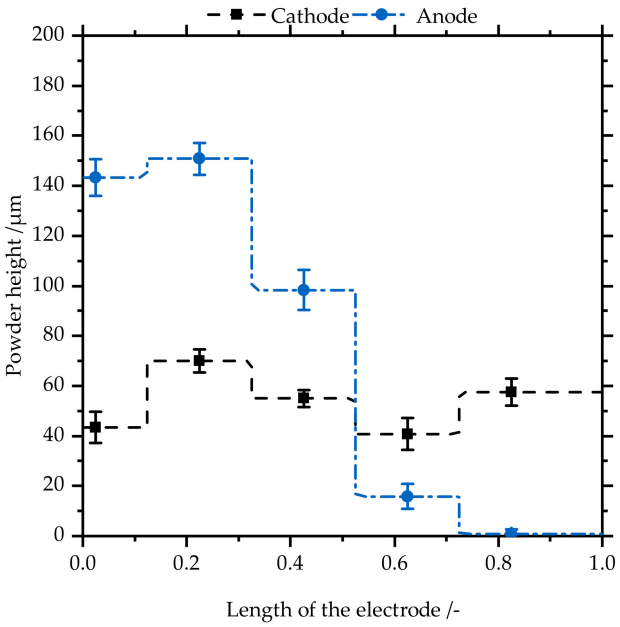

Figure 4. Powder height along the cathode and the anode. Powder height is approximately constant on the cathode, but mostly separates over the first half of the anode.

3.2.2. Protein Content

Figure 5 shows the protein content on the cathode in the three measurement areas at initial protein contents of 15 and 30 wt %. The protein content was consistently higher for the sample with the higher initial protein content. Independently of the initial protein content, the protein content increased in the second area (relative to the first area). In the third area, the protein content decreased at the initial protein content of 15 wt %, but remained high at the higher initial protein content. If we compare the protein content with the powder height, the two quantities are apparently independent because the powder height was approximately constant along the electrode, whereas the protein content extensively varied.

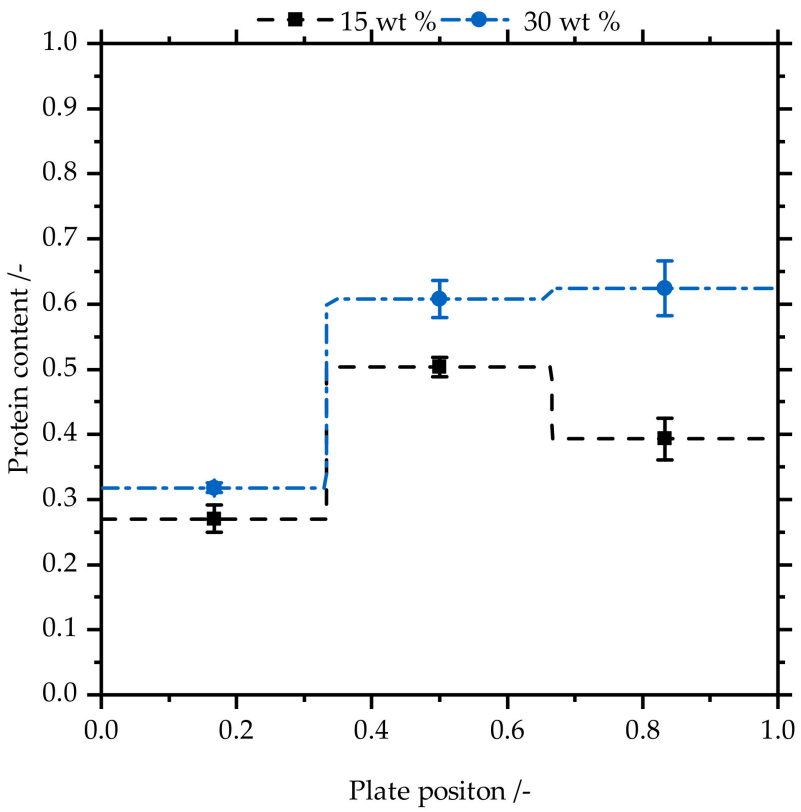

Figure 5. Protein content on the cathode in three different measurement areas for initial protein contents of 15 and 30 wt %. The protein content increases form the first to the second area regardless of initial protein content. In the third area, the protein content decreases (15 wt %) or remains the same (30 wt %).

3.3. Estimation of the Charge Correlated with the In Situ Particle Size Distribution

To estimate the minimum charge at which particles will separate in the separation chamber (enabling an in situ particle size analysis), the particles were tracked in a CFD study. Figure 6 shows the trajectories of spherical particles with different accelerations (varied by changing the electrical force in Equation (1)). In a homogenous electrical field, the net charge of the particles is a multiple of the elementary charge. Uncharged particles might be undetectable in every measuring region. Particles with a net charge of 1.45×10^3 q_e can be detected in regions II and III, whereas those with charges of 7.26×10^3 q_e and 1.16×10^4 q_e might be measurable only in region II. Particles with a net charge of 3.77×10^4 q_e and higher are visible in region I. When generating Figure 6 and calculating the associated particle charge, we assumed spherical particles with a mean diameter of 16 µm corresponding to the mean particle size of the powders used for the experiments. According to Equation (1), the particle size affects both the charge on a single particle and the particle trajectories. In all cases, varying the particle size only slightly affected the trajectories.

The background of Figure 6 shows the velocity profile in the separation chamber. The profile shows a jet at the charging tube outlet followed by homogeneity. The jet formed at the outlet of the tube affected the particle trajectories considerably. Regardless of their net charge, the particles remained within the jet to ~100 mm from the outlet. Then, they lost speed and were deflected toward the electrode by the Coulomb force. Thus, the simulation visualized the influence of the particle net charge on the particle trajectories within a complex velocity profile. Observing these particle trajectories, we can understand how particles might be charged to ensure their separation in the measuring regions of in situ particle size analyses.

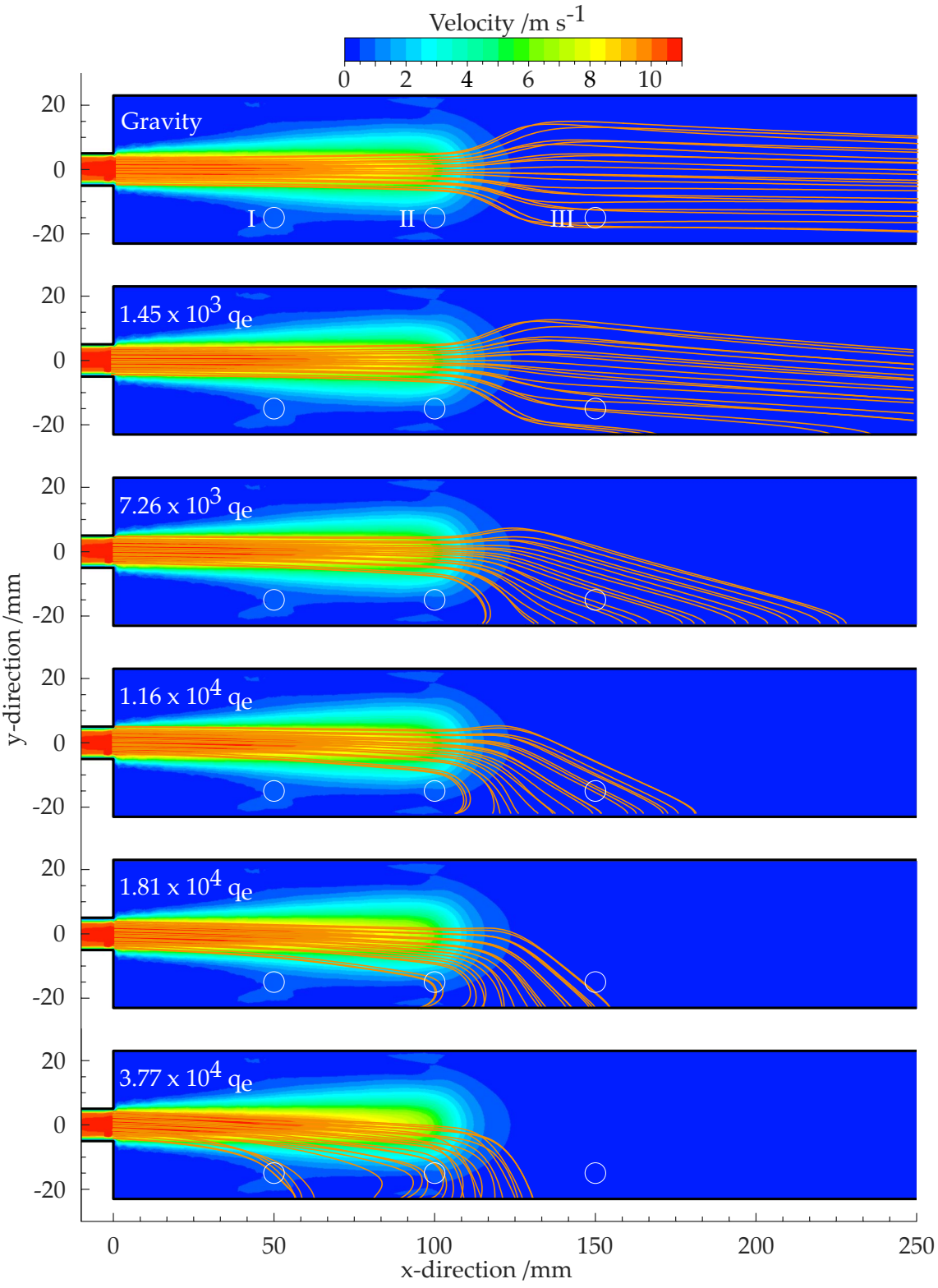

Figure 6. Trajectories of 16 µm diameter spherical particles with different particle charges (multiples of the elementary charge calculated by Equation (1)). The measuring regions I, II, and III of the in situ particle size distribution are indicated by the white open circles. Depending on their net charges, certain particles are not detectable in every measuring region. The background visualizes the velocity profile. The jet formed at the outlet of the charging tube is clearly visible.

4. Discussion

To use triboelectric separation as a tailor-made particle separation tool, one must separate the particles by their specific chargeabilities. Accordingly, it is necessary to disperse the particles before the charging step and avoid their agglomeration during the charging step. The selected setup enables the appropriate conditions for dispersal and aggregation prevention (Figure 2). Hence, detailed investigations of the separation step are required to establish triboelectric separation as an industrial separation technique.

Assuming that the charge distribution of fine particles is sourced from the triboelectric charging of the particles and that the charge distribution also possibly depends on the particle size and the chemical composition [34], the particle size distributions were determined at different locations close to the electrodes (Figure 3). As expected, the particle size distribution was coarser on the anode than on the cathode, because increasing the protein content refined the particle size distribution (Figure 2) and the protein was enriched on the cathode [47,48]. Moreover, along the measuring regions close to the electrodes, the decreased particle size accompanying the refined particles was demonstrated for different initial protein contents. These results were identical on the cathode and the anode, suggesting (as a first hint) that the net charges of the particles after triboelectric charging are independently distributed of the particle sizes.

The local distribution of the separated powder on the electrodes indicates the strength of the particle charges because particles with a higher and lower net charge are separated at the inlet and the near-outlet of the electrode, respectively. The powder height profiles on the cathode and the anode exhibited very different characteristics (Figure 4). The powder was dispersed almost homogeneously on the cathode but was separated close to the inlet on the anode. The absence of powder at the anode outlet indicates that the negative particles were more highly charged than the positive ones. The same results were reported in single-particle charge measurements [49]. This result further indicates independent distributions of the particle charges and sizes because the particle size distributions were similar on the cathode and anode (Figure 3). Furthermore, the homogeneously distributed powder exhibited a distributed protein content with a peak in the middle of the electrode at 15 wt % initial protein content, and level peaks in the second and third parts of the electrode at 30 wt % initial protein content (Figure 5). This suggests a lower net charge of protein particles than of starch particles (Figure 6). These results are underpinned by the decreased particle size (higher protein content) along the cathode than along the anode (Figure 3). The particle trajectories were affected by the inhomogeneous flow profile in the separation chamber; however, in the flow simulation, they were predominantly influenced by the charge. Moreover, they showed a charge-dependent separation region. To summarize, the binary powder mixture with a polydispersed particle size distribution showed no clear relationship between particle size and particle charge in the separation region. These results contradict previous studies, which reported that smaller particles are predominantly negatively charged [25–30]. The results support an effect of particle size on triboelectric charging, but no clear tendency was found regarding the fine and coarse particles. Thus, the hypothesis of this study, i.e., that particle size distribution (as a measure of surface area) plays a major role in triboelectric charging and subsequent separation, is questionable. Indeed, there is a dependence of particle size along the electrodes, but the results show a more complex connection between the particle material and particle size.

5. Conclusions

The dispersing and agglomeration characteristics of powders with different initial protein contents were consistent along the charging tube. The in situ particle size measurements were consistent at different regions in the separation camber. After estimating the minimum charge for particle separation, it was found that large charge differences were required for separation in every measuring region of the chamber. This wide charge distribution might lead to different separation regions of the particles, as indicated by the roughly homogeneous powder height on the cathode and the steep decrease in powder height on the anode. These results show a complex dependency of triboelectric charging and

subsequent separation on the size and material of the particles. As the mechanism of triboelectric or contact charging has not been accurately determined, determining the primary influencing factors is very challenging. The present results indicate the high complexity of triboelectric charging and indicate that particle size is not a highly important factor in triboelectric separation but affects the triboelectric charging through surface-area differences.

Author Contributions: Conceptualization, J.L.; methodology, J.L.; data curation, J.L.; writing—original draft preparation, J.L.; writing—review and editing, J.L. and P.F.; visualization, J.L.; supervision, P.F.

Funding: This research received no external funding.

Acknowledgments: The authors would like to thank Lukas Hans for help with performing in situ particle size measurement and Heiko Briesen for the possibility to carry out this study.

Conflicts of Interest: The authors declare no conflict of interest.

References

1. Iversen, P.; Lacks, D.J. A life of its own: The tenuous connection between Thales of Miletus and the study of electrostatic charging. *J. Electrost.* **2012**, *70*, 309–311. [CrossRef]
2. O'Grady, P.F. *Thales of Miletus. The Beginnings of Western Science and Philosophy*; Ashgate: Aldershot, UK, 2002; ISBN 0754605337.
3. Harper, W.R. The Volta Effect as a Cause of Static Electrification. *Proc. R. Soc. A Math. Phys. Eng. Sci.* **1951**, *205*, 83–103. [CrossRef]
4. Harper, W.R. *Contact and Frictional Electrification. Monographs on the Physics and Chemistry of Materials*; Clarendon Press: Oxford, UK, 1967.
5. Davies, D.K. Charge generation on dielectric surfaces. *J. Phys. D Appl. Phys.* **1969**, *2*, 1533. [CrossRef]
6. Lowell, J.; Rose-Innes, A.C. Contact electrification. *Adv. Phys.* **1980**, *29*, 947–1023. [CrossRef]
7. Liu, C.; Bard, A.J. Electrostatic electrochemistry at insulators. *Nat. Mater.* **2008**, *7*, 505–509. [CrossRef]
8. McCarty, L.S.; Whitesides, G.M. Electrostatic charging due to separation of ions at interfaces: Contact electrification of ionic electrets. *Angew. Chem. Int. Ed. Engl.* **2008**, *47*, 2188–2207. [CrossRef]
9. Ducati, T.R.D.; Simoes, L.H.; Galembeck, F. Charge partitioning at gas-solid interfaces: Humidity causes electricity buildup on metals. *Langmuir* **2010**, *26*, 13763–13766. [CrossRef]
10. Baytekin, H.T.; Patashinski, A.Z.; Branicki, M.; Baytekin, B.; Soh, S.; Grzybowski, B.A. The mosaic of surface charge in contact electrification. *Science* **2011**, *333*, 308–312. [CrossRef]
11. Salaneck, W.R. Double mass transfer during polymer-polymer contacts. *J. Appl. Phys.* **1976**, *47*, 144–147. [CrossRef]
12. Schella, A.; Herminghaus, S.; Schröter, M. Influence of humidity on tribo-electric charging and segregation in shaken granular media. *Soft Matter* **2017**, *13*, 394–401. [CrossRef]
13. Németh, E.; Albrecht, V.; Schubert, G.; Simon, F. Polymer tribo-electric charging: Dependence on thermodynamic surface properties and relative humidity. *J. Electrost.* **2003**, *58*, 3–16. [CrossRef]
14. Baytekin, H.T.; Baytekin, B.; Soh, S.; Grzybowski, B.A. Is water necessary for contact electrification? *Angew. Chem. Int. Ed. Engl.* **2011**, *50*, 6766–6770. [CrossRef]
15. Matsusyama, T.; Yamamoto, H. Impact charging of particulate materials. *Chem. Eng. Sci.* **2006**, *61*, 2230–2238. [CrossRef]
16. Matsuyama, T.; Yamamoto, H. Electrification of single polymer particles by successive impacts with metal targets. *IEEE Trans. Ind. Appl.* **1995**, *31*, 1441–1445. [CrossRef]
17. Watanabe, H.; Ghadiri, M.; Matsuyama, T.; Maruyama, H.; Matsusaka, S.; Ghadiri, M.; Matsuyama, T.; Ding, Y.L.; Pitt, K.G.; Maruyama, H.; et al. Triboelectrification of pharmaceutical powders by particle impact. *Int. J. Pharm.* **2007**, *334*, 149–155. [CrossRef] [PubMed]
18. Grosshans, H.; Papalexandris, M.V. Large Eddy simulation of triboelectric charging in pneumatic powder transport. *Powder Technol.* **2016**, *301*, 1008–1015. [CrossRef]
19. Ireland, P.M. Triboelectrification of particulate flows on surfaces: Part I—Experiments. *Powder Technol.* **2010**, *198*, 189–198. [CrossRef]
20. Fotovat, F.; Bi, X.T.; Grace, J.R. A perspective on electrostatics in gas-solid fluidized beds: Challenges and future research needs. *Powder Technol.* **2018**, *329*, 65–75. [CrossRef]

21. Mehrani, P.; Murtomaa, M.; Lacks, D.J. An overview of advances in understanding electrostatic charge buildup in gas-solid fluidized beds. *J. Electrost.* **2017**, *87*, 64–78. [CrossRef]
22. Engers, D.A.; Fricke, M.N.; Storey, R.P.; Newman, A.W.; Morris, K.R. Triboelectrification of pharmaceutically relevant powders during low-shear tumble blending. *J. Electrost.* **2006**, *64*, 826–835. [CrossRef]
23. Karner, S.; Urbanetz, N.A. Arising of electrostatic charge in the mixing process and its influencing factors. *Powder Technol.* **2012**, *226*, 261–268. [CrossRef]
24. Ghori, M.U.; Supuk, E.; Conway, B.R. Tribo-electric charging and adhesion of cellulose ethers and their mixtures with flurbiprofen. *Eur. J. Pharm. Sci.* **2014**, *65*, 1–8. [CrossRef] [PubMed]
25. Forward, K.M.; Lacks, D.J.; Sankaran, R.M. Particle-size dependent bipolar charging of Martian regolith simulant. *Geophys. Res. Lett.* **2009**, *36*, 139. [CrossRef]
26. Waitukaitis, S.R.; Lee, V.; Pierson, J.M.; Forman, S.L.; Jaeger, H.M. Size-Dependent Same-Material Tribocharging in Insulating Grains. *Phys. Rev. Lett.* **2014**, *112*. [CrossRef]
27. Lacks, D.J.; Levandovsky, A. Effect of particle size distribution on the polarity of triboelectric charging in granular insulator systems. *J. Electrost.* **2007**, *65*, 107–112. [CrossRef]
28. Zhao, H.; Castle, G.S.P.; Inculet, I.I.; Bailey, A.G. Bipolar charging of poly-disperse polymer powders in fluidized beds. *IEEE Trans. Ind. Appl.* **2003**, *39*, 612–618. [CrossRef]
29. Mukherjee, R.; Gupta, V.; Naik, S.; Sarkar, S.; Sharma, V.; Peri, P.; Chaudhuri, B. Effects of particle size on the triboelectrification phenomenon in pharmaceutical excipients: Experiments and multi-scale modeling. *Asian J. Pharm. Sci.* **2016**, *11*, 603–617. [CrossRef]
30. Trigwell, S.; Grable, N.; Yurteri, C.U.; Sharma, R.; Mazumder, M.K. Effects of surface properties on the tribocharging characteristics of polymer powder as applied to industrial processes. *IEEE Trans. Ind. Appl.* **2003**, *39*, 79–86. [CrossRef]
31. Karner, S.; Maier, M.; Littringer, E.; Urbanetz, N.A. Surface roughness effects on the tribo-charging and mixing homogeneity of adhesive mixtures used in dry powder inhalers. *Powder Technol.* **2014**, *264*, 544–549. [CrossRef]
32. Lacks, D.J.; Duff, N.; Kumar, S.K. Nonequilibrium accumulation of surface species and triboelectric charging in single component particulate systems. *Phys. Rev. Lett.* **2008**, *100*, 188305. [CrossRef]
33. Burgo, T.A.L.; Silva, C.A.; Balestrin, L.B.S.; Galembeck, F. Friction coefficient dependence on electrostatic tribocharging. *Sci. Rep.* **2013**, *3*. [CrossRef] [PubMed]
34. Diaz, A.F.; Felix-Navarro, R.M. A semi-quantitative tribo-electric series for polymeric materials: The influence of chemical structure and properties. *J. Electrost.* **2004**, *62*, 277–290. [CrossRef]
35. Grosshans, H.; Papalexandris, M.V. A model for the non-uniform contact charging of particles. *Powder Technol.* **2017**, *305*, 518–527. [CrossRef]
36. Haeberle, J.; Schella, A.; Sperl, M.; Schröter, M.; Born, P. Double origin of stochastic granular tribocharging. *Soft Matter* **2018**, *14*, 4987–4995. [CrossRef] [PubMed]
37. Hu, J.; Zhou, Q.; Liang, C.; Chen, X.; Liu, D.; Zhao, C. Experimental investigation on electrostatic characteristics of a single grain in the sliding process. *Powder Technol.* **2018**, *334*, 132–142. [CrossRef]
38. Ireland, P.M. Impact tribocharging of soft elastic spheres. *Powder Technol.* **2019**, *348*, 70–79. [CrossRef]
39. Wang, J.; Zhao, J.; de Wit, M.; Boom, R.M.; Schutyser, M.A.I. Lupine protein enrichment by milling and electrostatic separation. *Innov. Food Sci. Emerg. Technol.* **2016**, *33*, 596–602. [CrossRef]
40. Wang, J.; de Wit, M.; Boom, R.M.; Schutyser, M.A.I. Charging and separation behavior of gluten–starch mixtures assessed with a custom-built electrostatic separator. *Sep. Purif. Technol.* **2015**, *152*, 164–171. [CrossRef]
41. Xing, Q.; de Wit, M.; Kyriakopoulou, K.; Boom, R.M.; Schutyser, M.A.I. Protein enrichment of defatted soybean flour by fine milling and electrostatic separation. *Innov. Food Sci. Emerg. Technol.* **2018**, *50*, 42–49. [CrossRef]
42. Wang, J.; de Wit, M.; Schutyser, M.A.I.; Boom, R.M. Analysis of electrostatic powder charging for fractionation of foods. *Innov. Food Sci. Emerg. Technol.* **2014**, *26*, 360–365. [CrossRef]
43. Wang, J.; Suo, G.; de Wit, M.; Boom, R.M.; Schutyser, M.A.I. Dietary fibre enrichment from defatted rice bran by dry fractionation. *J. Food Eng.* **2016**, *186*, 50–57. [CrossRef]
44. Tabtabaei, S.; Jafari, M.; Rajabzadeh, A.R.; Legge, R.L. Development and optimization of a triboelectrification bioseparation process for dry fractionation of legume flours. *Sep. Purif. Technol.* **2016**, *163*, 48–58. [CrossRef]

45. Tabtabaei, S.; Jafari, M.; Rajabzadeh, A.R.; Legge, R.L. Solvent-free production of protein-enriched fractions from navy bean flour using a triboelectrification-based approach. *J. Food Eng.* **2016**, *174*, 21–28. [CrossRef]
46. Chen, Z.; Liu, F.; Wang, L.; Li, Y.; Wang, R.; Chen, Z. Tribocharging properties of wheat bran fragments in air–solid pipe flow. *Food Res. Int.* **2014**, *62*, 262–271. [CrossRef]
47. Landauer, J.; Aigner, F.; Kuhn, M.; Foerst, P. Effect of particle-wall interaction on triboelectric separation of fine particles in a turbulent flow. *Adv. Powder Technol.* **2019**, *30*, 1099–1107. [CrossRef]
48. Landauer, J.; Foerst, P. Triboelectric separation of a starch-protein mixture—Impact of electric field strength and flow rate. *Adv. Powder Technol.* **2018**, *29*, 117–123. [CrossRef]
49. Landauer, J.; Tauwald, S.M.; Foerst, P. A Simple μ-PTV Setup to Estimate Single-Particle Charge of Triboelectrically Charged Particles. *Front. Chem.* **2019**, *7*, 1. [CrossRef]

© 2019 by the authors. Licensee MDPI, Basel, Switzerland. This article is an open access article distributed under the terms and conditions of the Creative Commons Attribution (CC BY) license (http://creativecommons.org/licenses/by/4.0/).

3. Discussion

In process engineering, several separation techniques are used to separate powders mainly according to their particle size. Further separation features, like particle morphology or chemical composition, are usually linked with particle size. If particles should be separated in the same size and density range according to their chemical composition *classical* separation techniques are not able to separate these powders. Therefore, a further separation technique which addresses the chemical composition of particles is necessary. Triboelectric separation could be this new separation technique, because triboelectric or contact charging is a surface-physical effect and depends on the state of surfaces (Lacks and Shinbrot, 2019). Hitherto, triboelectric separation is no common technique to separate fine organic powders due to their chemical composition, because factors that influence and control triboelectric charging are not yet clearly understood. Several studies accompanying this thesis were carried out to gain knowledge about factors influencing triboelectric separation of binary organic powder mixtures below 50 µm.

It is shown that triboelectric separation is a suitable tool to separate fine organic powders and that the main parameters influencing triboelectric separation are the flow conditions and the particle size distribution. Thus, **H I** has to be accepted. In *Paper I*, *II*, and *III* fine organic powder containing starch and protein are separated with a high selectivity and efficiency. These findings agree with previous studies that investigated the separation performance of ground organic material (Tabtabaei et al., 2016a,b, 2017; Wang et al., 2015a, 2014, 2016a,b). A variation in the flow conditions characterised by Reynolds number provides evidence for the triboelectric separation selectivity (*Paper I*). These findings underpin the results of *Paper III*. The increase of particle interaction results in higher separation selectivity. Since an increase in turbulence dissipation results in an increase of particle contact number (Saffman and Turner, 1956), the findings of *Paper I* indicate that **H II**, which concerns the particle-particle interaction plays a decisive role in triboelectric charging and separation might be accepted. *Paper II* and *III* agree with previous findings and support the decisive role of particle-particle interactions. An increase in contact numbers of particles results in an increase in separation selectivity. Therefore, the main charging mechanism of fine powders is found to be particle-particle interactions. These results agree with the findings of simulation studies (Lacks et al., 2008; Lacks and Levandovsky, 2007). Thus, **H III** which questions the influence of particle-wall interaction should be accepted? Indeed, *Paper II* and *III* showed no differences in separation selectivity by varying the charging tube material according to the empirical triboelectric series. In fluidised beds, the same findings were made (Yu et al., 2010). Furthermore, boundary-layer-control showed only a slight decrease in separation performance (*Paper II*), but these differences are deduced from the lower contact numbers of

particles (*Paper III*). However, these findings only correspond to few studies which addresses particle-particle interaction to be most important (Forward et al., 2009; Zhao et al., 2002, 2003), whereas most triboelectric separation studies emphasise particle-wall interaction as the dominant charging mechanism (Chen et al., 2014; Park et al., 2008a; Tabtabaei et al., 2016b; Wang et al., 2014; Xing et al., 2018); nevertheless the choice of the wall material whether it is conductive or insulating should not lead to any differences in the separation performance.

The main process parameter to control or reinforce triboelectric charging is particle collision rate. Since every contact between two particles generates charge and every particle collides statistically, it is hypothesized in **H IV** that a charge distribution for both positively and negatively charged particles exists. These charge distributions might be multimodal, because different amounts of net charge are generated by the contact of different and same materials. These multimodal distributions are determined only for positively charged starch particles, whereas negatively charged starch particles exhibit a monomodal charge distribution (*Paper IV*). On the contrary, positively and negatively charged protein particles show the same charge distribution. In protein powder mixtures, similar charge distributions as for pure starch powders are measured. Thus, **H IV** has to be accepted. Furthermore, the findings of this study underpin the influence of particle surface on triboelectric charging and might show that particle morphology and surface properties are closely linked. Different charge distributions of pure powders and powder mixtures might indicate an evidence of charge generation due to the contact between different materials (*Paper IV*). These findings also suggest the dependency of triboelectric series on the combination of materials and questions its absoluteness. Therefore, **H V** deals with the amount and polarity of charge which should be independent from particle size in a binary powder mixture. Due to in-situ particle size measurement in *Paper V*, the same high range of particle charge was measured like in *Paper IV*, but no correlation between particle size and particle charge is detected. Only slight differences of size were measured along both electrodes. Thus, these findings suggest no correlation between charge and particle size in binary mixtures and **H V** is accepted. However, for single component powders charge might depend on particle size (Forward et al., 2009; Kok and Lacks, 2009; Lacks et al., 2008; Lacks and Levandovsky, 2007; Mehrani et al., 2005; Sowinski et al., 2010; Zhao et al., 2002, 2003). Therefore, it can be assumed that the charge generation between different materials superimposes the charge generation brought about differences in particle size.

The results of this thesis substantiate the high potential of triboelectric separation to separate dry organic powders. For binary powder mixtures the separation feature is the different ability for the generation of charge depending on the surface properties (*Paper IV*). These findings could be expected, because differences of surfaces are discussed in detail to determine charging mechanism(s) of contact charging (Baytekin et al., 2012a, 2011b; McCarty and Whitesides, 2008) (cf. 1.2.2). However, it is unknown that differences in surface properties within the same material caused by differences in particle morphology and size affect the charge distribution of binary powder mixtures. This might indicate a charge generation

and elimination at every particle-particle contact independent of particle size (*Paper V*). Nevertheless, particle size distribution has a huge influence on the contact number of particles (*Paper II, III*) and thereby particle size distribution influences the net charge of particles. The net charge of particle might reach a maximum by increasing contact number over a certain number (Haeberle et al., 2018) and a highest possible separation performance could be reached (*Paper III*). Both contact number and separation performance are linked with the flow profile (*Paper I, II, III, V*). Higher turbulence dissipation rates promote dispersing of powder, (Masuda, 2009) and contact rate between particles (Saffman and Turner, 1956; Wang et al., 1998). Thus, triboelectric separation of fine organic powders is mainly influenced by particle contact number and surface properties. These findings coincide with the initial example of the child with a balloon generating charge by rubbing an air balloon on its hair; the rubbing corresponds to the contact number, whereas the surface properties correspond to the balloon and the hair.

4. Conclusion and future prospects

The aim of this thesis was to apply triboelectric separation to fine organic powders and to figure out the main process parameters influencing triboelectric charging. Since the physical understanding is only insufficiently elucidated, different studies dealing with particle interaction and powder composition parameters were carried out. Triboelectric separation is a suitable way to separate fine organic powders, where starch and protein particles have approximately the same true density and are in the same size range. Separation experiments were carried out using a simple self-designed triboelectric separator consisting of a charging section (Venturi nozzle and charging tube) and a separation chamber (parallel-plate capacitor). In the charging section, the flow conditions can be adjusted by different setups and the separation performance can be adapted by the electrical-field strength.

Figure 4.1 shows the determined main process parameters influencing triboelectric separation. Since particle-wall interactions play a subordinate role, particle-particle interaction is related to contact number. The contact number of fine particles in a flow depends on the flow conditions (turbulent eddy dissipation rate) and the particle size. Furthermore, triboelectric separation is also influenced by the surface properties of the particles. The surface properties depend on particle size, particle origin, humidity, ions, etc. In this thesis, only particle size and origin were varied. Besides these parameters, contact number and surface property can interact, as adhesion forces of particles might lead to agglomerates within the charging step or dispersion is incomplete in the chosen flow conditions. Thus, efficiency and selectivity of triboelectric separation is reduced.

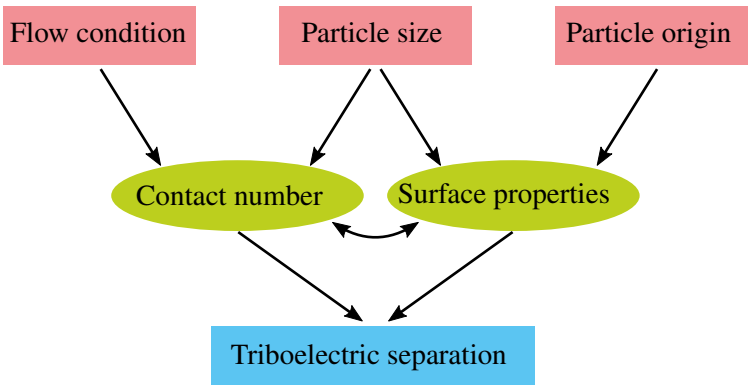

Figure 4.1.: Summary of the main process parameters influencing triboelectric separation investigated in this thesis.

Further studies dealing with triboelectric separation should focus on both central influencing parameters. Contact number of particles and dispersing properties have to be adjusted

to different particle sizes in order to use triboelectric separation for a wide range of particle sizes. For larger particles, the turbulence dissipation rate in a simple tube flow would not be sufficient and vortexes in the turbulent flow have to be adjusted to the used particle sizes. Thus, a combination of charging-setup design using CFD simulation and contact models appropriate to the flow conditions and particle size is necessary to achieve a sufficiently high contact number. To adjust the sufficient contact number for different powders predominantly plant design has to be carried out.

Surface properties of particles might play a decisive role in triboelectric charging, and thus possibilities to influence triboelectric charging are manifold. The comminution of powder decreases particle size as well as varies particle morphology, the crystalline or amorphous state of the particle surface or even *activates* the surface (referred as mechanochemistry (Ribas-Arino and Marx, 2012)). Furthermore, the surface properties can be changed by adjusting the relative humidity. This might be very interesting for organic powders with a biological origin (no plastics meant). Organic powders show different water absorption kinetics and particles are predominately soluble in water; particles often tend to swell at higher humidities. These properties of organic powders might strongly influence triboelectric charge generation and the separation performance could be optimised.

In addition to the main parameters affecting triboelectric separation, powder preparation of raw organic materials like soya beans, wheat flour, or other crops containing protein and starch is essential. In order to separate protein and starch of these organic materials, the raw material has to comminuted that protein and starch are present in different particles within the powder. Indeed, comminution requires high energy input, but it is impossible to separate according to the chemical composition and the different materials are not divided in different particles.

The very early discovered physical effect of triboelectric charging consisting in the simple game of rubbing remains still unknown. The triboelectric effect is delighting for both children and scientists; a child rubbing a balloon on one's hair and rejoicing on the attractive effect between hair and balloon. A scientist is delighted by the surprise that the simple game of rubbing (contact) defies a precise measurement technique, because it is an unstable, multiscale and time-dependent process. Thus, triboelectric charging remains an exciting and challenging topic as currently reviewed by Lacks and Shinbrot (2019). However, the unknown exact physical mechanism of the triboelectric effect should not deter to use triboelectric separation which expands separation possibilities in process engineering.

5. References

Akande, A. R. and J. Lowell
1987. Charge transfer in metal/polymer contacts. *Journal of Physics D: Applied Physics*, 20(5):565–578.

Albrecht, V., A. Janke, E. Németh, S. Spange, G. Schubert, and F. Simon
2009. Some aspects of the polymers' electrostatic charging effects. *Journal of Electrostatics*, 67(1):7–11.

Allen, T.
1997. *Particle size measurement*, Powder technology series, 5. ed. edition. London: Chapman & Hall.

Anderson, J. H.
1994. A comparison of experimental data and model predictions for tribocharging of two-component electrophotographic developers. *Journal of Imaging Science and Technology*, 38(4):378.

Anderson, R., S. Gathman, J. Hughes, S. Björnsson, S. Jónasson, D. C. Blanchard, C. B. Moore, H. J. Survilas, and B. Vonnegut
1965. Electricity in volcanic clouds: Investigations show that lightning can result from charge-separation processes in a volcanic crater. *Science (New York, N.Y.)*, 148(3674):1179–1189.

Apodaca, M. M., P. J. Wesson, K. J. M. Bishop, M. A. Ratner, and B. A. Grzybowski
2010. Contact electrification between identical materials. *Angewandte Chemie International Edition*, 49(5):946–949.

Atroune, S., A. Tilmatine, R. Alkama, A. Samuila, and L. Dascalescu
2015. Comparative experimental study of triboelectric charging of two size classes of granular plastics. *Particulate Science and Technology*, 33(6):652–658.

Bailey, A. G.
2001. The charging of insulator surfaces. *Journal of Electrostatics*, 51-52:82–90.

Baytekin, B., H. T. Baytekin, and B. A. Grzybowski
2012a. What really drives chemical reactions on contact charged surfaces? *Journal of the American Chemical Society*, 134(17):7223–7226.

Baytekin, H. T., B. Baytekin, J. T. Incorvati, and B. A. Grzybowski
2012b. Material transfer and polarity reversal in contact charging. *Angewandte Chemie*, 124(20):4927–4931.

Baytekin, H. T., B. Baytekin, S. Soh, and B. A. Grzybowski
2011a. Is water necessary for contact electrification? *Angewandte Chemie (International ed. in English)*, 50(30):6766–6770.

Baytekin, H. T., A. Z. Patashinski, M. Branicki, B. Baytekin, S. Soh, and B. A. Grzybowski
2011b. The mosaic of surface charge in contact electrification. *Science (New York, N.Y.)*, 333(6040):308–312.

Bloch, F.
1929. Über die quantenmechanik der elektronen in kristallgittern. *Zeitschrift für Physik*, 52(7):555–600.

Boland and D. Geldart
1972. Electrostatic charging in gas fluidised beds. *Powder Technology*, 5(5):289–297.

Bunchatheeravate, P., J. Curtis, Y. Fujii, and S. Matsusaka
2013. Prediction of particle charging in a dilute pneumatic conveying system. *AChE Journal*, 59(7):2308–2316.

Burgo, T. A., F. Galembeck, and G. H. Pollack
2016. Where is water in the triboelectric series? *Journal of Electrostatics*, 80:30–33.

Calin, L., L. Caliap, V. Neamtu, R. Morar, A. Iuga, A. Samuila, and L. Dascalescu
2008. Tribocharging of granular plastic mixtures in view of electrostatic separation. *IEEE Transactions on Industry Applications*, 44(4):1045–1051.

Cangialosi, F., L. Liberti, M. Notarnicola, and J. Stencel
2006. Monte carlo simulation of pneumatic tribocharging in two-phase flow for high-inertia particles. *Powder Technology*, 165(1):39–51.

Chen, A. H., H. T. Bi, and J. R. Grace
2003. Measurement of particle charge-to-mass ratios in a gas–solids fluidized bed by a collision probe. *Powder Technology*, 135-136:181–191.

Chen, J. and R. Honaker
2015. Dry separation on coal–silica mixture using rotary triboelectrostatic separator. *Fuel Processing Technology*, 131:317–324.

Chen, Z., F. Liu, L. Wang, Y. Li, R. Wang, and Z. Chen
2014. Tribocharging properties of wheat bran fragments in air–solid pipe flow. *Food Research International*, 62:262–271.

Clint, J. H. and T. S. Dunstan
2001. Acid-base components of solid surfaces and the triboelectric series. *EPL (Europhysics Letters)*, 54(3):320.

Coehn, A.
1898. Ueber ein gesetz der electricitätserregung. *Annalen der Physik*, 300(2):217–232.

Davies, D. K.
1969. Charge generation on dielectric surfaces. *Journal of Physics D: Applied Physics*, 2(11):1533.

Diaz, A. F. and R. M. Felix-Navarro
2004. A semi-quantitative tribo-electric series for polymeric materials: the influence of chemical structure and properties: The influence of chemical structure and properties. *Journal of Electrostatics*, 62(4):277–290.

Dizdar, T. O., G. Kocausta, E. Gülcan, and Ö. Y. Gülsoy
2018. A new method to produce high voltage static electric load for electrostatic separation – triboelectric charging. *Powder Technology*, 327:89–95.

Dong, K., Q. Zhang, Z. Huang, Z. Liao, J. Wang, and Y. Yang
2015a. Experimental investigation of electrostatic effect on bubble behaviors in gas–solid fluidized bed. *AIChE Journal*, 61(4):1160–1171.

Dong, K., Q. Zhang, Z. Huang, Z. Liao, J. Wang, Y. Yang, and F. Wang
2015b. Experimental investigation of electrostatic effect on particle motions in gas–solid fluidized beds. *AIChE Journal*, 61(11):3628–3638.

Dötterl, M., U. Wachsmuth, L. Waldmann, H. Flachberger, M. Mirkowska, L. Brands, P.-M. Beier, and I. Stahl†
2000. Electrostatic separation. In *Ullmann's Encyclopedia of Industrial Chemistry*, volume 37, Pp. 1–35. Chichester: Wiley.

Ducati, T. R. D., L. H. Simoes, and F. Galembeck
2010. Charge partitioning at gas-solid interfaces: humidity causes electricity buildup on metals. *Langmuir : the ACS journal of surfaces and colloids*, 26(17):13763–13766.

Dwari, R. K., S. K. Mohanta, B. Rout, R. K. Soni, P. Reddy, and B. K. Mishra
2015. Studies on the effect of electrode plate position and feed temperature on the tribo-electrostatic separation of high ash indian coking coal. *Advanced Powder Technology*, 26(1):31–41.

Ema, A., D. Yasuda, K.-i. Tanoue, and H. Masuda
2003. Tribo-charge and rebound characteristics of particles impact on inclined or rotating metal target. *Powder Technology*, 135-136:2–13.

Fenzel-Alexander, D., P. Brock, and A. Diaz
1994. Control of contact charge in polymers with ionomers. *Langmuir : the ACS journal of surfaces and colloids*, 10(9):3323–3327.

Fermi, E.
1926. Zur quantelung des idealen einatomigen gases. *Zeitschrift für Physik*, 36(11):902–912.

Forward, K. M., D. J. Lacks, and R. M. Sankaran
2009. Particle-size dependent bipolar charging of martian regolith simulant. *Geophysical Research Letters*, 36(13):139.

Fowkes, F. M.
1987. Role of acid-base interfacial bonding in adhesion. *Journal of Adhesion Science and Technology*, 1(1):7–27.

Fowkes, F. M.
1990. Quantitative characterization of the acid-base properties of solvents, polymers, and inorganic surfaces. *Journal of Adhesion Science and Technology*, 4(1):669–691.

Furchner, B. and S. Zampini
2010. Air classifying. In *Ullmann's encyclopedia of industrial chemistry*, volume 24, P. 91. Chichester: Wiley.

Galk, J., W. Peukert, and J. Krahnen
1999. Industrial classification in a new impeller wheel classifier. *Powder Technology*, 105(1-3):186–189.

Gallo, C. F. and W. L. Lama
1976. Some charge exchange phenomena explained by a classical model of the work function. *Journal of Electrostatics*, 2(2):145–150.

Geldart, D.
1973. Types of gas fluidization. *Powder Technology*, 7(5):285–292.

Glor, M.
2003. Ignition hazard due to static electricity in particulate processes. *Powder Technology*, 135-136:223–233.

Gooding, D. M. and G. K. Kaufman
2011. Tribocharging and the triboelectric series. In *Encyclopedia of Inorganic and Bioinorganic Chemistry*, R. A. Scott, ed., volume 47, Pp. 1–9. Wiley.

Gouveia, R. F. and F. Galembeck
2009. Electrostatic charging of hydrophilic particles due to water adsorption. *Journal of the American Chemical Society*, 131(32):11381–11386.

Grosshans, H. and M. V. Papalexandris
2016. Large eddy simulation of triboelectric charging in pneumatic powder transport. *Powder Technology*, 301:1008–1015.

Gupta, R., D. Gidaspow, and D. T. Wasan
1993. Electrostatic separation of powder mixtures based on the work functions of its constituents. *Powder Technology*, 75(1):79–87.

Haeberle, J., A. Schella, M. Sperl, M. Schröter, and P. Born
2018. Double origin of stochastic granular tribocharging. *Soft matter*, 14(24):4987–4995.

Harper, W. R.
1951. The volta effect as a cause of static electrification. *Proceedings of the Royal Society A: Mathematical, Physical and Engineering Sciences*, 205(1080):83–103.

Harper, W. R.
1967. *Contact and frictional electrification: Monographs on the physics and chemistry of materials*, Monographs on the physics and chemistry of materials. Oxford: Clarendon Press.

Hemery, Y., U. Holopainen, A.-M. Lampi, P. Lehtinen, T. Nurmi, V. Piironen, M. Edelmann, and X. Rouau
2011. Potential of dry fractionation of wheat bran for the development of food ingredients, part ii: Electrostatic separation of particles. *Journal of Cereal Science*, 53(1):9–18.

Hemery, Y., X. Rouau, C. Dragan, M. Bilici, R. Beleca, and L. Dascalescu
2009. Electrostatic properties of wheat bran and its constitutive layers: Influence of particle size, composition, and moisture content. *Journal of Food Engineering*, 93(1):114–124.

Hendrickson, G.
2006. Electrostatics and gas phase fluidized bed polymerization reactor wall sheeting. *Chemical Engineering Science*, 61(4):1041–1064.

Henniker, J.
1962. Triboelectricity in polymers. *Nature*, 196(4853):474.

Hersh, S. P. and D. J. Montgomery
1955. Static electrification of filaments. *Textile Research Journal*, 25(4):279–295.

Hertz, H.
1881. Über die berührung fester elastischer körper. *Journal für die reine und angewandte Mathematik*, 92:156–171.

Hölzl, J. and F. K. Schulte
1979. Work function of metals. In *Solid Surface Physics*, J. Hölzl, F. K. Schulte, and H. Wagner, eds., Springer Tracts in Modern Physics, Pp. 1–150. Berlin and Heidelberg: Springer.

Horn, R. G. and D. T. Smith
1992. Contact electrification and adhesion between dissimilar materials. *Science (New York, N.Y.)*, 256(5055):362–364.

Horn, R. G., D. T. Smith, and A. Grabbe
1993. Contact electrification induced by monolayer modification of a surface and relation to acid–base interactions. *Nature*, 366(6454):442–443.

Ireland, P. M.
2010. Triboelectrification of particulate flows on surfaces: Part i — experiments. *Powder Technology*, 198(2):189–198.

Ireland, P. M.
2019. Impact tribocharging of soft elastic spheres. *Powder Technology*, 348:70–79.

Iversen, P. and D. J. Lacks
2012. A life of its own: The tenuous connection between thales of miletus and the study of electrostatic charging. *Journal of Electrostatics*, 70(3):309–311.

Jackson, T. L., W. M. Farrell, and M. I. Zimmerman
2015. Rover wheel charging on the lunar surface. *Advances in Space Research*, 55(6):1710–1720.

Karner, S. and N. A. Urbanetz
2012. Arising of electrostatic charge in the mixing process and its influencing factors. *Powder Technology*, 226:261–268.

Kok, J. F. and D. J. Lacks
2009. Electrification of granular systems of identical insulators. *Physical Review E*, 79(5 // 5 Pt 1):051304.

Kolehmainen, J., P. Sippola, O. Raitanen, A. Ozel, C. M. Boyce, P. Saarenrinne, and S. Sundaresan
2017. Effect of humidity on triboelectric charging in a vertically vibrated granular bed: Experiments and modeling. *Chemical Engineering Science*, 173:363–373.

Korevaar, M. W., J. T. Padding, M. A. van der Hoef, and Kuipers, J. A. M.
2014. Integrated dem–cfd modeling of the contact charging of pneumatically conveyed powders. *Powder Technology*, 258:144–156.

Lacks, D. J.
2012. The unpredictability of electrostatic charging. *Angewandte Chemie International Edition*, 51(28):6822–6823.

Lacks, D. J., N. Duff, and S. K. Kumar
2008. Nonequilibrium accumulation of surface species and triboelectric charging in single component particulate systems. *Physical review letters*, 100(18):188305.

Lacks, D. J. and A. Levandovsky
2007. Effect of particle size distribution on the polarity of triboelectric charging in granular insulator systems. *Journal of Electrostatics*, 65(2):107–112.

Lacks, D. J. and R. Mohan Sankaran
2011. Contact electrification of insulating materials. *Journal of Physics D: Applied Physics*, 44(45):453001.

Lacks, D. J. and T. Shinbrot
2019. Long-standing and unresolved issues in triboelectric charging. *Nature Reviews Chemistry*, 3(8):465–476.

Landauer, J., F. Aigner, M. Kuhn, and P. Foerst
2019a. Effect of particle-wall interaction on triboelectric separation of fine particles in a turbulent flow. *Advanced Powder Technology*, 30(5):1099–1107.

Landauer, J. and P. Foerst
2018. Triboelectric separation of a starch-protein mixture – impact of electric field strength and flow rate. *Advanced Powder Technology*, 29(1):117–123.

Landauer, J. and P. Foerst
2019a. Influence of particle charge and size distribution on triboelectric separation—new evidence revealed by in situ particle size measurements. *Processes*, 7(6):381.

Landauer, J. and P. Foerst
2019b. Influence of particle contact number on triboelectric separation selectivity. *Processes*, 7(10):716.

Landauer, J., S. M. Tauwald, and P. Foerst

2019b. A simple \textmu-ptv setup to estimate single-particle charge of triboelectrically charged particles. *Frontiers in Chemistry*, 7:1.

Lee, V., S. R. Waitukaitis, M. Z. Miskin, and H. M. Jaeger

2015. Direct observation of particle interactions and clustering in charged granular streams. *Nature Physics*, 11(9):733–737.

Liu, C. and A. J. Bard

2008. Electrostatic electrochemistry at insulators. *Nature materials*, 7(6):505–509.

Liu, C.-y. and A. J. Bard

2009. Chemical redox reactions induced by cryptoelectrons on a pmma surface. *Journal of the American Chemical Society*, 131(18):6397–6401.

Liu, K., F. T. Barrows, and D. Obert

2009. Dry fractionation methods to produce barley meals varying in protein, beta-glucan, and starch contents. *Journal of food science*, 74(6):C487–99.

Lowell, J. and A. C. Rose-Innes

1980. Contact electrification. *Advances in Physics*, 29(6):947–1023.

Lowell, J. and W. S. Truscott

1986a. Triboelectrification of identical insulators. i. an experimental investigation. *Journal of Physics D: Applied Physics*, 19(7):1273–1280.

Lowell, J. and W. S. Truscott

1986b. Triboelectrification of identical insulators. ii. theory and further experiments. *Journal of Physics D: Applied Physics*, 19(7):1281–1298.

Lu, L.-S. and S.-S. Hsiau

2005. Mixing in vibrated granular beds with the effect of electrostatic force. *Powder Technology*, 160(3):170–179.

Mareev, E. A. and S. O. Dementyeva

2017. The role of turbulence in thunderstorm, snowstorm, and dust storm electrification. *Journal of Geophysical Research: Atmospheres*, 122(13):6976–6988.

Masuda, H.

2009. Dry dispersion of fine particles in gaseous phase. *Advanced Powder Technology*, 20(2):113–122.

Matsusaka, S., H. Maruyama, T. Matsuyama, and M. Ghadiri

2010. Triboelectric charging of powders: A review. *Chemical Engineering Science*, 65(22):5781–5807.

Matsusaka, S. and H. Masuda

2003. Electrostatics of particles. *Advanced Powder Technology*, 14(2):143–166.

Matsusaka, S., M. Oki, and H. Masuda

2007. Control of electrostatic charge on particles by impact charging. *Advanced Powder Technology*, 18(2):229–244.

Matsusyama, T. and H. Yamamoto

2006. Impact charging of particulate materials. *Chemical Engineering Science*, 61(7):2230–2238.

Matsuyama, T., M. Ogu, H. Yamamoto, J. C. Marijnissen, and B. Scarlett

2003. Impact charging experiments with single particles of hundred micrometre size. *Powder Technology*, 135-136:14–22.

Matsuyama, T. and H. Yamamoto

1994. Charge transfer between a polymer particle and a metal plate due to impact. *IEEE Transactions on Industry Applications*, 30(3):602–607.

Matsuyama, T. and H. Yamamoto

1995. Electrification of single polymer particles by successive impacts with metal targets. *IEEE Transactions on Industry Applications*, 31(6):1441–1445.

McCarty, L. S. and G. M. Whitesides

2008. Electrostatic charging due to separation of ions at interfaces: contact electrification of ionic electrets. *Angewandte Chemie (International ed. in English)*, 47(12):2188–2207.

Mehrani, P., H. T. Bi, and J. R. Grace

2005. Electrostatic charge generation in gas–solid fluidized beds. *Journal of Electrostatics*, 63(2):165–173.

Messafeur, R., I. Mahi, R. Ouiddir, K. Medles, L. Dascalescu, and A. Tilmatine

2019. Tribo-electrostatic separation of a quaternary granular mixture of plastics. *Particulate Science and Technology*, 37(6):760–765.

Mizes, H. A., E. M. Conwell, and D. P. Salamida

1998. Direct observation of ion transfer in contact charging between a metal and a polymer. *Applied Physics Letters*, 56(16):1597.

Mohanta, S. K., B. Rout, R. K. Dwari, P. Reddy, and B. K. Mishra

2016. Tribo-electrostatic separation of high ash coking coal washery rejects: Effect of moisture on separation efficiency. *Powder Technology*, 294:292–300.

Nernst, W.

1896. Ueber berührungselectricität. *Annalen der Physik*, 294(8):i–xiii.

O'Grady, P. F.

2002. *Thales of Miletus: The beginnings of western science and philosophy*, Western philosophy series. Aldershot, Hants: Ashgate.

Pähtz, T., H. J. Herrmann, and T. Shinbrot

2010. Why do particle clouds generate electric charges? *Nature Physics*, 6(5):364–368.

Park, B.

1898. *A history of electricity (The intellectual rise in electricity) from antiquity to the days of Benjamin Franklin*. New York, NY: John Wiley & Sons.

Park, C.-H., H.-S. Jeon, H.-S. Yu, O.-H. Han, and J.-K. Park

2008a. Application of electrostatic separation to the recycling of plastic wastes: Separation of pvc, pet, and abs. *Environmental Science & Technology*, 42(1):249–255.

Park, C. H., J. K. Park, H. S. Jeon, and B. C. Chun

2008b. Triboelectric series and charging properties of plastics using the designed vertical-reciprocation charger. *Journal of Electrostatics*, 66(11-12):578–583.

Pelgrom, P. J., J. Wang, R. M. Boom, and M. A. Schutyser

2015. Pre- and post-treatment enhance the protein enrichment from milling and air classification of legumes. *Journal of Food Engineering*, 155(-):53–61.

Pence, S., V. J. Novotny, and A. F. Diaz

1994. Effect of surface moisture on contact charge of polymers containing ions. *Langmuir : the ACS journal of surfaces and colloids*, 10(2):592–596.

Piperno, S., H. Cohen, T. Bendikov, M. Lahav, and I. Lubomirsky
2011. The absence of redox reactions for palladium(ii) and copper(ii) on electrostatically charged teflon: relevance to the concept of "cryptoelectrons". *Angewandte Chemie (International ed. in English)*, 50(25):5654–5657.

Ribas-Arino, J. and D. Marx
2012. Covalent mechanochemistry: theoretical concepts and computational tools with applications to molecular nanomechanics. *Chemical reviews*, 112(10):5412–5487.

Rumpf, H. and K. Leschonski
1967. Prinzipien und neuere verfahren der windsichtung. *Chemie Ingenieur Technik - CIT*, 39(21):1231–1241.

Saffman, P. G. and J. S. Turner
1956. On the collision of drops in turbulent clouds. *Journal of Fluid Mechanics*, 1(01):16.

Sakaguchi, M., M. Makino, T. Ohura, and T. Iwata
2014. Contact electrification of polymers due to electron transfer among mechano anions, mechano cations and mechano radicals. *Journal of Electrostatics*, 72(5):412–416.

Sakaguchi, M., S. Shimada, and H. Kashiwabara
1990. Mechanoions produced by mechanical fracture of solid polymer. 6. a generation mechanism of triboelectricity due to the reaction of mechanoradicals with mechanoanions on the friction surface. *Macromolecules*, 23(23):5038–5040.

Salaneck, W. R.
1976. Double mass transfer during polymer-polymer contacts. *Journal of Applied Physics*, 47(1):144.

Schella, A., S. Herminghaus, and M. Schröter
2017. Influence of humidity on tribo-electric charging and segregation in shaken granular media. *Soft matter*, 13(2):394–401.

Schlichting, H. and K. Gersten
2017. *Boundary-Layer Theory*. Berlin, Heidelberg: Springer Berlin Heidelberg.

Schmidt, P.
2010. Screening. In *Ullmann's encyclopedia of industrial chemistry*, volume 1, P. 434. Chichester: Wiley.

Schönert, K., K. Eichas, and F. Niermöller
1996. Charge distribution and state of agglomeration after tribocharging fine particulate materials. *Powder Technology*, 86(1):41–47.

Shapiro, M. and V. Galperin
2005. Air classification of solid particles: a review. *Chemical Engineering and Processing: Process Intensification*, 44(2):279–285.

Shaw, P. E.
1917. Experiments on tribo-electricity. i. the tribo-electric series. *Proceedings of the Royal Society A: Mathematical, Physical and Engineering Sciences*, 94(656):16–33.

Shin, J.-H. and J.-K. Lee
2002. Pvc separation and flow visualization of triboeletrostatically charged plastic particles using fluidized bed tribocharger. *Geosystem Engineering*, 5(2):25–30.

Sibakov, J., J. Abecassis, C. Barron, and K. Poutanen
2014. Electrostatic separation combined with ultra-fine grinding to produce \textbeta-glucan enriched ingredients from oat bran. *Innovative Food Science & Emerging Technologies*, 26:445–455.

Smoluchowski, M.

1917. Versuch einer mathematischen theorie der koagulationskinetik kolloider lösungen. *Zeitschrift fuer physikalische Chemie (Leipzig)*, 92:129–168.

Sommerfeld, M.

1992. Modelling of particle-wall collisions in confined gas-particle flows. *International Journal of Multiphase Flow*, 18(6):905–926.

Soong, Y., M. Schoffstall, and T. Link

2001. Triboelectrostatic beneficiation of fly ash. *Fuel*, 80(6):879–884.

Sow, M., D. J. Lacks, and R. M. Sankaran

2012. Dependence of contact electrification on the magnitude of strain in polymeric materials. *Journal of Applied Physics*, 112(8):084909.

Sowinski, A., L. Miller, and P. Mehrani

2010. Investigation of electrostatic charge distribution in gas–solid fluidized beds. *Chemical Engineering Science*, 65(9):2771–2781.

Tabtabaei, S., M. Jafari, A. R. Rajabzadeh, and R. L. Legge

2016a. Development and optimization of a triboelectrification bioseparation process for dry fractionation of legume flours. *Separation and Purification Technology*, 163:48–58.

Tabtabaei, S., M. Jafari, A. R. Rajabzadeh, and R. L. Legge

2016b. Solvent-free production of protein-enriched fractions from navy bean flour using a triboelectrification-based approach. *Journal of Food Engineering*, 174:21–28.

Tabtabaei, S., M. Vitelli, A. R. Rajabzadeh, and R. L. Legge

2017. Analysis of protein enrichment during single- and multi-stage tribo-electrostatic bioseparation processes for dry fractionation of legume flour. *Separation and Purification Technology*, 176:48–58.

Tanaka, Y., T. Miura, and T. Koyaguchi

2002. Measurements of electric charge distribution in volcanic plumes at sakurajima volcano, japan. *Bulletin of Volcanology*, 64(2):75–93.

Tiyapiboonchaiya, P., D. Gidaspow, and S. Damronglerd

2012. Hydrodynamics of electrostatic charge in polypropylene fluidized beds. *Industrial & Engineering Chemistry Research*, 51(25):8661–8668.

Tomas, J.

2004. Gravity separation of particulate solids in turbulent fluid flow. *Particulate Science and Technology*, 22(2):169–187.

Trigwell, S., N. Grable, C. U. Yurteri, R. Sharma, and M. K. Mazumder

2003a. Effects of surface properties on the tribocharging characteristics of polymer powder as applied to industrial processes. *IEEE Transactions on Industry Applications*, 39(1):79–86.

Trigwell, S., K. B. Tennal, M. K. Mazumder, and D. A. Lindquist

2003b. Precombustion cleaning of coal by triboelectric separation of minerals. *Particulate Science and Technology*, 21(4):353–364.

Vollrath, R. E.

1932. A high voltage direct current generator. *Physical Review*, 42(2):298.

Vose, J. R.

1978. Separating grain components by air classification. *Separation & Purification Reviews*, 7(1):1–29.

Waitukaitis, S. R., V. Lee, J. M. Pierson, S. L. Forman, and H. M. Jaeger
2014. Size-dependent same-material tribocharging in insulating grains. *Physical review letters*, 112(21).

Wang, H., F. Fotovat, X. T. Bi, and J. R. Grace
2019. Tribo-charging of binary mixtures composed of coarse and fine particles in gas–solid pipe flow. *Particuology*, 43:101–109.

Wang, H., G. Zhang, X. Zhang, W. Xie, Y. He, H. Li, and Q. Chen
2017. Improving the efficiency of coal triboelectric separation by chemical conditioning. *Separation Science and Technology*, 52(6):1122–1128.

Wang, J., M. de Wit, R. M. Boom, and M. A. Schutyser
2015a. Charging and separation behavior of gluten–starch mixtures assessed with a custom-built electrostatic separator. *Separation and Purification Technology*, 152:164–171.

Wang, J., M. de Wit, M. A. Schutyser, and R. M. Boom
2014. Analysis of electrostatic powder charging for fractionation of foods. *Innovative Food Science & Emerging Technologies*, 26:360–365.

Wang, J., G. Suo, M. de Wit, R. M. Boom, and M. A. Schutyser
2016a. Dietary fibre enrichment from defatted rice bran by dry fractionation. *Journal of Food Engineering*, 186:50–57.

Wang, J., J. Zhao, M. de Wit, R. M. Boom, and M. A. Schutyser
2016b. Lupine protein enrichment by milling and electrostatic separation. *Innovative Food Science & Emerging Technologies*, 33:596–602.

Wang, L.-P., A. S. Wexler, and Y. Zhou
1998. On the collision rate of small particles in isotropic turbulence. i. zero-inertia case. *Physics of Fluids*, 10(1):266.

Wang, Z. L., J. Chen, and L. Lin
2015b. Progress in triboelectric nanogenerators as a new energy technology and self-powered sensors. *Energy & Environmental Science*, 8(8):2250–2282.

Watanabe, H., M. Ghadiri, T. Matsuyama, Y. L. Ding, and K. G. Pitt
2007. New instrument for tribocharge measurement due to single particle impacts. *Review of Scientific Instruments*, 78(2):024706.

Wiles, J. A., B. A. Grzybowski, A. Winkleman, and G. M. Whitesides
2003. A tool for studying contact electrification in systems comprising metals and insulating polymers. *Analytical Chemistry*, 75(18):4859–4867.

Wu, C., A. C. Wang, W. Ding, H. Guo, and Z. L. Wang
2019. Triboelectric nanogenerator: A foundation of the energy for the new era. *Advanced Energy Materials*, 9(1).

Wu, G., J. Li, and Z. Xu
2013. Triboelectrostatic separation for granular plastic waste recycling: a review. *Waste management (New York, N.Y.)*, 33(3):585–597.

Wu, J. and H. T. Bi
2011. Addition of fines for the reduction of powder charging in particle mixers. *Advanced Powder Technology*, 22(3):332–335.

Xie, L., P. F. He, J. Zhou, and D. J. Lacks

2014. Correlation of contact deformation with contact electrification of identical materials. *Journal of Physics D: Applied Physics*, 47(21):215501.

Xie, L., G. Li, N. Bao, and J. Zhou

2013. Contact electrification by collision of homogenous particles. *Journal of Applied Physics*, 113(18):184908.

Xing, Q., M. de Wit, K. Kyriakopoulou, R. M. Boom, and M. A. Schutyser

2018. Protein enrichment of defatted soybean flour by fine milling and electrostatic separation. *Innovative Food Science & Emerging Technologies*, 50:42–49.

Yao, J., S. Ge, Y. Zhao, S. Cong, C.-H. Wang, and N. Li

2016. Investigation of granule electrostatic charge generation with normal stress effect. *Advanced Powder Technology*, 27(5):2094–2101.

Yoshimatsu, R., N. A. M. Araújo, T. Shinbrot, and H. J. Herrmann

2018. Segregation of charged particles under shear. *Granular Matter*, 20(3):641.

Yu, X., W. Li, Y. Xu, J. Wang, Y. Yang, N. Xu, and H. Wang

2010. Effect of polymer granules on the electrostatic behavior in gas−solid fluidized beds. *Industrial & Engineering Chemistry Research*, 49(1):132–139.

Zelmat, M. E.-M., R. Ouiddir, A. Tilmatine, A. Benabboun, A. Bendaoud, K. Medles, and L. Dascalescu

2015. Experimental investigation of a new-electrostatic separation process for micronized plastics. *2015 IEEE Industry Applications Society Annual Meeting*, Pp. 1–5.

Zhao, H., G. Castle, and I. I. Inculet

2002. The measurement of bipolar charge in polydisperse powders using a vertical array of faraday pail sensors. *Journal of Electrostatics*, 55(3-4):261–278.

Zhao, H., G. Castle, I. I. Inculet, and A. G. Bailey

2003. Bipolar charging of poly-disperse polymer powders in fluidized beds. *IEEE Transactions on Industry Applications*, 39(3):612–618.

A. List of Publications

Peer-Reviewed Publications

Johann Landauer and Petra Foerst, 2018, Triboelectric separation of a starch-protein mixture – impact of electric field strength and flow rate. Advanced Powder Technology, 29(1):117–123.

Johann Landauer, Felicitas Aigner, Michael Kuhn, and Petra Foerst, 2019, Effect of particle-wall interaction on triboelectric separation of fine particles in a turbulent flow. Advanced Powder Technology, 30(5):1099–1107.

Johann Landauer and Petra Foerst, 2019, Influence of particle charge and size distribution on triboelectric separation—new evidence revealed by in situ particle size measurements. Processes, 7(6):381.

Johann Landauer, Sandra M. Tauwald, and Petra Foerst, 2019, A simple µ-ptv setup to estimate single-particle charge of triboelectrically charged particles. Frontiers in Chemistry, 7:1.

Johann Landauer and Petra Foerst, 2019, Influence of particle contact number on triboelectric separation selectivity. Processes, 7(10):716

Johann Landauer, Michael Kuhn, Daniel S. Nasato, Petra Foerst, and Heiko Briesen, 2020, Particle shape matters – Using 3D-printed particles to investigate fundamental particle and packing properties. Powder Technology, 361:711-718.

Oral Presentations

Johann Landauer and Petra Foerst, 2017, Triboelectric separation of starch and protein particles. ESCC 2017, Izmir, Turkey.

Johann Landauer and Petra Foerst, 2019, Factors influencing triboelectric separation of fine organic powders. ESCC 2019, Leeds, UK.

Poster Presentations

Johann Landauer and Petra Foerst, 2017, Einfluss der Verteilung von Feststoffdichte auf das Zerkleinerungsergebnis. ProcessNet 2017 Fachgruppe Agglomertaion und Schüttguttechnik, Bruchsal, Germany.

Johann Landauer, Felicitas Aigner, and Petra Foerst, 2018, Triboelektrische Trennung von feinen binären Partikelsystemen gleicher Größe. ProcessNet 2018 Fachgruppe Zerkleinern und Klassieren, Neuss, Germany.

Johann Landauer, Sandra M. Tauwald, and Petra Foerst, 2019, Measurement of single particle charge using a µ-PTV system in a dry gas flow. Partec 2019, Nürnberg, Germany.

Non-Peer-Reviewed Publications

Johann Landauer, Dominik Nöninger, Heiko Briesen, and Petra Foerst, 2016, Mechanische Aufbereitung von Gerstenmalz. Der Weihenstephaner, 84(4):152-154.

Johann Landauer and Petra Foerst, 2019, Triboelektrik – Eine spannende Aufbereitungsmethode für Malz?. Der Weihenstephaner, 87(1):30-32.

B. Supplementary of embedded publications

Influence of particle contact number on triboelectric separation selectivity S1

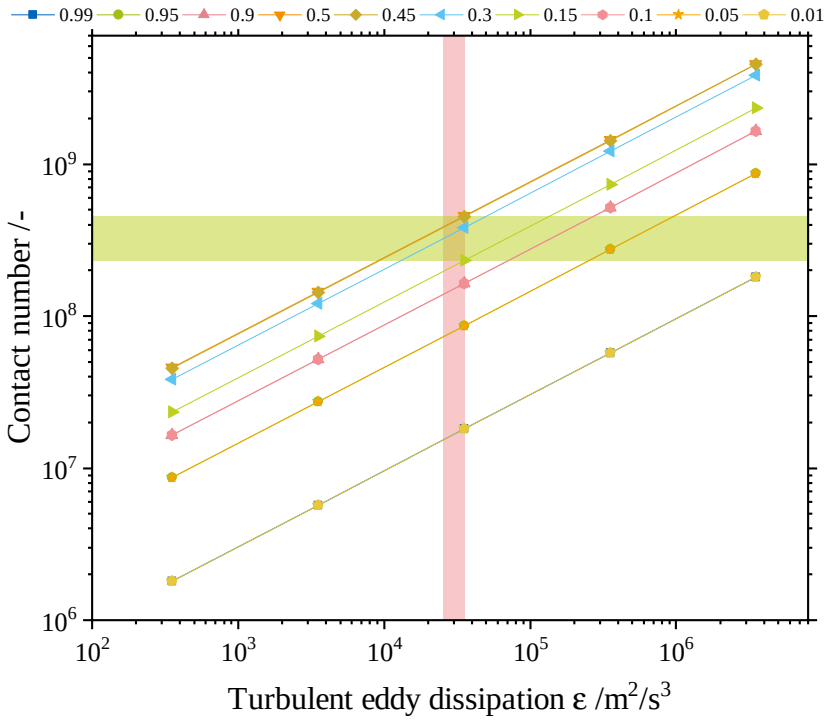

Figure S1: Sensitivity analysis of Eq. (2) to estimate the influence of turbulence eddy dissipation rate and protein content in the initial powder (from 0.99 to 0.01) on the contact number. Contact numbers and turbulent eddy dissipation rates used in this study are highlighted.

A simple µ-PTV Setup S1

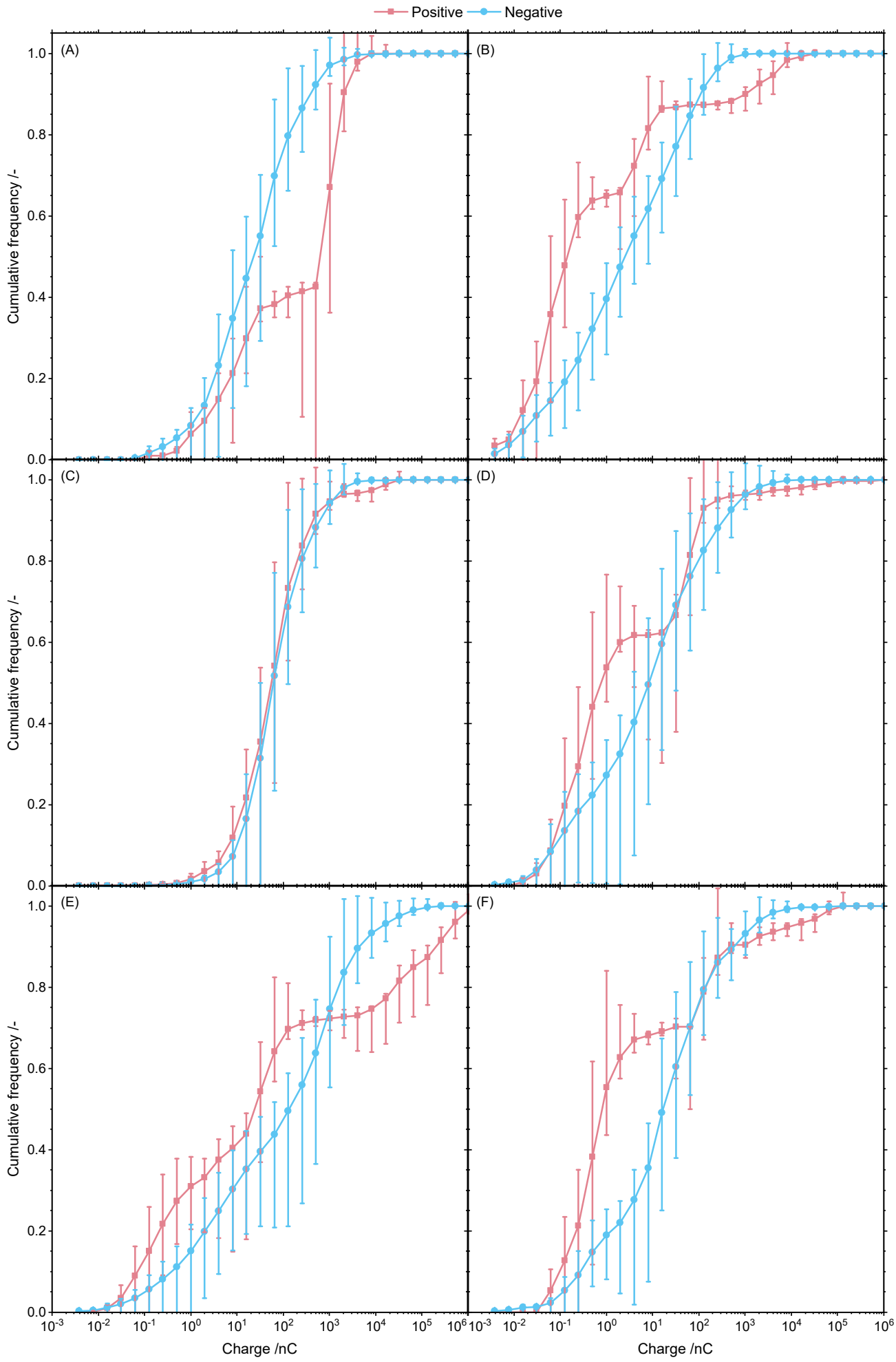

Figure 1S: Cumulative frequency of corn starch (A), potato starch (B), and whey protein (C) as well as starch-protein mixtures containing 15 wt.% protein and barley (D), corn (E), and potato starch (F). Error bars indicating the uncertainty in calculating the charge using data of a particle size distribution with a given standard derivation.